VOLUME 84, NO. EM3
JULY 1958

JOURNAL of the

Engineering Mechanics Division

PROCEEDINGS OF THE
AMERICAN SOCIETY
OF CIVIL ENGINEERS

BASIC REQUIREMENTS FOR MANUSCRIPTS

This Journal represents an effort by the Society to deliver information to the reader with the greatest possible speed. To this end the material herein has none of the usual editing required in more formal publications.

Original papers and discussions of current papers should be submitted to the Manager of Technical Publications, ASCE. Authors should indicate the technical division to which the paper should be referred. The final date on which a discussion should reach the Society is given as a footnote with each paper. Those who are planning to submit material will expedite the review and publication procedures by complying with the following basic requirements:

1. Titles should have a length not exceeding 50 characters and spaces.

2. A 50-word summary should accompany the paper.

3. The manuscript (a ribbon copy and two copies) should be double-spaced on one side of 8½-in. by 11-in. paper. Papers that were originally prepared for oral presentation must be rewritten into the third person before being submitted.

4. The author's full name, Society membership grade, and footnote reference stating present employment should appear on the first page of the paper.

5. Mathematics are reproduced directly from the copy that is submitted. Because of this, it is necessary that capital letters be drawn, in black ink, 3/16-in. high (with all other symbols and characters in the proportions dictated by standard drafting practice) and that no line of mathematics be longer than 6½-in. Ribbon copies of typed equations may be used but they will be proportionately smaller in the printed version.

6. Tables should be typed (ribbon copies) on one side of 8½-in. by 11-in. paper within a 6½-in. by 10½-in. invisible frame. Small tables should be grouped within this frame. Specific reference and explanation should be made in the text for each table.

7. Illustrations should be drawn in black ink on one side of 8½-in. by 11-in. paper within an invisible frame that measures 6½-in. by 10½-in.; the caption should also be included within the frame. Because illustrations will be reduced to 69% of the original size, the capital letters should be ⅛-in. high. Photographs should be submitted as glossy prints in a size that is less than 6½-in. by 10½-in. Explanations and descriptions should be made within the text for each illustration.

8. Papers should average about 12,000 words in length and should be no longer than 18,000 words. As an approximation, each full page of typed text, table, or illustration is the equivalent of 300 words.

Further information concerning the preparation of technical papers is contained in the "Technical Publications Handbook" which can be obtained from the Society.

This Journal is published quarterly by the American Society of Civil Engineers. Publication office is at 2500 South State Street, Ann Arbor, Michigan. Editorial and General Offices are at 33 West 39 Street, New York 18, New York. [illegible] of a member's dues are applied as a subscription to this Journal. Second-class postage privileges are authorized at Ann Arbor, Michigan.

1M,SM.

Journal of the
ENGINEERING MECHANICS DIVISION
Proceedings of the American Society of Civil Engineers

CONTENTS

July, 1958

Papers

Paper 1692 July, 1958 EM 3

Journal of the
ENGINEERING MECHANICS DIVISION
Proceedings of the American Society of Civil Engineers

STRONG CYLINDRICAL BENDING OF ELASTIC PLATES

S. J. Medwadowski,[1] A. M. ASCE, and K. S. Pister,[2] J. M. ASCE
(Proc. Paper 1692)

ABSTRACT

The effect of shear deformation on strong cylindrical bending of an elastic plate under uniform transverse load is considered. A system of differential equations governing the problem is stated, utilizing the refined theory of plates due principally to Reissner and Eringen. The problem is solved and graphs are given, from which numerical results are obtainable. The solution is compared with the corresponding result of the classical theory.

NOTATION

The following nomenclature is used in this paper:

u, v, w = displacements of the middle surface of the plate

w_x, w_y = rotations of the normal to the undeformed middle surface

E = Young's modulus in the x, y plane

F = Airy stress function defined in Eq. (3)

ν = Poisson's ratio in the x, y plane

E_z = Young's modulus in the z direction

G_z = Shearing modulus in the z direction

$D = \frac{E h^3}{12 (1 - \nu^2)}$

Note: Discussion open until December 1, 1958. To extend the closing date one month, a written request must be filed with the Executive Secretary, ASCE. Paper 1692 is part of the copyrighted Journal of the Engineering Mechanics Division, Proceedings of the American Society of Civil Engineers, Vol. 84, No. EM 3, July, 1958.

1. Head, Structural Dept., John A. Carollo, Cons. Engrs., Berkeley, Calif.
2. Associate Prof. of Civ. Eng., Univ. of California, Berkeley, Calif.

$M_x \ldots, N_x \ldots, V_x \ldots$ = stress resultants as defined in Reference (6)

p = transverse load on plate surface

INTRODUCTION

The classical formulation of the equations governing the flexural behavior of thin elastic plates disregards the effect of transverse shear deformation. This is characteristic of both the Poisson-Kirchhoff small deflection theory and the Fδppl-v. Karman large deflection theory. Refinements of the small deflection theory to include the above effect may be found in the work of Levy[1] or Reissner,[2] who further considered the effect of transverse normal stress. These refinements were also extended to the problem of strong bending of sandwich plates by Reissner.[3,4] A recent paper by Eringen[5] on the finite flexural motion of visco-elastic plates contains Reissner's static plate equations as special cases, for both small and large deflection theories, although no applications to specific problems are presented.

In this paper the refined plate theory is applied to the problem of strong cylindrical bending of a uniformly loaded, simply supported strip. The solution is compared with the results from classical plate theory. The material of the plate will be assumed isotropic.

Fundamental System of Equations

The fundamental system of partial differential equations governing the problem of large deflection of elastic plates including the effect of shear deformation has been derived and adequately discussed in references cited above. In general there are thirteen unknown functions to be determined; introducing the Airy stress function F and then choosing F, w, V_x and V_y (see NOTATION) as the fundamental unknowns it can be shown that the following fundamental system of four partial differential equations must be satisfied:

$$\nabla^4 F = E\left(w_{,xy}^2 - w_{,xx}\, w_{,yy}\right) \tag{1a}$$

$$D\nabla^4 w = p + N - \frac{Eh^2}{10(1-\nu^2)G_z}\nabla^2(p+N) \tag{1b}$$

$$V_x - \frac{Eh^2}{20(1+\nu)G_z}\nabla^2 V_x = -D\nabla^2 w_{,x} - \frac{Eh^2}{20(1-\nu)G_z}\left(p_{,x} + N_{,x}\right) \tag{1c}$$

$$V_y - \frac{Eh^2}{20(1+\nu)G_z}\nabla^2 V_y = -D\nabla^2 w_{,y} - \frac{Eh^2}{20(1-\nu)G_z}\left(p_{,y} + N_{,y}\right) \tag{1d}$$

where subscripts following a comma denote differentiation and

$$N \equiv N_x w_{,xx} + 2N_{xy} w_{,xy} + N_y w_{,yy} \tag{2}$$

The remaining ten unknowns are then given directly in terms of the fundamental four as follows:

$$N_x = h F_{,yy} \qquad N_y = h F_{,xx} \qquad N_{xy} = -h F_{,xy} \tag{3}$$

$$M_x = -D\left(w_{,xx} + \nu w_{,yy}\right) + \underline{\frac{6}{5h}\frac{D}{G_z}(1-\nu)V_{x,x}} - \underline{\frac{6}{5h}\frac{D\nu}{G_z}(p+N)} \tag{4a}$$

$$M_y = -D\left(w_{,yy} + \nu w_{,xx}\right) + \underline{\frac{6}{5h}\frac{D}{G_z}(1-\nu)V_{y,y}} - \underline{\frac{6}{5h}\frac{D\nu}{G_z}(p+N)} \tag{4b}$$

$$M_{xy} = -D(1-\nu)w_{,xy} + \underline{(V_{x,y} + V_{y,x})\frac{Eh^2}{20(1+\nu)G_z}} \tag{4c}$$

$$u_{,x} = \frac{N_x}{Eh} - \frac{\nu N_y}{Eh} - \frac{1}{2}w_{,x}^2 \tag{5a}$$

$$v_{,y} = -\frac{\nu N_x}{Eh} + \frac{N_y}{Eh} - \frac{1}{2}w_{,y}^2 \tag{5b}$$

$$w_x = -w_{,x} + \underline{\frac{6V_x}{5hG_z}} \tag{5c}$$

$$w_y = -w_{,y} + \underline{\frac{6V_y}{5hG_z}} \tag{5d}$$

As indicated in the introduction the present theory differs from the classical theory in that the effect of shear deformation is considered. Those terms which do not appear in the classical theory have been underlined for easier comparison. It is seen that one of the equations of the fundamental system, Eq. (1a), is identical to the corresponding equation of the classical theory.

The remaining three Eqs. (1b, c, d) contain additional terms. If the effect of shear deformation is neglected the terms multiplied by h^2 in Eqs. (1b, c, d) vanish and the resultant shears V_x and V_y become entirely defined once the stress function $F(x,y)$ and weighted displacement $w(x,y)$ become known.

Cylindrical Bending of an Infinite Strip

Consider the problem of cylindrical bending of an isotropic infinite strip bounded by lines $x = 0$ and $x = a$ and acted upon by a transverse normal load $p = \text{const}$. For a simply supported plate we have the following set of boundary conditions:

$$w(0,y) = w(a,y) = 0 \tag{6a}$$

$$M_x(0,y) = M_x(a,y) = 0 \tag{6b}$$

either $w_y(0,y) = w_y(a,y) = 0$

or $M_{xy}(0,y) = M_{xy}(a,y) = 0$ (6c)

and

$$u(0,y) = u(a,y) = 0 \tag{6d}$$

$$v(0,y) = v(a,y) = 0 \tag{6e}$$

The solution of the corresponding problem of the classical plate theory can be found in reference (6).

We observe that in this problem none of the quantitites to be found depend on y. Also we have $M_{xy} = 0$; $V_y = 0$; $N_{xy} = 0$; hence $N_x = \text{const.}$, $N_y = \text{constant}$. Then Eqs. (1a, d) are identically satisfied and Eq. (1b), for an isotropic material with $G_z = \frac{E}{2(1+\nu)}$, becomes

$$D\,w_{,xxxx} = p + N_x\,w_{,xx} - \frac{h^2}{5(1-\nu)}\,N_x\,w_{,xxxx} \tag{7}$$

We note next that for the given problem $V_{x,xx} = -N_x w_{,xxx}$ and thus Eq. (1c) becomes:

$$V_x = -\left(D + \frac{h^2}{5(1-\nu)}\,N_x\right) w_{,xxx} \tag{8}$$

Thus the order of the fundamental system has been lowered. This is due to the fact that we are dealing with a problem of irrotational bending as defined by Bolle.[7] To integrate Eq. (7) write it in a different form:

$$w_{,xxxx} - \frac{4\lambda^2}{a^2}\,w_{,xx} = \frac{pt^2}{D} \tag{9}$$

where

$$\lambda^2 = \frac{a^2}{4} \frac{N_x}{D + \frac{h^2 N_x}{5(1-\nu)}} \tag{10a}$$

$$t^2 = 1 - \frac{4h^2}{5a^2} \cdot \frac{\lambda^2}{1-\nu} \tag{10b}$$

The general solution of (9) is

$$w = C_1 + C_2 x + C_3 \sinh \frac{2\lambda x}{a} + C_4 \cosh \frac{2\lambda x}{a} - \frac{P a^2 t^2 x^2}{8 D \lambda^2} \tag{11}$$

Using boundary conditions (6a) and (6b) we find:

$$C_1 = -\frac{P}{16D} \cdot \frac{a^4 t^4}{\lambda^4} \tag{12a}$$

$$C_3 = \frac{P}{16D} \frac{a^4 t^4}{\lambda^4} \tanh \lambda \tag{12b}$$

$$C_2 = \frac{P}{8D} \cdot \frac{a^3 t^2}{\lambda^2} \tag{12c}$$

$$C_4 = \frac{P}{16D} \frac{a^4 t^4}{\lambda^4} \tag{12d}$$

It follows that deflection w(x), maximum deflection $w(\frac{a}{2})$ and maximum bending moment $M_x(\frac{a}{2})$ are given respectively by:

$$w(x) = \frac{P a^4 t^4}{16 D \lambda^4} \left[-1 + \frac{2\lambda^2 x}{a t^2} + \tanh \lambda \sinh \frac{2\lambda x}{a} + \cosh \frac{2\lambda x}{a} - \frac{2\lambda^2 x^2}{a^2 t^2} \right] \tag{13a}$$

$$w(\tfrac{a}{2}) = \frac{5 P a^4}{384 D} f_1(\lambda) \tag{13b}$$

$$M_x(\tfrac{a}{2}) = \frac{P a^2}{8} f_2(\lambda) \tag{13c}$$

where

$$f_1(\lambda) = \frac{24 t^4}{5 \lambda^4} \left[\operatorname{sech} \lambda - 1 + \frac{\lambda^2}{2 t^2} \right] \tag{14a}$$

$$f_2(\lambda) = \frac{2}{\lambda^2} \left[1 - \operatorname{sech} \lambda + \frac{4}{5} \cdot \frac{\lambda^2}{1-\nu} \cdot \frac{h^2}{a^2} \operatorname{sech} \lambda \right] - \frac{8 h^2}{5(1-\nu) a^2} \tag{14b}$$

It is now necessary to find the quantity λ. This will be done using boundary conditions (6d). On integrating Eq. (5a) and using the first of boundary conditions (6d) we find:

$$\frac{1-\nu^2}{Eh} N_x a - \frac{1}{2}\int_0^a w_{,x}^2 \, dx = 0 \tag{15}$$

On substitution of the proper expression for $w_{,x}$ and performing operations indicated we get, after some manipulation:

$$\frac{E^2 h^8}{(1-\nu^2)^2 p^2 a^8} = \frac{9}{8}\frac{t^6}{\lambda^6} - \frac{27}{16}\frac{t^8}{\lambda^8}(t^2+4) + \frac{27}{16}\frac{t^{10}}{\lambda^8}\tanh^2\lambda + \frac{27}{16}\frac{t^8}{\lambda^8}(t^2+4)\tanh\lambda \tag{16}$$

which replaces Timoshenko's formula[8] for classical theory, reference (6). This equation can be solved for a given value of the left-hand side (with $\nu = 0.3$) using appended graph given in Fig. 3.

The function $f_1(\lambda)$ and $f_2(\lambda)$ can be found from graphs given in Fig. 1 and Fig. 2 respectively.

It should be noted that the range of applicability of the figures is limited by the requirement that $N_x \geq 0$. From Eq. (10a) this condition is met if the following inequality is satisfied: (for $\nu = 0.3$)

$$\left(\frac{\lambda}{\alpha}\right)^2 \leq \frac{1}{8} \tag{17}$$

where

$$\alpha = \frac{a}{h}$$

For the case of $N_x = 0$ ($\lambda = 0$) the limiting value of $f_1(\lambda)$ depends upon the span-depth ratio, α. The value of $f_1(0)$ is the shear correction for maximum deflection of a simply supported beam under uniform load.

It may also be noted that upon setting $N_x = -P$ in Eq. (10a) and by choosing $-\frac{4\lambda^2}{a^2} = \frac{\pi^2}{a^2}$ the Euler buckling load, modified for the effect of shear deformation, is recovered.

Example

To indicate the significance of the results obtained and to illustrate the application of the graphs given in Figs. 1, 2 and 3 consider a steel plate strip, $E = 3 \times 10^7$ psi and $\nu = 0.3$. Let $a = 20"$, $h = 1"$ and $p = 100$ lb./in. Then $\sqrt{f_3(\lambda)} = 2.06$ and from Fig. 3 we have $\lambda = 0.70$. From Figs. 1 and 2, $f_1(\lambda) = 0.83$ and $f_2(\lambda) = 0.70$ while the corresponding values from the classical theory are $f_1(\lambda) = 0.83$ and $f_2(\lambda) = 0.83$. Thus we note that while the effect of shear deformation on deflection cannot be observed for the span-depth ratio chosen, its effect on maximum bending moment is pronounced. Expressions for bending and axial stress are obtainable from Eqs. (13c) and (10a) respectively:

$$\sigma_{bend.} = 0.75\, p\alpha^2 f_2(\lambda) \qquad (18)$$

$$\sigma_{axial} = \frac{N_x}{h} = \frac{4\lambda^2 D}{h a^2}\left[\frac{1}{1 - \frac{4\lambda^2}{5(1-\nu)\alpha^2}}\right] \qquad (19)$$

The maximum stress obtained by adding Eqs. (18) and (19) for the case considered is 35 ksi as compared to 39 ksi by classical plate theory. A comparison of maximum stresses found by the refined and classical theories for span-depth ratios of 20 and 40 is shown below:

$\alpha = 20$			$\alpha = 40$	
p	σ_{Max}	σ^*_{Max}	σ_{Max}	σ^*_{Max}
60	23	26	52	56
80	29	33	66	70
100	35	39	77	83
200	57	66	110	120
400	96	115	—	—

σ^*_{Max} computed neglecting shear effect.

It may be noted from the table that maximum stress predicted by classical theory is on the safe side. The difference in maximum stress from the classical and refined theories decreases as α increases, due to the increasing importance of axial stress and decreasing importance of bending stress. It is clear from Eqs. (18) and (19) that the difference occurs in the bending stress, while the axial stress is the same by either refined or classical theories. While it appears from the results shown that little is to be gained in employing the refined theory for normal strength steel plates, its use is justified for high strength plates if full advantage of high strength is to be taken.

CONCLUDING REMARKS

The problem of strong cylindrical bending of an elastic plate-strip under uniformly distributed load has been solved in this paper. The behavior of the plate was considered in light of the refined plate theory of Reissner, which includes the effect of shear deformation. Graphs are given to simplify

numerical solution of problems and results are compared with those of the classical theory as given by Timoshenko. It is shown that, as might be expected, the effect of shear deformation is more pronounced for plates whose thickness is large compared to their span. In the case of maximum bending moment, however, the effect of shear deformation appears to be large even for fairly thin plates. The importance of the refined theory for efficient design of high strength plates is indicated. Plate strips with other types of boundary conditions may be treated by the method described.

BIBLIOGRAPHY

1. Levy, M., "Memoire sur la theorie des plaques élastiques planes", Journal de mathematiques pures et appliquees, 3. serie, 3-4 (1877-1878), pp. 219-306.

2. Reissner, E., "On the Theory of Bending of Elastic Plates", J. Math. Phys., 23 (1944) pp. 184-191.

3. Reissner, E., "Finite Deflections of Sandwich Plates", J. Aero. Sci., 15, No. 7 (1948), pp. 435-440.

4. Reissner, E., "Errata - Finite Deflections of Sandwich Plates", J. Aero. Sci., 17, No. 2 (1950), p. 125.

5. Eringen, A. C., "On the Nonlinear Oscillations of Viscoelastic Plates", J. Appl. Mech., 22 (1955), pp. 563-567.

6. Timoshenko, S., "Theory of Plates and Shells", McGraw-Hill Book Company, Inc., New York and London, 1940, pp. 4-10.

7. Bolle, L., "Contribution au probleme lineaire de flexion d'une plaque elastique", Bulletin Technique de la Suisse Romande, 73 (1947), part 1 and 2, pp. 281-285 and 293-298.

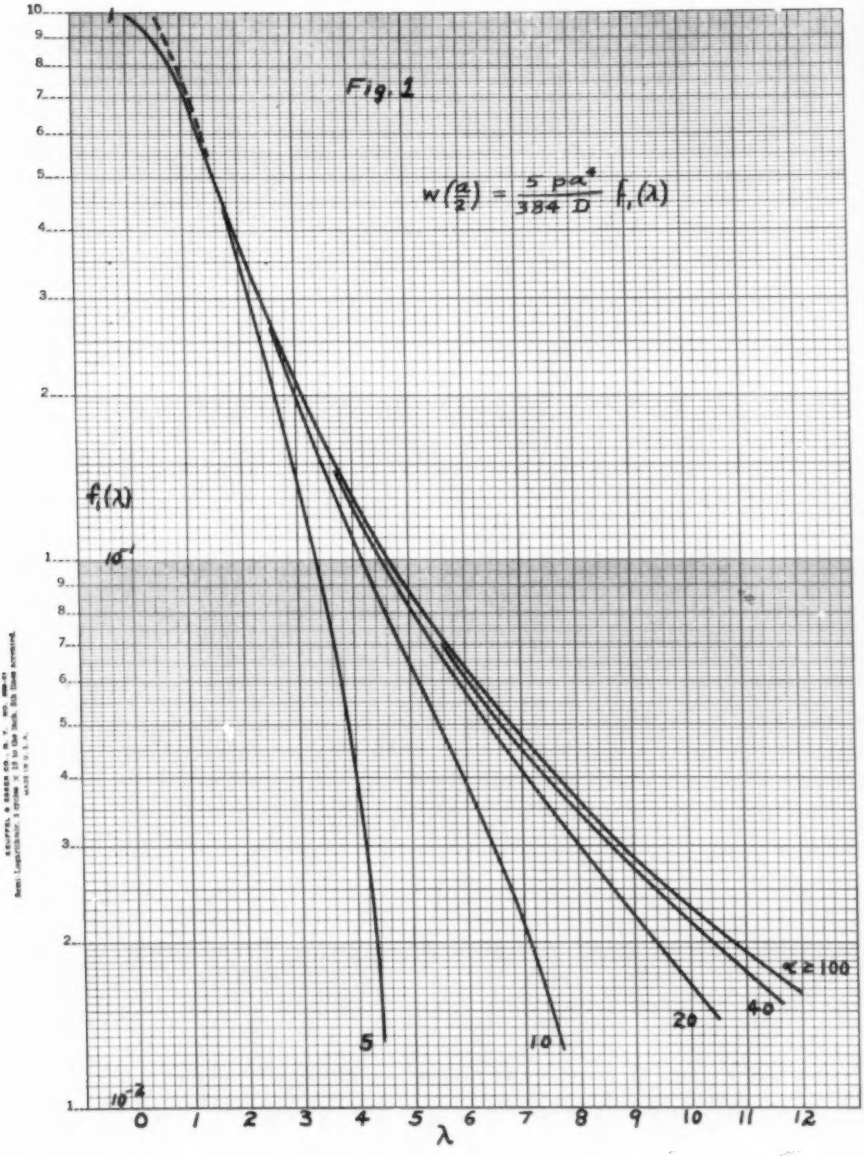
Fig. 1
$w\left(\frac{a}{2}\right) = \frac{5\,p a^4}{384\,D} f_1(\lambda)$
$f_1(\lambda)$
10^{-1}
10^{-2}
λ
0 1 2 3 4 5 6 7 8 9 10 11 12
5
10
20
40
$\infty \geq 100$

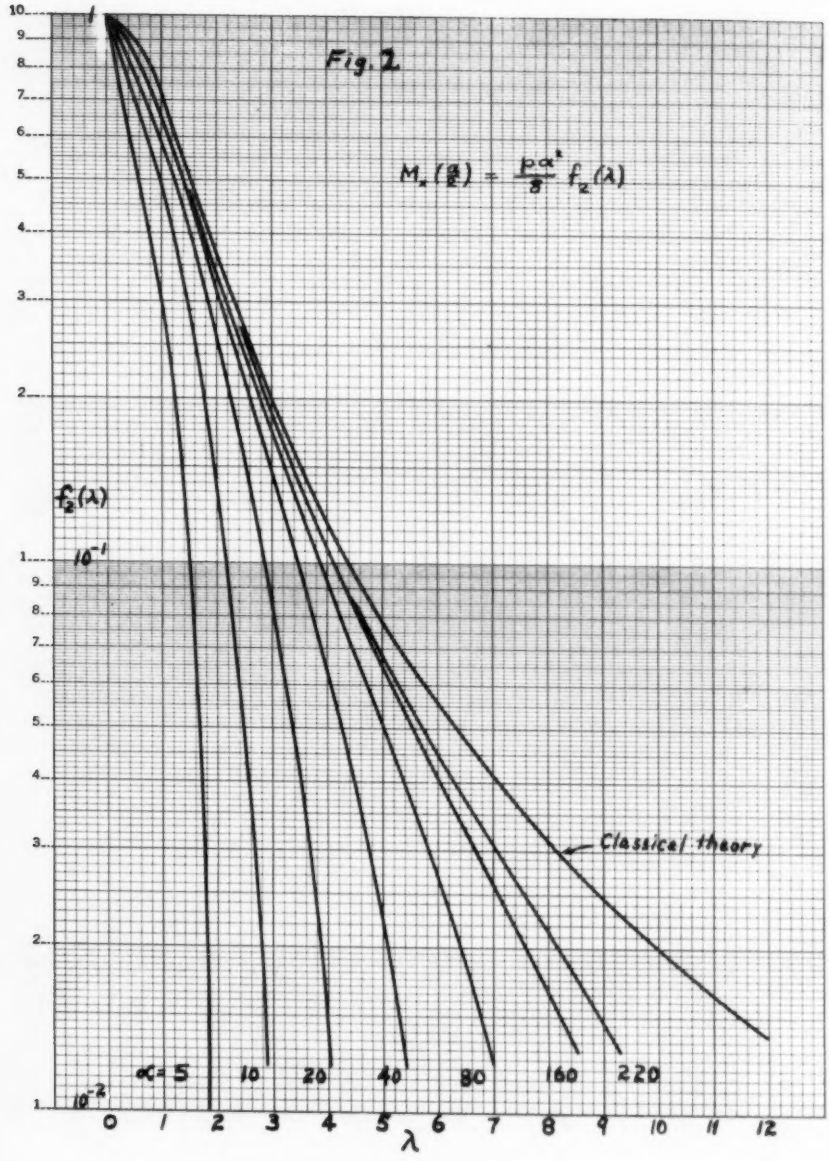
Fig. 2.
$M_z(\frac{\beta}{2}) = \frac{p\alpha^2}{8} f_z(\lambda)$
$f_2(\lambda)$
1
10^{-1}
10^{-2}
Classical theory
α= 5
10
20
40
80
160
220
0 1 2 3 4 5 6 7 8 9 10 11 12
λ

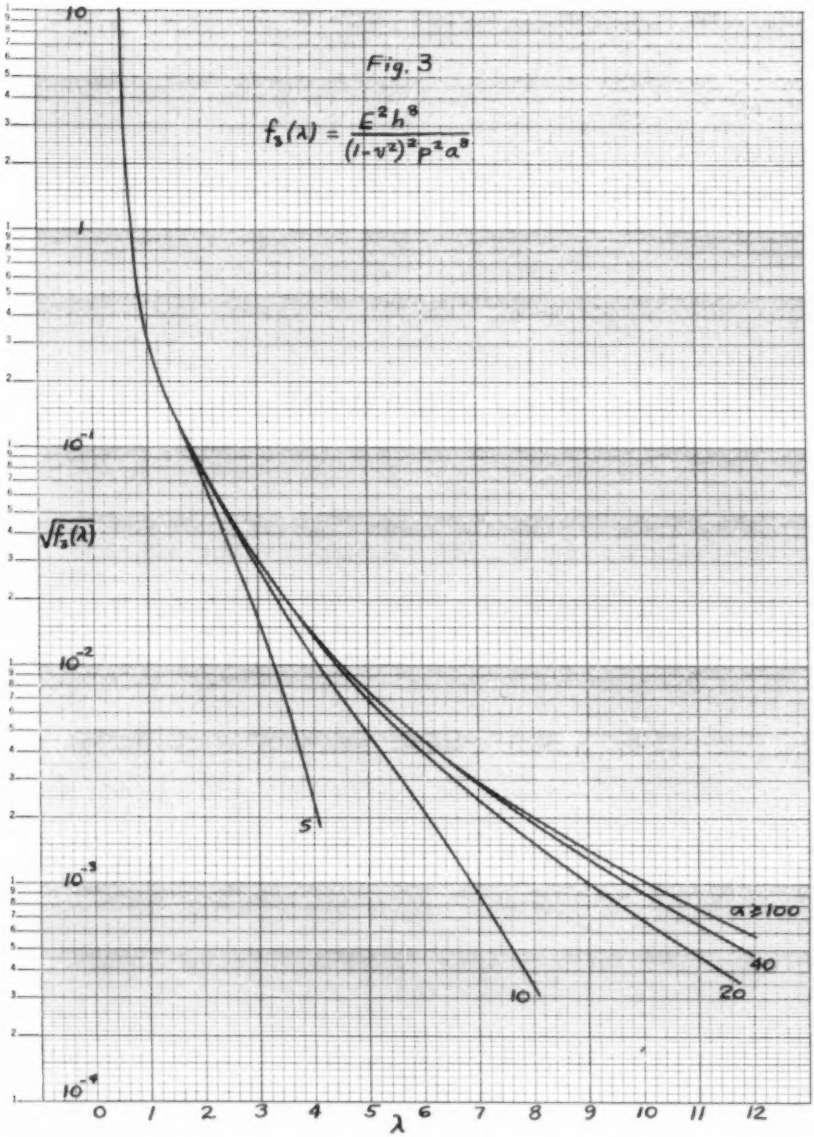
Fig. 3
$f_3(\lambda) = \frac{E^2 h^8}{(1-\nu^2)^2 p^2 a^8}$
10
1
10^{-1}
$\sqrt{f_3(\lambda)}$
10^{-2}
10^{-3}
10^{-4}
5
10
20
40
$\alpha \geq 100$
0 1 2 3 4 5 6 7 8 9 10 11 12
λ

Paper 1693 July, 1958 EM 3

Journal of the
ENGINEERING MECHANICS DIVISION
Proceedings of the American Society of Civil Engineers

DYNAMIC ELASTO-PLASTIC RESPONSE OF RIGID FRAMES

Frank L. DiMaggio,[1] A. M., ASCE
(Proc. Paper 1693)

INTRODUCTION

The procedure for determining the elastic response of structures to transient loads in terms of the elastic normal modes is well known.(1) Assuming ideal plasticity, Bleich and Salvadori(2) recently proposed a method for obtaining the response beyond the elastic range in terms of elasto-plastic normal modes. They applied the method to free-free beams acted on by impulsive loads.

In this paper, the method of Bleich and Salvadori is applied in general to two hinged and fixed rigid frames acted upon by a time dependent concentrated force at the knee and in particular to a two hinged frame (for which the elastic normal modes are known(3)) and a linearly decaying forcing function.

General Analysis

The structure and loading considered in this paper are shown in Fig. 1, where the ends A and D may be either both pinned or both fixed.

First Elastic Stage

The forced elastic deflections of the columns and beam (see Fig. 2) may be represented by

$$y_E^u(x^u,t) = \sum_{i=1}^{\infty} q_i(t)\,\phi_i^u(x^u)$$

Note: Discussion open until December 1, 1958. To extend the closing date one month, a written request must be filed with the Executive Secretary, ASCE. Paper 1693 is part of the copyrighted Journal of the Engineering Mechanics Division, Proceedings of the American Society of Civil Engineers, Vol. 84, No. EM 3, July, 1958.

1. Asst. Prof. of Civ. Eng., Columbia Univ., New York, N. Y.

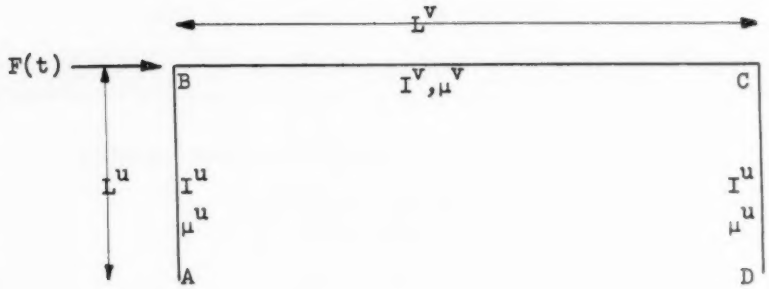

Fig. 1. Loaded Rigid Frame

$$y_E^v(x^v,t) = \sum_{i=1}^{\infty} q_i(t)\, \phi_i^v(x^v) \tag{1b}$$

in which ϕ_i are the antisymmetrical normal modes of the frame (the symmetrical modes are not excited by the load considered) and q_i, the generalized coordinates, satisfy the differential equations

$$\ddot{q}_i + \omega_i^2 q_i = Q_i/C_i \tag{2}$$

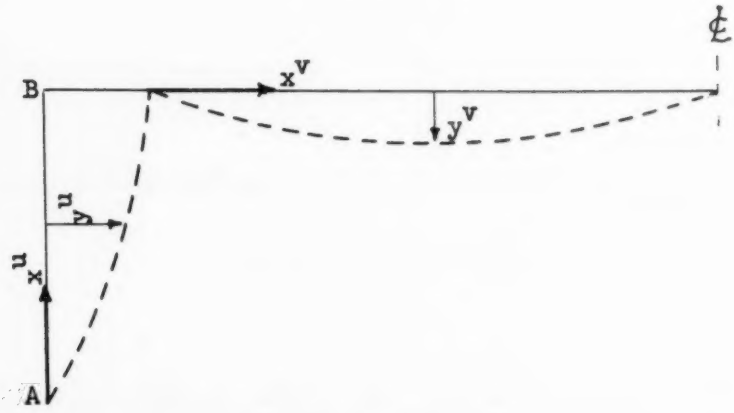

Fig. 2. First Antisymmetrical Mode

where ω_i are the natural frequencies, C_i the generalized masses:

$$C_i = 2\mu^u \int_0^{L^u} (\phi_i^u)^2 \, dx + \mu^v \int_0^{L^v} (\phi_i^v)^2 \, dx + \mu^v L^v \left[\phi_i^u(L^u)\right]^2 \tag{3}$$

and Q_i the generalized forces due to the applied force F(t):

$$Q_i(t) = F(t) \, \phi_i^u(L^u) \tag{4}$$

In Eq. (2), dots denote differentiation with respect to time t. If the structure is initially at rest

$$q_i(0) = \dot{q}_i(0) = 0$$

and the general solutions of (2) are

$$q_i(t) = \frac{\phi_i^u(L^u)}{C_i \omega_i} \int_0^t F(\tau) \sin \omega_i (t - \tau) \, d\tau \tag{6}$$

When, at time t_o, the elastic moment at the knees, computed from

$$M_E^u (L^u, t_e) = - EI^u y_E^{u''} (L^u, t_e) = - EI^u \sum_{i=1}^{\infty} q_i(t_e) \, \phi_i^{u''}(L^u) \tag{7}$$

where t_e denotes the time variable during the elastic phase reaches the capacity value M_o, plastic hinges are assumed to form there and the first plastic stage begins. In Eq. (7) and hereafter, primes indicate differentiation with respect to x.

First Plastic Stage

On the assumption of an ideal plastic hinge, the moment at the knees remains constant and equal to M_o throughout the elasto-plastic stage. If the capacity moment is not reached at any other section during this stage, the motion of the frame may be determined by considering two separate elastic systems as shown in Fig. 3.

Consider the translational motion of the beam. Newton's second law yields

$$S(t) = \frac{1}{2}\left[F(t) - \mu^v L^v \ddot{y}^u(L^u)\right] \tag{8}$$

where S(t) is the shear at the column top as shown in Fig. 3. Thus the effect of the mass of the beam on the lateral motion of the column may be reproduced by adding a concentrated mass $.5\mu^v L^v$ to the column at $x^u = L^u$. This permits the use of the systems shown in Fig. 4 to determine the elasto-plastic response.

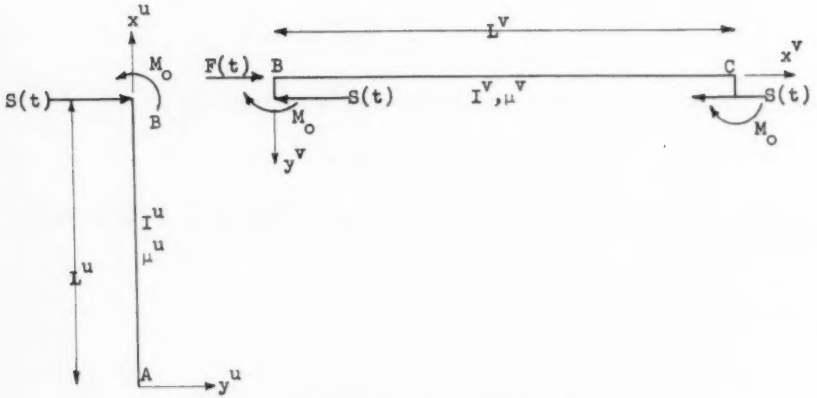

Fig. 3. Column and Beam Elastic Systems

Denoting the modes of free vibration of the column with concentrated mass (Fig. 4a) by $\psi_i^u(x^u)$, the lateral deflections may be expressed as*

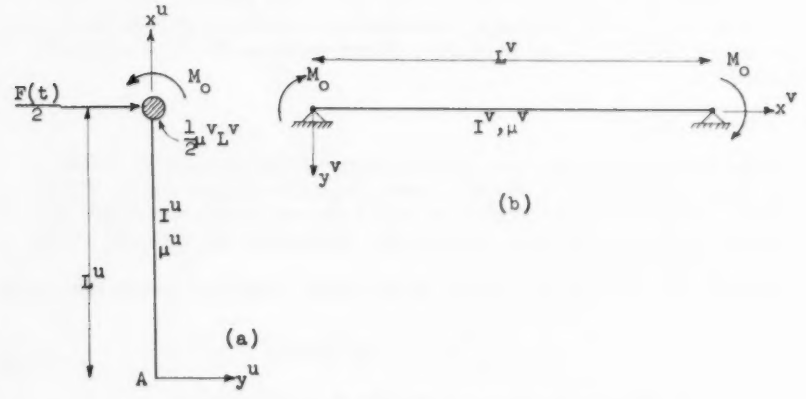

Fig. 4. Column and Beam Elasto-Plastic Systems

*The symbol $\sum_i$ will be used to denote $\sum_{i=0}^{\infty}$ for the two hinged frame, where i = 0 corresponds to the rigid body mode, and $\sum_{i=1}^{\infty}$ for the fixed frame.

$$y_P^u(x^u,t) = \sum_i \psi_i^u(x^u)\, p_i^u(t) \tag{9}$$

where the generalized coordinates p_i^u satisfy the differential equations

$$\ddot{p}_i^u + (\Omega_i^u)^2 p_i^u = \frac{P_i^u}{\alpha_i^u} \tag{10}$$

In Eq. (10), Ω_i^u are the natural frequencies associated with the ψ_i^u, α_i^u are the generalized masses:

$$\alpha_i^u = \mu^u \int_0^{L^u} (\psi_i^u)^2\, dx + \tfrac{1}{2}\mu^v L^v \left[\psi_i^u(L^u)\right]^2 \tag{11}$$

and P_i^u are the generalized forces associated with the external force and couple:

$$P_i^u(t) = \tfrac{1}{2}F(t)\ \psi_i^u(L^u) - M_o\ \psi_i^{u\prime}(L^u) \tag{12}$$

Similarly, the lateral deflection of the simple beam of Fig. 4b is given by

$$y_P^v(x^v,t) = \sum_{i=1}^{\infty} \psi_i^v(x^v)\, p_i^v(t) \tag{13}$$

where ψ_i^v are the antisymmetrical modes and the generalized coordinates $p_i^v(t)$ satisfy the equations

$$\ddot{p}_i^v + (\Omega_i^v)^2 p_i^v = \frac{P_i^v}{\alpha_i^v} \tag{14}$$

with

$$\alpha_i^v = \mu^v \int_0^{L^v} (\psi_i^v)^2\, dx \tag{15}$$

$$P_i(t) = 2M_o\ \psi_i^{v\prime}(0) \tag{16}$$

Initial conditions on the elasto-plastic generalized coordinates p_i^u and p_i^v are obtained by requiring continuity of displacements and velocities at the instant t_o when the transition from the elastic to the elasto-plastic stage occurs.

Considering the column first,

$$y_E^u(x^u,t_o) = y_P^u(x^u,t_o) \tag{17a}$$

$$\dot{y}_E^u(x^u,t_o) = \dot{y}_P^u(x^u,t_o) \tag{17b}$$

Using Eqs. (1a) and (9), Eq. (17a) becomes

$$\sum_{i=1}^{\infty} q_i(t_o)\ \phi_i^u(x^u) = \sum_i p_i^u(t_o)\ \psi_i^u(x^u) \tag{18}$$

Eq. (18) holds at $x^u = L^u$:

$$\sum_{i=1}^{\infty} q_i(t_o)\, \phi_i^u(L^u) = \sum_i p_i^u(t_o)\ \psi_i^u(L^u) \tag{19}$$

Multiplying both sides of (18) by $\mu^u \psi_k^u(x^u)$ and integrating along the column yields

$$\mu^u \sum_{i=1}^{\infty} q_i(t_o) \int_0^{L^u} \phi_i^u(x)\ \psi_k^u(x)\, dx = \mu^u \sum_i p_i^u(t_o) \int_0^{L^u} \psi_i^u(x)\ \psi_k^u(x)\, dx \tag{20}$$

Both sides of Eq. (19) are now multiplied by $\frac{1}{2}\mu^v L^v \psi_k^u(L^u)$:

$$\tfrac{1}{2}\mu^v L^v \sum_{i=1}^{\infty} q_i(t_o)\, \phi_i^u(L^u)\ \psi_k^u(L^u) = \tfrac{1}{2}\mu^v L^v \sum_i p_i^u(t_o)\ \psi_i^u(L^u)\, \psi_k^u(L^u) \tag{21}$$

Adding Eqs. (20) and (21) results in

$$\sum_{i=1}^{\infty} q_i(t_o) \left[\mu^u \int_0^{L^u} \phi_i^u(x)\ \psi_k^u(x)\, dx + \tfrac{1}{2}\mu^v L^v\, \phi_i^u(L^u)\ \psi_k^u(L^u) \right] =$$
$$\sum_i p_i^u(t_o) \left[\mu^u \int_0^{L^u} \psi_i^u(x)\ \psi_k^u(x)\, dx + \tfrac{1}{2}\mu^v L^v\ \psi_i^u(L^u)\ \psi_k^u(L^u) \right] \tag{22}$$

Making use of Eq. (11) and the orthogonality condition for the modes ψ_i^u, i.e.,

$$\mu^u \int_0^{L^u} \psi_i^u(x)\ \psi_k^u(x)\, dx + \tfrac{1}{2}\mu^v L^v\ \psi_i^u(L^u)\ \psi_k^u(L^u) = 0 \quad \text{for } i \neq k \tag{23}$$

Eq. (22) reduces to

$$p_k^u(t_o) = \frac{1}{\alpha_k^u} \sum_{i=1}^{\infty} \alpha_{ik}^u\, q_i(t_o) \tag{24}$$

where

$$\alpha_{ik}^u = \mu^u \int_0^{L^u} \phi_i^u(x)\ \psi_k^u(x)\, dx + \tfrac{1}{2}\mu^v L^v\, \phi_i^u(L^u)\ \psi_k^u(L^u) \tag{25}$$

In the same way, Eq. (17b) leads to the condition

$$\dot{p}_k^u(t_o) = \frac{1}{\alpha_k^u} \sum_{i=1}^{\infty} \alpha_{ik}^u\, \dot{q}_i(t_o)$$

Considering the beam, the requirement that

$$y_E^v(x^v, t_o) = y_P^v(x^v, t_o) \tag{27a}$$

$$\dot{y}_E(x^v, t_o) = \dot{y}_P^v(x^v, t_o) \tag{27b}$$

and the orthogonality condition for the modes ϕ_i^v :

$$\int_0^{L^u} \psi_i^v(x)\ \psi_k^v(x)\ dx = 0 \tag{28}$$

leads to the relations

$$p_k^v(t_o) = \frac{1}{\alpha_k^v} \sum_{i=1}^{\infty} \alpha_{ik}^v\ q_i(t_o) \tag{29}$$

$$\dot{p}_k^v(t_o) = \frac{1}{\alpha_k^v} \sum_{i=1}^{\infty} \alpha_{ik}^v\ \dot{q}_i(t_o) \tag{30}$$

in which α_k^v is given by Eq. (15) and

$$\alpha_{ik}^v = \mu^v \int_0^{L^v} \phi_i^v(x)\ \psi_k^v(x)\ dx \tag{31}$$

Let

$$t - t_o = \tau \tag{32}$$

Then the solution of Eqs. (10) and (14) for $i \neq 0$ may be written as

$$p_i^u(\tau) = p_i^u(0) \cos\ \Omega_i^u \tau + \frac{\dot{p}_i^u(0)}{\Omega_i^u} \sin\ \Omega_i^u \tau$$

$$- \frac{M_o\ \psi_i^{u'}(L^u)}{\alpha_i^u\ \Omega_i^u} \int_0^{\tau} \sin\ \Omega_i^u(\tau - T)\ dT$$

$$+ \frac{\psi_i^u(L^u)}{2\ \alpha_i^u \Omega_i^u} \int_0^{\tau} F(T + t_o) \sin\ \Omega_i^u(\tau - T)\ dT$$

$$p_i^v(\tau) = p_i^v(0) \cos\ \Omega_i^v \tau + \frac{\dot{p}_i^v(0)}{\Omega_i^v} \sin\ \Omega_i^v \tau$$

$$+ \frac{2M_o\ \psi_i^{v'}(0)}{\alpha_i^v\ \Omega_i^v} \int_0^{\tau} \sin\ \Omega_i^v(\tau - T)\ dT \tag{34}$$

The initial values (i.e., values at $t = t_o$ or $\tau = 0$) appearing in Eqs. (33) and (34) are computed from Eqs. (24), (26), (29) and (30). Since

$$\int_0^{\tau} \sin\ \Omega\ (\tau - T)\ dT = \frac{1}{\Omega}\ (1 - \cos\ \Omega \tau)$$

Eqs. (33) and (34) simplify to

$$p_1^u(\tau) = p_1^u(0) \cos \Omega_1^u \tau + \frac{\dot{p}_1^u(0)}{\Omega_1^u} \sin \Omega_1^u \tau$$

$$- \frac{M_o \psi_1^{u'}(L^u)}{\alpha_1^u (\Omega_1^u)^2} (1 - \cos \Omega_1^u \tau)$$

$$+ \frac{\psi_1^u(L^u)}{2\alpha_1^u \Omega_1^u} \int_0^\tau F(T + t_o) \sin \Omega_1^u (\tau - T) \, dT \qquad (35)$$

$$p_1^v(\tau) = p_1^v(0) \cos \Omega_1^v \tau + \frac{\dot{p}_1^v(0)}{\Omega_1^v} \sin \Omega_1^v \tau$$

$$+ \frac{2M_o \psi_1^{v'}(0)}{\alpha_1^v (\Omega_1^v)^2} (1 - \cos \Omega_1^v \tau) \qquad (36)$$

In the case of a two hinged frame, a rigid body rotation of the column is possible in the plastic stage. Denoting this mode of motion by ψ_o^u, it may be expressed as

$$\psi_o^u = \frac{x^u}{L^u} \qquad (37)$$

The differential equation governing the generalized coordinate p_o^u associated with this mode is obtained by setting $\Omega_o^u = 0$ in Eq. (10). Eqs. (11) and (12) remain valid. Thus, making use of (37):

$$\ddot{p}_o^u = \frac{F(t)}{2\alpha_o} - \frac{M_o}{\alpha_o L^u} \qquad (38)$$

The solution of (38) is

$$p_o^u(\tau) = p_o^u(0) + \dot{p}_o^u(0)\tau + \int_0^\tau \left\{ \int_0^z \left(\frac{F(T + t_o)}{2\alpha_o} - \frac{M_o}{\alpha_o L^u} \right) dT \right\} dz \qquad (39)$$

Since

$$\int_0^\tau \left\{ \int_0^z \frac{M_o}{L^u} \, dT \right\} dz = \frac{M_o}{2L^u} \tau^2,$$

Eq. (39) may be written as

$$p_o^u(\tau) = p_o^u(0) + \dot{p}_o^u(0)\tau - \frac{M_o}{2L^u \alpha_o} \tau^2 + \frac{1}{2\alpha_o} \int_0^\tau \left\{ \int_0^z F(T + t_o) \, dT \right\} dz \qquad (40)$$

Except for Eq. (35), all other equations derived for the p_1^u are valid for the rigid body mode.

During the first elastic stage, the beam remains perpendicular to the columns at the knees of the frame. After a plastic hinge forms, this constraint no longer exists and energy is dissipated as work is done by the couples with

moment M_o in moving through a plastic angle. The plastic angle θ_p (see Fig. 5) is given by

$$\theta_p = y_p^{u'}(L^u) - y_p^{v'}(0) \tag{41}$$

which becomes, using Eqs. (9) and (13),

$$\theta_p(\tau) = \sum_1 p_1^u(\tau)\ \psi_1^{u'}(L^u) - \sum_{1=1}^{\infty} p_1^v(\tau)\ \psi_1^{v'}(0) \tag{42}$$

Plasticity at any section is characterized by the condition that the rate of plastic work is positive, i.e.,

$$\dot{W}_p = M_o \dot{\theta}_p > 0 \tag{43}$$

Assuming that the capacity moment M_o has not been exceeded at any other section of the frame, the time τ_o at which the first elasto-plastic stage ends and the second elastic stage begins is determined from

$$\dot{\theta}_p(\tau_o) = 0 \tag{44}$$

It is to be noted that the bending moment at the knee of the frame may not be computed from an expression like (7) since each $\psi_i^{u''}(L^u) = 0$. For points near the knee, the convergence will be very slow. In order to find bending moments near the top of the column, therefore, the equilibrium of the column under the action of external and inertia forces is considered. This will be illustrated here only for the case of a two hinged frame. Fig. 6 is a free body diagram of the column, excluding longitudinal forces, whose effect on bending is neglected in this study.

Equilibrium of forces in the y direction requires that

$$H = \frac{1}{2}\left[F - \mu^v L^v \ddot{y}_p^u(L^u)\right] - \mu^u \int_0^{L^u} \ddot{y}_p^u(x)\, dx \tag{45}$$

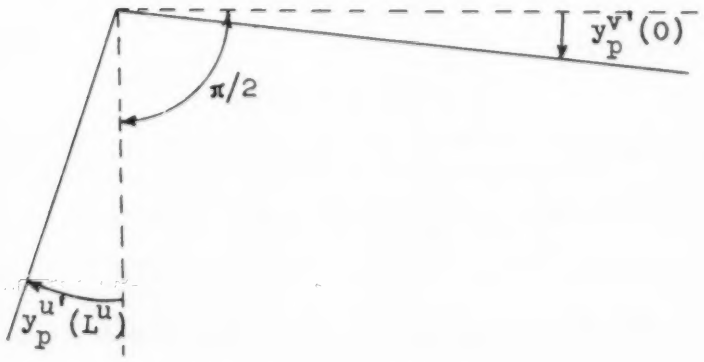

Fig. 5. Plastic Angle

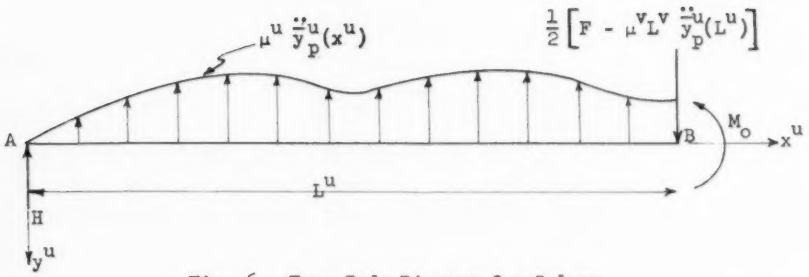

Fig. 6. Free Body Diagram for Column

The bending moment at any section x^u, found by considering forces acting to the left of the section, is

$$M(x^u) = Hx^u + \mu^u \int_0^{x^u} y_p^u(\xi)\left[x^u - \xi\right] d\xi \tag{46}$$

which becomes, using (45),

$$M(x^u) = \tfrac{1}{2}Fx^u - \tfrac{1}{2}\mu^v L^v x^u \ddot{y}_p^u(L^u) - \mu^u x^u \int_0^{L^u} \ddot{y}_p^u(x^u)\, dx + \mu^u \int_0^{x^u} \dot{y}_p^u(\xi)\left[x^u - \xi\right] d\xi \tag{47}$$

Introducing the series expansion for $\ddot{y}_p$ into (47), i.e.,

$$\ddot{y}_p^u(x^u) = \sum_1 \ddot{p}_1^u(\tau)\ \psi_1^u(x^u) \tag{48}$$

and letting

$$\int_0^{x^u} \psi_1^u(x)\, dx = K_1^P(x^u) \tag{49}$$

$$\int_0^{x^u} x\, \psi_1^u(x)\, dx = r_1^P(x^u) \tag{50}$$

Eq. (47) becomes

$$M(x^u) = \tfrac{1}{2}Fx^u - \sum_1 \ddot{p}_1^u \left\{ \mu^u x^u \left[K_1^P(L^u) - K_1^P(x^u) \right] + \mu^u r_1^P(x^u) + \tfrac{1}{2}\mu^v L^v x^u\ \psi_1^u(L^u) \right\} \tag{51}$$

At the knee ($x^u = L^u$) it is easy to show that (51) reduces to $M_P(L^u) = -M_o$.

Second Elastic Stage

In the second elastic stage, the displacements are again given by Eqs. (1) with new generalized coordinates $\bar{q}_i$ satisfying Eq. (2) and initial conditions determined from

$$\bar{y}^u_E(x^u,0) = y^u_P(x^u,\tau_o) \quad ; \quad \dot{\bar{y}}^u_E(x^u,0) = \dot{y}^u_P(x^u,\tau_o) \tag{52}$$

$$\bar{y}^v_E(x^v,0) = y^v_P(x^v,\tau_o) \quad ; \quad \dot{\bar{y}}^v_E(x^v,0) = \dot{y}^v_P(x^v,\tau_o) \tag{53}$$

in which a new time variable has been introduced in the second elastic stage:

$$t^* = t - (t_o + \tau_o) \tag{54}$$

Consider the first of Eqs. (52) and (53) and the particular case of Eq. (52) for $x^u = L^u$. Substituting the appropriate series expansions, these become

$$\sum_{i=1}^{\infty} \bar{q}_i(0)\, \phi^u_i(x^u) = \sum_i p^u_i(\tau_o)\ \psi^u_i(x^u) \tag{55}$$

$$\sum_{i=1}^{\infty} \bar{q}_i(0)\, \phi^u_i(L^u) = \sum_i p^u_i(\tau_o)\ \psi^u_i(L^u) \tag{55a}$$

$$\sum_{i=1}^{\infty} \bar{q}_i(0)\, \phi^v_i(x^v) = \sum_i p^v_i(\tau_o)\ \psi^v_i(x^v) \tag{56}$$

The following operations are now performed: (1) both sides of Eq. (55) are multiplied by $\mu^u\phi^u(x^u_k)$ and integrated along the column, (2) both sides of Eq. (55a) are multiplied by $\frac{1}{2}\mu^v L^v \phi^u_k(L^u)$, (3) both sides of Eq. (56) are multiplied by $\mu^v\phi^v_k(x^v)$ and integrated along the beam.

If the three equations resulting from these operations are added up using the orthogonality condition for the elastic modes, i.e.,

$$2\mu^u \int_0^{L^u} \phi^u_i(x)\, \phi^u_k(x)\, dx + \mu^v L^v\, \phi^u_i(L^u)\, \phi^u_k(L^u) = 0 \quad \text{for } i \neq k \tag{57}$$

the result is

$$\bar{q}_i(0) = \frac{2}{C_i}\left\{\sum_k \alpha^u_{ik}\, p^u_k(\tau_o) + \sum_{k=1}^{\infty} \alpha^v_{ik}\, p^v_k(\tau_o)\right\} \tag{58}$$

where C_i, α^u_{ik} and α^v_{ik} are given by Eqs. (3), (25) and (31) respectively. Similarly, using Eq. (53), initial conditions on the $\dot{\bar{q}}_i$ are obtained as

$$\dot{\bar{q}}_i(0) = \frac{2}{C_i}\left\{\sum_k \alpha^u_{ik}\, \dot{p}^u_k(\tau_o) + \sum_{k=1}^{\infty} \alpha^v_{ik}\, \dot{p}^v_k(\tau_o)\right\} \tag{59}$$

Using the initial conditions obtained from Eqs. (58) and (59), the solution of Eq. (2) is

$$\bar{q}_i(t^*) = \bar{q}_i(0)\cos\omega_i t^* + \frac{\dot{\bar{q}}_i(0)}{\omega_i}\sin\omega_i t^* + \frac{\phi^u_i(L^u)}{C_i\omega_i}\int_0^{t^*} F(T - t_o - \tau_o)\sin\omega_i\,(t^* - T)\, dT \tag{60}$$

Eq. (7) can no longer be used to find the bending moment at the knee because the series obtained by differentiating the series expression for $\bar{y}_E$ twice with respect to x does not converge to $\bar{y}''_E$ at the knee. This can be seen by realizing that the series obtained by differentiating each term once does not converge to $\bar{y}'_E$ since this series of derivatives can never lead to a plastic angle at the knee. At points near the knee, the series of second derivatives will converge slowly to the curvature.

Using inertia forces, a series expression similar to Eq. (51) is obtained. For the numerical examples considered in section III, however, this series did not seem to converge either.

It therefore appears that it is not possible to compute the moments near the knee after the first plastic stage and thus impossible to know whether a plastic hinge reappears there.

Two Hinged Frame and Linearly Decaying Load

In this section, the results of section II will be particularized for the case of a frame supported by smooth hinges and a linearly decaying load, i.e.,

$$\left.\begin{aligned} F(t) &= F_o\left(1 - \frac{t}{t_e}\right), \quad t \leq t_e \\ &= 0 \qquad\qquad , \quad t > t_e \end{aligned}\right\} \tag{61}$$

First Elastic Stage

In a recent study, DeHart[3] obtained the modes and frequencies for a two hinged frame and determined the response to the loading given by Eq. (61) up to the end of the first elastic stage. His results will be summarized in this subsection. The elastic frequencies ω_i associated with the antisymmetrical modes were obtained from the equation

$$\frac{I^v}{I^u}\left(\frac{I^u}{I^v}\frac{\mu^v}{\mu^u}\right)^{\frac{1}{4}}\left[\frac{\frac{\mu^v}{\mu^u}\frac{L^v}{L^u}\frac{k^u L^u}{2}\eta_1^u - \eta_2^u}{\frac{\mu^v}{\mu^u}\frac{L^v}{L^u}\frac{k^u L^u}{2}\eta_3^u + \eta_1^u}\right] = -\frac{\eta_1^v}{\eta_3^v} \tag{62}$$

where

$$\omega_1^2 = \frac{(k_1^u)^4 EI^u}{\mu^u} = \frac{(k_1^v)^4 EI^v}{\mu^v} \tag{63}$$

and

$$\eta_1^v = \sin\frac{k_1^v L^v}{2}\cosh\frac{k_1^v L^v}{2} - \cos\frac{k_1^v L^v}{2}\sinh\frac{k_1^v L^v}{2} \tag{64}$$

$$\eta_3^v = 2 \sin \frac{k_1^v L^v}{2} \sinh \frac{k_1^v L^v}{2} \tag{65}$$

$$\eta_1^u = \sin k_1^u L^u \cosh k_1^u L^u - \cos k_1^u L^u \sinh k_1^u L^u \tag{66}$$

$$\eta_2^u = 2 \cos k_1^u L^u \cosh k_1^u L^u \tag{67}$$

$$\eta_3^u = 2 \sin k_1^u L^u \sinh k_1^u L^u \tag{68}$$

The antisymmetrical modes are given by

$$\phi_1^u = \sin k_1^u x^u + D_1 \sinh k_1^u x^u \tag{69}$$

$$\phi_1^v = \lambda_1 \left[- \tan \frac{k_1^v L^v}{2} (\cos k_1^v x^v - \cosh k_1^v x^v) + \sin k_1^v x^v - \frac{\tan \frac{k_1^v L^v}{2}}{\tanh \frac{k_1^v L^v}{2}} \sinh k_1^v x^v \right] \tag{70}$$

in which

$$D_1 = \frac{- \cos k_1^u L^u + \frac{k_1^v L^v}{2} \left(\frac{I^v}{I^u} \frac{\mu^u}{\mu^v} \right)^{\frac{1}{4}} \frac{\mu^v}{\mu^u} \sin k_1^u L^u}{- \frac{k_1^v L^v}{2} \left(\frac{I^v}{I^u} \frac{\mu^u}{\mu^v} \right)^{\frac{1}{4}} \sinh k_1^u L^u - \cosh k_1^u L^u} \tag{71}$$

$$\lambda_1 = 2 \left(\frac{I^v}{I^u} \frac{\mu^v}{\mu^u} \right)^{\frac{1}{2}} \left[\frac{\tan \frac{k_1^v L^v}{2}}{- \sin k_1^u L^u + D_1 \sinh k_1^u L^u} \right] \tag{72}$$

Using the modes given by Eqs. (70) and (71), the generalized mass C_i of Eq. (3) is obtained as

$$C_i = \mu^v L^v \left[\sin k_i^u L^u + D_i \sinh k_i^u L^u \right]^2$$

$$+ \frac{1}{2} \mu^u L^u \left\{ 1 - \frac{1}{k_i^u L^u} \cos k_i^u L^u \sin k_i^u L^u \right.$$

$$+ \frac{2D_i}{k_i^u L^u} \left(\cosh k_i^u L^u \sin k_i^u L^u - \sinh k_i^u L^u \cos k_i^u L^u \right)$$

$$\left. + \frac{D_i^2}{k_i^u L^u} \left(\sinh k_i^u L^u \cosh k_i^u L^u - k_i^u L^u \right) \right\}$$

$$+ \frac{1}{\alpha_i} \mu^v L^v \left\{ \frac{1}{2} + \frac{1}{k_i^v L^v} \sin \frac{k_i^v L^v}{2} \cos \frac{k_i^v L^v}{2} \right.$$

$$\left. + \tan^2 \frac{k_i^v L^v}{2} \left[\frac{1}{2} \left(1 - \frac{1}{\sinh^2 \frac{k_i^v L^v}{2}} \right) + \frac{1}{k_i^v L^v} \sin \frac{k_i^v L^v}{2} \cos \frac{k_i^v L^v}{2} \right.\right.$$

$$\left.\left. \frac{1}{k_i^v L^v} \coth \frac{k_i^v L^v}{2} \right] \right\} \tag{73}$$

and, for the forcing function given by Eq. (61), the elastic generalized coordinates of Eq. (6) become, for $t < t_e$,

$$q_i(t) = \frac{F_o \phi_i^u(L^u)}{C_i \omega_i t_e} \left[t_e \left(1 - \cos \omega_i t \right) - t + \frac{1}{\omega_i} \sin \omega_i t \right] \tag{74}$$

First Plastic Stage

The normal modes of the column with concentrated mass (Fig. 4a) satisfy the differential equation

$$EI^u \psi_i^{u\,iv} = \mu^u (\Omega_i^u)^2 \psi_i^u \tag{75}$$

and the boundary conditions

$$\psi_i^u(0) = \psi_i^{u\,''}(0) = \psi_i^{u\,''}(L^u) = 0$$

$$EI^u \psi_i^{u\,'''}(L^u) + \frac{1}{2} \mu^v L^v (\Omega_i^u)^2 \psi_i^u(L^u) = 0 \tag{76}$$

In the usual manner, it is found that solutions to Eq. (75), satisfying the conditions (76), exist only for discrete values of the frequency determined from

$$\frac{1}{\beta_1^u L^u}\left(\cot \beta_1^u L^u - \coth \beta_1^u L^u\right) = \frac{\mu^v L^v}{\mu^u L^u} \tag{77}$$

where

$$\beta_1^4 = \frac{\mu^u (\Omega_1^u)^2}{EI^u} \tag{78}$$

Corresponding to the frequencies Ω_i^u found from Eq. (77) (which has a solution $\Omega_o = 0$) the normal modes are

$$\psi_o^u = \frac{x^u}{L^u} \tag{79}$$

$$\psi_i^u = \sin \beta_1^u x^u + \frac{\sin \beta_1^u L^u}{\sinh \beta_1^u L^u} \sinh \beta_1^u x^u \ , \quad i > 0 \tag{80}$$

For the simple beam of Fig. 4b, the well known antisymmetrical modes and frequencies are

$$\psi_i^v = \sin i \frac{\pi x^v}{L^v} \tag{81}$$

$$i = 2, 4, 6 \ldots$$

$$\Omega_i^v = i^2 \frac{\pi^2}{(L^v)^2} \sqrt{\frac{EI^v}{\mu^v}} \tag{82}$$

Using the expressions (69) and (70) for the elastic modes and (77) and (82) for the elasto-plastic modes, the generalized masses of Eq. (11) and (15) and the coupling constants of Eqs. (25) and (31) are obtained by integration as

$$\alpha_o^u = \frac{\mu^u L^u}{3} + \frac{\mu^v L^v}{2} \tag{83}$$

$$\alpha_i^u = \frac{1}{2}\mu^u L^u \left(1 - \frac{\sin^2 \beta_1^u L^u}{\sinh^2 \beta_1^u L^u} + 3 \sin^2 \beta_1^u L^u \coth \beta_1^u L^u \right.$$

$$\left. - \frac{3}{\beta_1^u L^u} \sin^2 \beta_1^u L^u \cot \beta_1^u L^u \right) + 2\mu^v L^v \sin^2 \beta_1^u L^u \ ; \ i > 0 \tag{84}$$

$$\alpha_1^v = \frac{\mu^v L^v}{2} \tag{85}$$

$$\alpha_{io} = \frac{1}{2}\mu^v L^v (\sin a + D_i \sinh a) + \frac{\mu^u L^u}{a^2}\left[\sin a - a \cos a + D_i \right. \tag{86}$$

$$\left. (a \cosh a - \sinh a)\right]$$

$$\alpha_{ij}^{u} = \mu^{v}L^{v} \sin b \,(\sin a + D_i \sinh b)$$

$$+ \frac{\mu^{u}L^{u}}{a^4 - b^4}\Big\{2a^3 \sin b \,(D_i \cosh a - \cos a)$$

$$+ a^2 b \,(\cos b + \sin b \coth b)(\sin a + D_i \sinh a)$$

$$+ b^3 \,(\cos b - \sin b \coth b)(\sin a - D_i \sinh a)\Big\}\,;\ j > 0 \qquad (87)$$

where

$$a = k_i^{u}L^{u}\,,\quad b = \beta_j^{u}L^{u} \qquad (88)$$

$$\alpha_{ij}^{v} = \frac{\pi\mu^{v}L^{v}}{r_i}\, j \tan\tfrac{1}{2}k_i^{v}L^{v}\, \frac{\left(\frac{k_i^{v}L^{v}}{2}\right)^2}{\left(\frac{k_i^{v}L^{v}}{2}\right)^4 - \left(\frac{j\pi}{2}\right)^2}\ ;\ j = 2,\ 4,\ 6\ldots \qquad (89)$$

For the forcing function of Eq. (61), the integrals in Eqs. (35) and (40) become, for $t < t_e$,

$$\int_0^{\tau} F(T + t_o) \sin\,\Omega_i^{u}(\tau - T)\,dT = \frac{F_o}{\Omega_i^{u}t_e}\Big[(t_e - t_o)(1 - \cos\,\Omega_i^{u}\tau) + \frac{1}{\Omega_i^{u}}\sin\,\Omega_i^{u}\tau - \tau\Big] \qquad (90)$$

$$\frac{1}{2\alpha_o}\int_0^{\tau}\left\{\int_0^{u} F(T + t_o)\,dT\right\}du = \frac{F_o}{\alpha_o}\left[\frac{1}{4}\left(1 - \frac{t_o}{t_e}\right)\tau^2 - \frac{1}{3t_e}\tau^3\right] \qquad (91)$$

If bending moments near the top of the column are desired, the integrals of Eqs. (49) and (50) must be evaluated. From Eqs. (79) and (80) these are obtained as

$$K_o^{P}(x^{u}) = \frac{(x^{u})^2}{2L^{u}} \qquad (92)$$

$$K_i^{P}(x^{u}) = \frac{1}{\beta_i^{u}}\left[1 - \cos\,\beta_i^{u}x^{u} + \frac{\sin\,\beta_i L^{u}}{\sinh\,\beta_i^{u}L^{u}}(\cosh\,\beta_i^{u}x^{u} - 1)\right];\quad i > 0 \qquad (93)$$

$$r_o^{P}(x^{u}) = \frac{(x^{u})^3}{3L^{u}} \qquad (94)$$

$$r_i^P(x^u) = \frac{1}{(\beta_i^u)^2}\left[\sin \beta_i^u x^u - \beta_i^u x^u \cos \beta_i^u x^u + \frac{\sin \beta_i^u L^u}{\sinh \beta_i^u L^u}\left(\beta_i^u x^u \cosh \beta_i^u x^u - \sinh \beta_i^u x^u\right)\right] ; \; i > 0 \tag{95}$$

Second Elastic Stage

The integral in Eq. (53) becomes, for the force function of Eq. (61)

$$\int_0^t F(T - t_o - \tau_o) \sin \omega_i (t^* - T)\, dT =$$

$$\frac{F_o}{\omega_i t_e}\left[t_e^* (1 - \cos \omega_i t^*) + \frac{1}{\omega_i} \sin \omega_i t^* - t^*\right] ; \; t < t_e \tag{96}$$

$$\frac{F_o}{\omega_i t_e}\left[t_e^* (1 - \cos \omega_i t_e^*) + \frac{1}{\omega_i} \sin \omega_i t_e^* - t_e^*\right] ; \; t > t_e \tag{97}$$

where

$$t_e^* = t_e - (t_o + \tau_o) \tag{98}$$

Numerical Examples

Using a forcing function given by Eq. (61) with time constant

$$t_e = .5 \text{ sec}$$

and two values of the maximum force

(1) $F_o = 345600$ lbs. (2) $F_o = 57600$ lbs.

response calculations were made for a two hinged steel frame with the following properties:

$$L^u = 144 \text{ in.} \qquad L^v = 360 \text{ in.}$$

$$I^u = 394 \text{ in.}^4 \qquad I^v = 1043 \text{ in.}^4$$

$$\mu^u = \mu^v = \tfrac{1}{3} \text{ lbs sec/in.}^2$$

$$M_o = 2.3 \times 10^6 \text{ in.lbs.}$$

This is the same structure used by DeHart,[3] who calculated the response in the first elastic stage to the higher of the two loads considered here.

Throughout the calculation, infinite series were approximated by the sum of the first five terms. All numerical work was done with an ordinary desk computer.

Elastic Modes and Frequencies

The first five frequencies were obtained from Eqs. (62) and (63) and substituted into Eqs. (69)-(73). Useful results are summarized in Table 1.

Elasto-Plastic Modes and Frequencies

The column and beams frequencies were obtained from Eqs. (77), (78) and (81) and substituted into Eqs. (79), (80), (83)-(89). These results are shown in Tables 2, 3 and 4.

Response to Load with F_o = 345600 lbs.

First Elastic Stage.—The deflection and bending moment at the knee, obtained by substituting the expressions (69) and (74) into Eqs. (1a) and (7), were calculated as functions of time using the constants of Table 1. The time at which the bending moment reached the capacity value M_o was found to be t_e = .044 seconds. In Figs. 7 and 8 these results are plotted.

While it was found that all modes other than the first contributed almost nothing to the deflection throughout this entire time range, the third mode was at least as important as the first mode in determining bending moment for early times. This is illustrated in Fig. 8.

It should be noticed that the deflection at the top of the column when the capacity moment is reached is almost exactly the same as that which would occur if the load were applied statically. This is, however, not generally true. For a different frame or forcing function, the static and dynamic deflections at incipient plasticity might be quite different.

Table 5 shows the values of the generalized coordinates and their derivatives at the end of the first elastic stage.

First Elasto-Plastic Stage.—Eqs. (24), (26), (29) and (30), when used in conjunction with Tables 2, 3, 4, and 5, furnish the initial values of the plastic generalized coordinates and their derivatives. These are recorded in Table 6.

It should be pointed out that the series expressions for $\dot{p}_i^u(t_o)$ and $\dot{p}_i^y(t_o)$ do not converge well enough to justify the number of significant figures presented in Table 6. For the higher values of i the first figure is in doubt. The numbers presented in these cases are merely the result of adding the five terms of the series, each of which is accurate to the number of decimal places in the sum. The spurious nature of these numbers does not, however, effect any further results appreciably.

It is interesting to see how well Eqs. (17a) and (17b) are satisfied at the top of the column using the values of the generalized coordinates of Tables 5 and 6. In conjunction with Tables 1 and 2, it is found that

$$y_E^u(L^u,t_o) = 1.970 + .014 + .000 + .000 + .000 = 1.984"$$

$$y_p^u(L^u,t_o) = 2.028 - .039 - .003 - .001 + .000 = 1.985"$$

$$\dot{y}_E(L^u,t_o) = 86.69 - .82 + .56 + .20 - .05 = 86.58"/sec$$

$$\dot{y}_p(L^u,t_o) = 89.41 - 2.61 - .09 + .11 - .02 = 86.80"/sec$$

Also of interest is a comparison of slopes at the knee:

$$y_E^{u'}(L^u,t_o) = y_E^{v'}(0,t_o) = .004266 + .001705 - .000002 - .000003 - .000002$$
$$= .005964 \text{ rad}$$

Table 1. Elastic Frequencies and Related Computed Quantities

i	$k_i^u L^u$	$\frac{1}{2} k_i^v L^v$	ω_i	D_i	λ_i	$\phi_i^u(L^u)$	$-EI\phi_i^{u''}(L^u)$	C_i
1	1.0481	1.0271	9.9759	-.1963	-4.8413	.6210	6963×10^2	62.56
2.	3.21861	3.15414	94.077	-.010963	-.6823	-.21373	3534×10^2	178.28
3.	4.0650	3.9836	150.06	.019478	2.6704	-.23038	-1286×10^4	68.54
4.	7.1831	7.0392	468.57	-9.7568×10^{-4}	-2.1520	.14079	4193×10^4	73.08
5.	10.330	10.123	969.05	4.476×10^{-5}	1.855	-.10091	-8955×10^4	78.02

Table 2. Elasto-Plastic Frequencies and Related Computed Quantities

i	$\beta_i^u L^u$	Ω_i^u	$\psi_i^u(L^u)$	$\psi_i^{u'}(L^u)$	α_i^u	i	Ω_i^v	$\psi_i^{v'}(0)$
0	0	0	1	.0069444	76	2	93.329	.017453
1	3.2507	95.961	-.21778	-.024906	24.710	4	373.32	.034907
2	6.3424	365.30	+.11836	.046572	24.210	6	839.96	.052360
3	9.4653	813.61	-.081022	-.068340	24.099	8	1493.3	.069813
4	12.597	1441.1	+.061450	.090127	24.056	10	2333.2	.087266

Table 3. Values for α_{ij}^{u}

i \ j	0	1	2	3	4
1	48.59	1.91	-.248	.072	-.034
2	.277	24.6	-.1309	.0369	-.01446
3	-3.964	24.06	5.400	-1.374	.5651
4	1.326	-4.965	22.68	6.478	-2.036
5	-.6614	2.398	-5.177	22.08	7.095

Table 4. Values for α_{ij}^{v}

i \ j	2	4	6	8	10
1	2.8225	.34904	.10336	.043600	.022323
2	-88.122	.1891	.05312	.02222	.011348
3	32.501	-7.6812	-1.9711	-.81324	-.41388
4	-6.9426	-36.51	9.0360	2.9125	1.4009
5	3.3601	7.818	40.16	-9.6864	-3.4695

Table 5. Generalized Coordinates and Derivatives at the End of the First Elastic Stage

i	1	2	3	4	5
q_i (.044)	3.172	-.06724	.001715	.003371	-.0003172
$\bar{q}_i$ (.044)	139.6	3.845	-2.426	1.386	.4480

Table 6. Initial Values of the Plastic Generalized Coordinates and Their Derivatives

i	$p_i^u(t_o)$	$\dot{p}_i^u(t_o)$	i	$p_i^v(t_o)$	$\dot{p}_i^v(t_o)$
0	2.028	89.41	2	.2485	-.529
1	.179	12.0	4	.01593	.3498
2	-.0284	-.79	6	.005645	.8322
3	.0099	-1.344	8	.002472	.1306
4	.0049	-.25	10	.001252	.07585

Table 7. Elasto-Plastic Generalized Coordinates at the End of the First Plastic Stage

i	$p_i^u(\tau_o)$	$\dot{p}_i^u(\tau_o)$	i	$p_i^v(\tau_o)$	$\dot{p}_i^v(\tau_o)$
0	35.16	12.0	2	.0730	3.92
1	.042	.5	4	.02062	1.30
2	-.0309	-.84	6	.006161	.772
3	.0094	-1.5	8	.002493	.113
4	-.0051	1.	10	.001273	.048

Table 8. Generalized Coordinates and Their First Derivatives at the Beginning of the Second Elastic Stage

i	1	2	3	4	5
$\bar{q}_i(0)$	54.60	.048	-3.980	1.22	-.5691
$\dot{\bar{q}}_i(0)$	19.1	-3.7	2	-2.3	.62

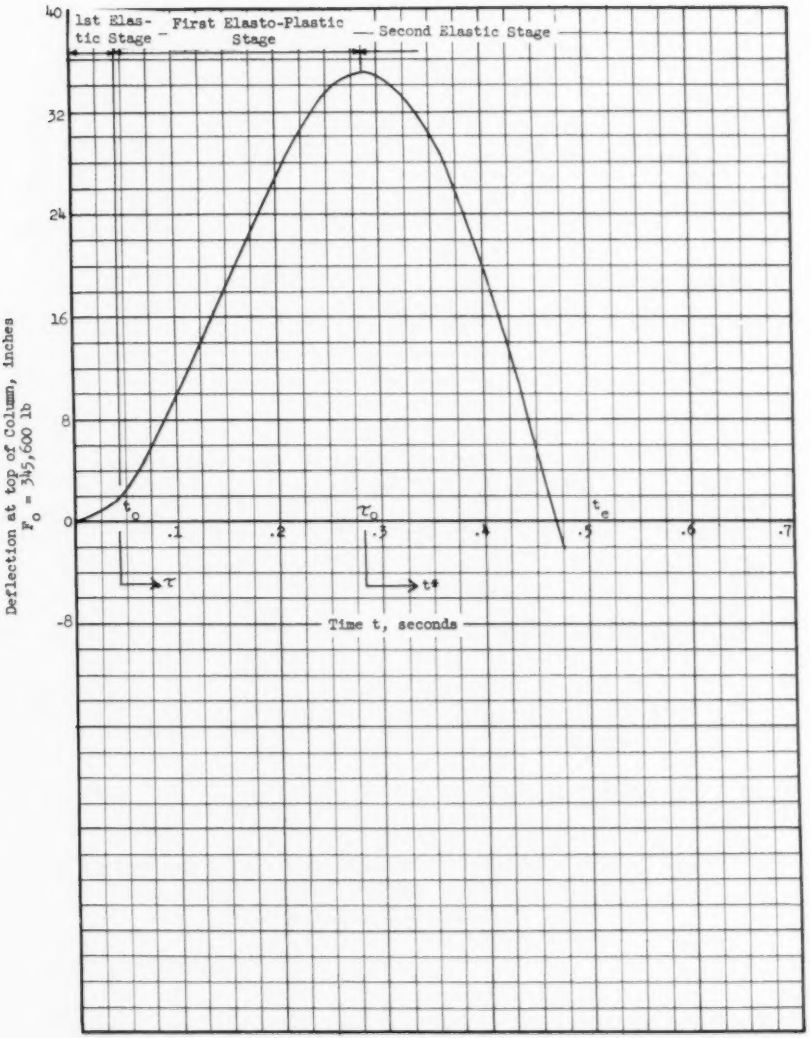

Figure 7. Relation Between Deflection and Time at Top of Column (F_o = 345,600 lbs.)

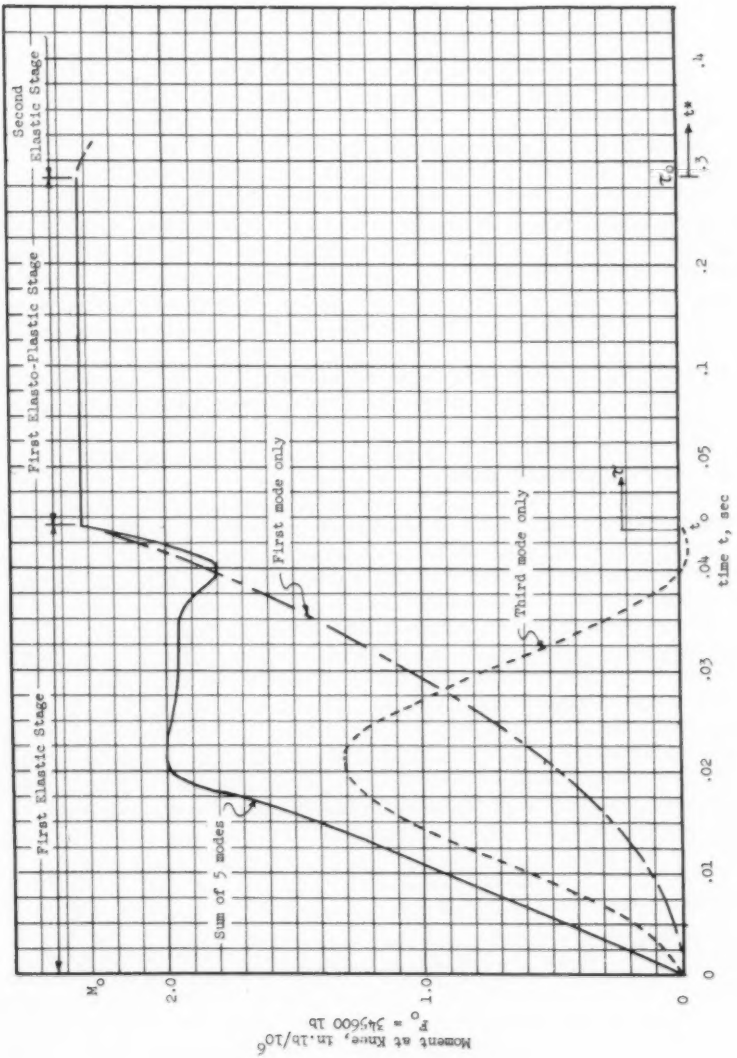

Figure 8. Relation Between Moment and Time at Top of Column (F_o = 345,600 lbs.)

$$y_p^{u'}(L^u, t_o) = .01408 - .00446 - .00132 - .00068 - .00044 = .00718 \text{ rad}$$

$$y_p^{v'}(0, t_o) = .004337 + .000556 + .000296 + .000173 + .000109$$
$$= .005471 \text{ rad}$$

It is seen that convergence in the elasto-plastic case is slow. As the plastic stage proceeds, however, this convergence improves as the rigid body mode becomes more and more important.

If Eqs. (90) and (91) are substituted into Eqs. (33) and (34), the plastic angle may be determined as a function of time from Eq. (42) by substituting the appropriate quantities from Tables 2, 3, 4 and 6. The result is plotted in Fig. 9. Except for the small values of τ, the contribution of the rigid body mode is by far the most important. The time τ_o when the first plastic stage ends is determined analytically from Eq. (44). From Fig. 9, it may be obtained graphically as $\tau_o = .240$ seconds. The maximum plastic angle is seen to be .238 radians.

From Eq. (9), the deflection at the top of the column is computed. This is plotted in Fig. 7. Again, the major portion of the response is from the rigid body mode.

At time τ_o, the end of the first plastic stage, the elasto-plastic generalized coordinates are given in Table 7.

A check was made of the bending moment at the center of the column during this stage using both Eq. (51) and one analogous to Eq. (7). The results, considering the convergence problem, were in fair agreement and established clearly that the bending moment at this section was well below the plastic capacity value throughout the stage. Thus, no plastic hinge other than the one at the knee is generated, in accordance with the assumptions made.

Second Elastic Stage.—Eqs. (51) and (52) together with quantities in Tables 1, 3, 4 and 7 are used to determine initial values of the new elastic generalized coordinates and their first derivatives. These are listed in Table 8.

Substituting Eqs. (96) and (97), as appropriate, into Eq. (53), with the necessary values from Tables 1 and 8, Eq. (1) may be used to find the deflection at the top of the column as a function of time. This is plotted in Fig. 7. Note that the assumption has been made that plastic hinges do not reappear. Again, the first mode was by far the most important in the series for the deflection at the top of the column.

Response to Load with $F_o = 57600$ lbs.

Figs. 10 and 11 and 12 show the results of this calculation.

The plot of Eq. (42) for $\tau > 0$ (not considering condition of Eq. (44)) shows the influence of the higher modes. Since the curve has two stationary points before it begins to decrease monotonically, two elastic and elasto-plastic stages might have to be examined to get the maximum plastic angle. It should be noted, however, that the first dip in the curve is of the same magnitude as the truncation error apparent at $\tau = 0$, so that the first stationary point may be unreal. Since, in any case, it appears impossible to determine when elastic stages other than the first come to an end, it seems appropriate to approximate the response in the first plastic stage by the rigid body mode only, giving the dotted curve shown on Fig. 12. Thus the stage ends, approximately, at $\tau_o = .160$ sec. and the maximum plastic angle is .0252 radians.

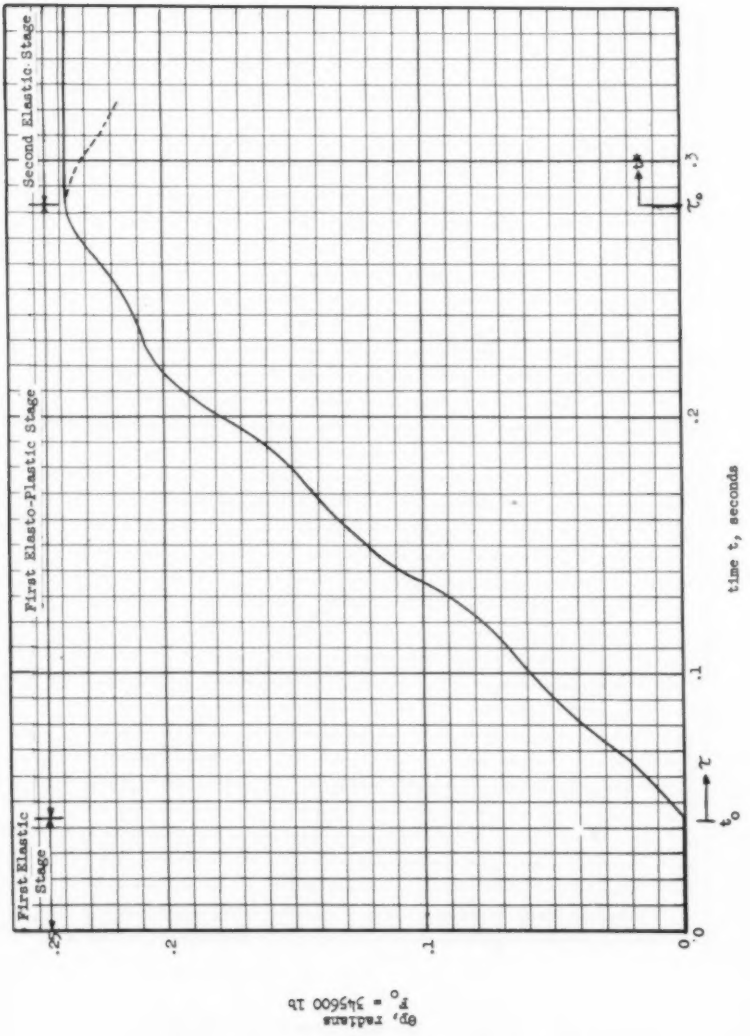

Figure 9. Relation Between Plastic Angle and Time at Top of Column (F_o = 345,600 lbs.)

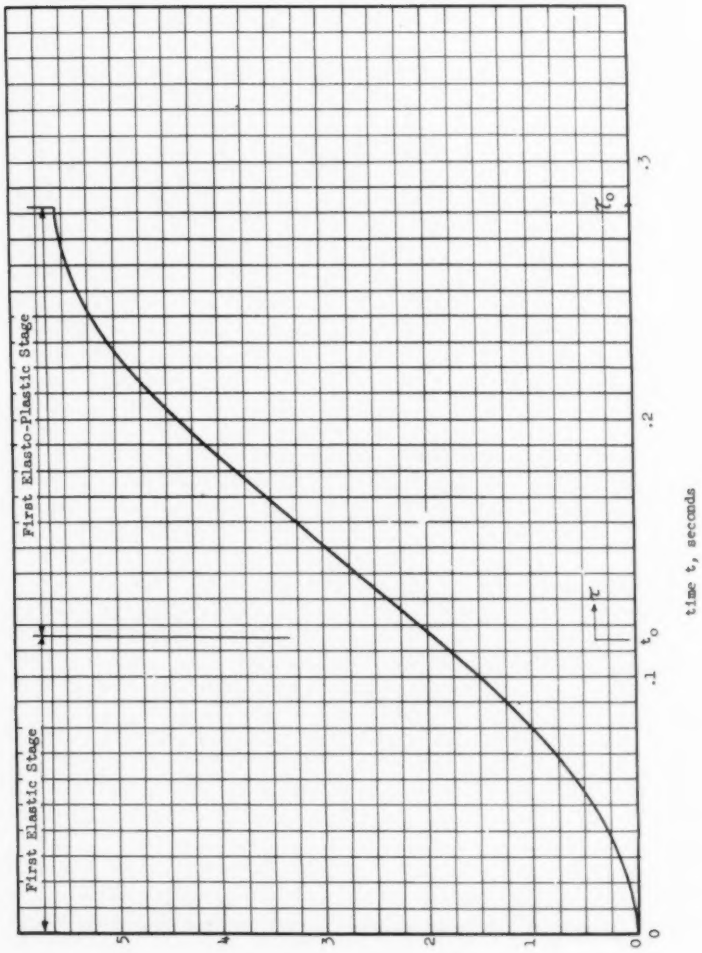

Figure 10. Relation Between Moment and Time at Top of Column (F_o = 57,600 lbs.)

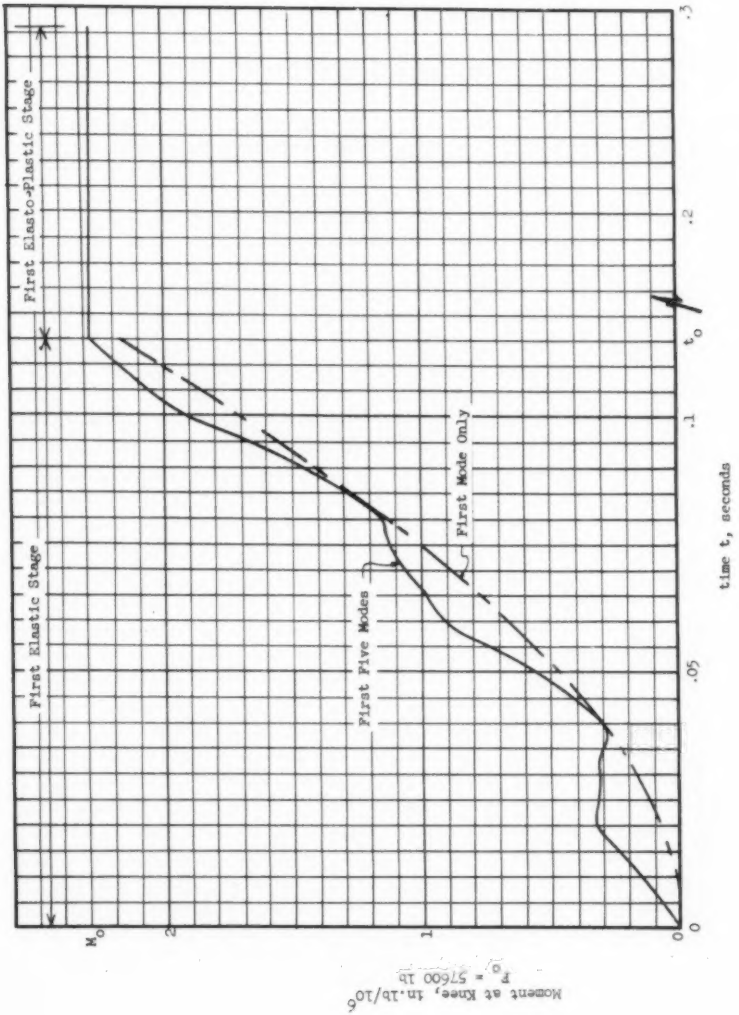

Figure 11. Relation Between Moment and Time at Top of Column (F_o = 57,600 lbs.)

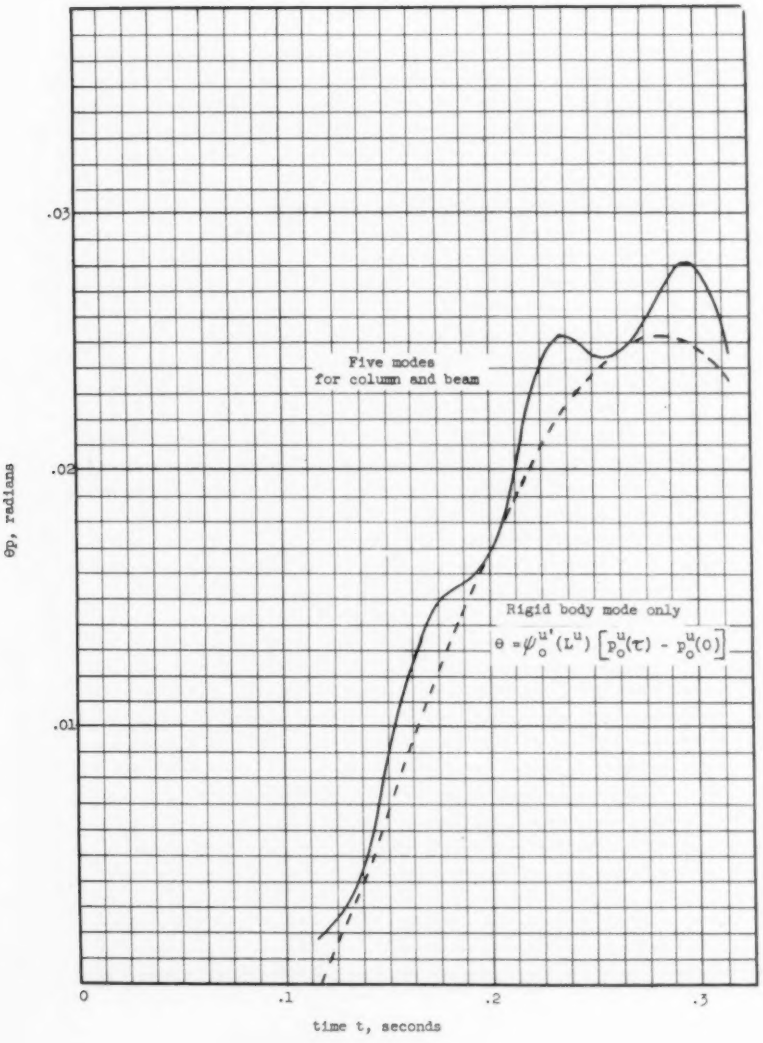

Figure 12. Relation Between Plastic Angle and Time at Top of Column (F_o = 57,600 lbs.)

CONCLUSION

It appears that, for engineering purposes, a good approximation of the maximum plastic angle which develops at the knee of a two hinged frame under a concentrated dynamic load applied at the knee may be obtained by considering the first elastic mode and the first (rigid body) elasto-plastic mode only.

ACKNOWLEDGEMENT

The author wishes to thank Dr. R. C. DeHart for his helpful advice in the solution of this problem and Mr. R. H. Anderson for carefully performing the numerical calculations.

REFERENCES

1. Timoshenko, S., "Vibration Problems in Engineering," D. Van Nostrand Co., New York, Second Edition, Chapter VI.
2. Bleich, H. H. and Salvadori, M. G., "Impulsive Motion of Elastoplastic Beams," Trans. ASCE 120:499.
3. DeHart, R. C., "Response of a Rigid Frame to a Distributed Transient Load," ASCE Proceedings Paper 1056.

Paper 1706 July, 1958 EM 3

Journal of the
ENGINEERING MECHANICS DIVISION
Proceedings of the American Society of Civil Engineers

LIMIT ANALYSIS OF SIMPLY SUPPORTED CIRCULAR SHELL ROOFS[a]

M. N. Fialkow,[1] M. ASCE
(Proc. Paper 1706)

SYNOPSIS

Plastic collapse of a partial circle cylindrical shell simply supported at each end with the longitudinal edges free is investigated for the case of uniform radial loading. The principles of Limit Analysis applicable to a plastic-rigid structure are utilized to develop upper and lower bounds for the collapse pressure parameter, $\bar{P}$. Bounds are obtained for a wide range in shell shape parameters with the deviation between the mean of the bounds and either bound varying between 2 and 25 per cent.

NOTATION

The letter symbols are defined where they first appear and at the end of the paper.

INTRODUCTION

In structural engineering, recent years have seen a more frequent adoption of cylindrical shells spanning between transverse supports in order to accomplish the roofing of large unobstructed areas. Such a typical shell roof is shown in Fig. 1. Current practice provides for the design of such shells on the basis of the elastic theory as developed by Flügge, Donnell, and Timoshenko.[1,2,3] The practical design of shell roofs by this elastic theory has in turn been greatly simplified by the tabulation in ASCE Manual No. 31[4] of values of the controlling stress resultants and deflections for various loading conditions and shape parameters. By this method, the design of cylindrical

Note: Discussion open until December 1, 1958. To extend the closing date one month, a written request must be filed with the Executive Secretary, ASCE. Paper 1706 is part of the copyrighted Journal of the Engineering Mechanics Division, Proceedings of the American Society of Civil Engineers, Vol. 84, No. EM 3, July, 1958.

1. Chief of Design Branch, U. S. Army Engr. District, New York, N. Y.

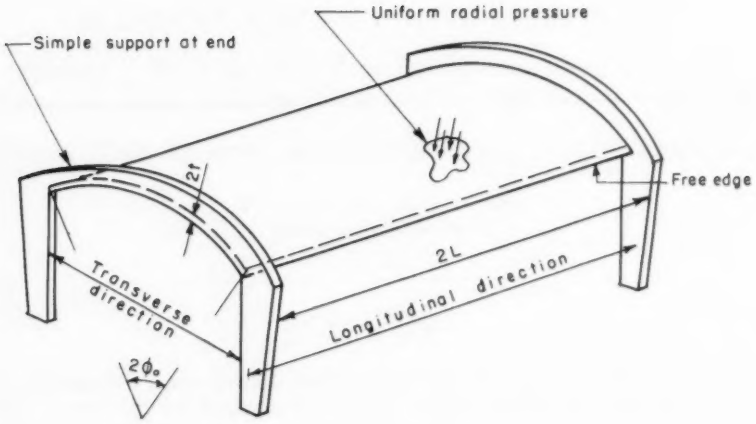

SHELL LAYOUT

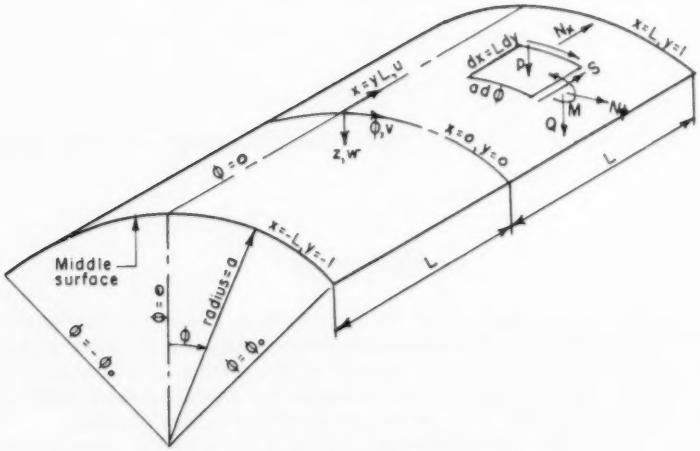

SHELL COORDINATE SYSTEM

FIGURE 1

shell roofs using working stresses less than the yield point can be readily accomplished.

However, for information as to the ultimate load carrying capacity of such structures, the theory of plastic collapse must be employed. Limit and plastic analyses of full circle cylindrical shells under axially symmetric loading have been accomplished by Drucker, Hodge, and Onat.[5,6,7] For shells of revolution under axially symmetric loading, Onat and Prager have used limit analysis to determine the collapse loading.[8] However, collapse loads for partial circle cylindrical shells with resultant non-axially symmetric loading are not available, and this paper concerns itself with the development of such results.

Several important distinctions between the plastic collapse of full circle shells and partial circle shells are to be noted. First, for collapse of the full circle shell to occur, the entire shell must be plastic. Although precise collapse modes are not derived herein, displacement patterns which are utilized to develop effective upper bounds on the collapse pressure tend to indicate that collapse occurs without the shell being fully plastic. Secondly, the symmetry about the axis of the cylinder which prevails for the full circle no longer is applicable to the partial circle with regard to the resultant stresses and deflections. Lastly, four controlling stress resultants must be considered for the partial circle, namely, three membrane stresses and the transverse moment whereas three stress resultants are predominant in the case of the full circle shell.

In this paper, a linear approximation to the Mises and Tresca conditions of plastic yielding is used and the material of the shell is assumed to be a rigid-perfectly plastic material. Thus, of the total strain rates the elastic components are neglected and only the plastic strain rates are considered significant. Likewise, by this assumption the effect of strain hardening is neglected.

A precise solution for the collapse of a rigid-plastic partial circle shell would define the zones of plastic action, give the collapse load and the displacement rate pattern and meet the following requirements.

a. Throughout the shell all equilibrium and stress boundary conditions must be satisfied.
b. Within the plastic zone, the stress combination must represent a yield condition. Outside the plastic zone, the stress combination must be less than that required for yielding.
c. Within the plastic zone, the displacement rate pattern must be related to the stresses by the appropriate plastic stress-strain-rate rule. Displacements at all boundaries must satisfy the appropriate boundary conditions. Outside the plastic zone the displacement pattern must be that of a rigid body or obey the laws of elasticity dependent on whether a plastic-rigid or a plastic-elastic analysis is contemplated.
d. Along the boundary between the plastic and non-plastic zones, appropriate continuity of stresses and displacement rates must prevail except for permissible discontinuities later discussed.

Development of the precise solution as described above is considered to be too involved mathematically to permit complete solution. By the methods of Limit Analysis for a rigid-plastic material, we obtain in effect partial solutions representing lower and upper bounds for the collapse load. Thus solutions satisfying subparagraphs a, b and d above define the lower bounds and solutions satisfying subparagraphs c and d above define the upper bounds.

General Theory

Yield Condition

Stress Yield Condition.—The yield condition defines the criteria under which plastic flow is possible. The condition can be expressed as an equality-inequality between a function of the stress components on the one hand and a material constant on the other. Only when the equality exists between this function and the constant is plastic flow feasible; when the inequality applies, no plastic flow is permitted. In this paper a linear yield condition which approximates both the Mises and Tresca conditions is used. This linear condition is developed from an approximation to the Mises condition for plane stress shown in Fig. 2.

Yield Condition in Terms of Stress Resultants.—As discussed below under Equilibrium, the four controlling stress resultants which are considered herein are N_x, $N\phi$, S, and M or in dimensionless form n_x, $n\phi$, s, and m. From the stress yield condition noted in Fig. 2, the corresponding yield condition in terms of stress resultants is obtained assuming the stresses in each half thickness of the shell to be constant across the half thickness as was done by Hodge;[6] the stress resultant yield condition is

$$\begin{aligned} &-1 \leq s \leq +1 \quad (a), \qquad -1 \leq n_\phi - m \leq +1 \quad (b), \\ &-1 \leq n_x \leq +1 \quad (c), \qquad -1 \leq n_\phi + m \leq +1 \quad (d), \\ &-1 \leq n_x - m - n_\phi \leq +1 \quad (e), \qquad -1 \leq n_x + m - n_\phi \leq +1 \quad (f) \end{aligned} \tag{17}$$

These yield conditions involve four variables. However, the shear stress resultant, s, does not combine in any of the inequalities with the other resultants, and it can conveniently be considered separately. Thus, assuming that the shear inequality is satisfied, the remaining yield conditions involve three variables. The equalities (b-f) can be pictured in a 3-dimensional space as defining a yield surface with all non-yielding combinations of stress resultants falling inside the surface and points on the surface representing yield conditions. The yield surface consists of ten bounding plane surfaces, and these are pictured in Fig. 3.

Because of the uniform loading and shape, the antisymmetric stress resultants must be zero at the corresponding planes of symmetry. Hence

$$\text{at } \varphi = 0, \quad s = 0 \quad (f), \quad \frac{\partial m}{\partial \varphi} = 0 \quad (g), \quad \text{and}$$

$$\text{at } y = 0, \quad s = 0 \quad (h). \tag{22}$$

At any transverse section, y = y, the total external longitudinal bending moment on the shell must equal the total internal longitudinal bending moment, M_y, resulting from summing N_x over the complete transverse section. This condition in non-dimensional form is

$$\text{at } y = y, \quad M_y = 2\sqrt{3}KTPL^2 (1 - y^2) \sin \varphi_o \quad (i). \tag{22}$$

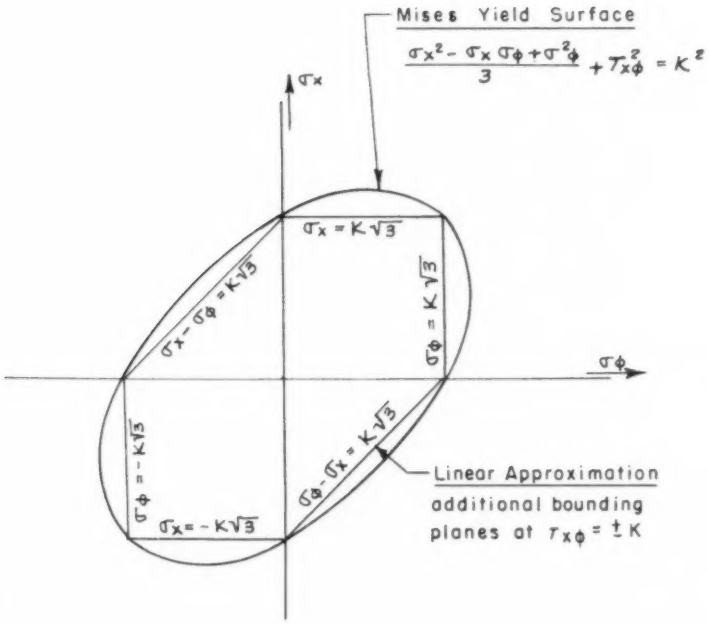

MISES YIELD CONDITION FOR PLANE STRESS
AND LINEAR APPROXIMATION THEREOF.
TRACE IN PLANE: $\tau_{x\phi} = 0$

FIGURE 2

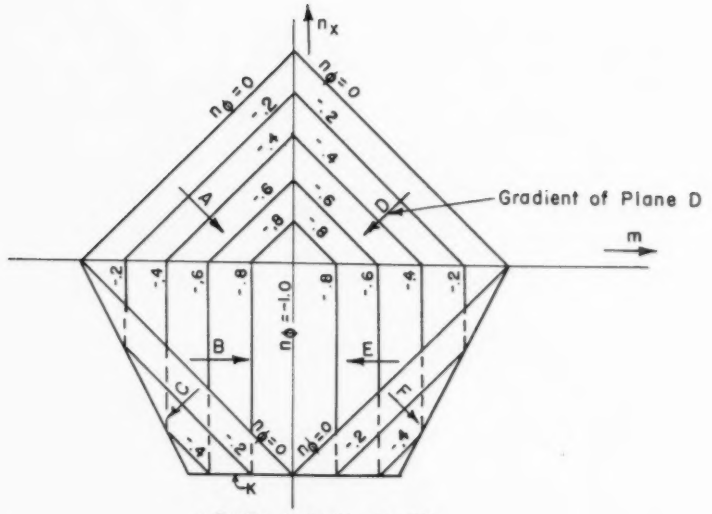

LEVEL LINES : $n_\phi \leq 0$

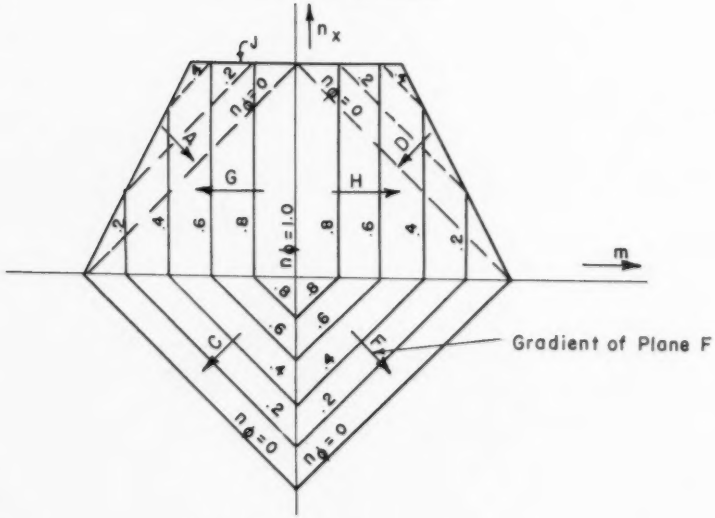

LEVEL LINES: $n_\phi \geq 0$

YIELD POLYHEDRON

$-1 < S < 1$

FIGURE 3

If we consider the five stress resultants involved in the equilibrium of a small element as indicated in Fig. 1, it is evident that certain discontinuities are permissible while enforcing equilibrium requirements. Thus, in the y-direction, discontinuities are permissible for m, $\frac{\sigma m}{\sigma \phi}$, and n_ϕ, but n_x and s must be continuous. For variation in the ϕ-direction, discontinuity of n_x is permissible but m, $\frac{\sigma m}{\sigma \phi}$, n_ϕ, and s must be continuous.

Displacement and Strain Rates

The expression for rate of internal work per unit area of the shell middle surface[3] is expressed in terms of dimensionless stress resultants by

$$D = 2\sqrt{3}\ \Sigma K \left[n_x \varepsilon_x + n_\phi \varepsilon_\phi + \frac{s}{\sqrt{3}} \gamma + mHX \right] \tag{24}$$

The strain rate resultants corresponding to the dimensionless stress resultants are expressed in terms of dimensionless variables by

$$\varepsilon_x = \frac{\partial U}{\partial y} \quad , \quad HX = -h\left(\frac{\partial V}{\partial \phi} + \frac{\partial^2 W}{\partial \phi^2}\right),$$

$$\varepsilon_\phi = \frac{\partial V}{\partial \phi} - W \quad , \quad \gamma = \frac{1}{r}\frac{\partial U}{\partial \phi} + r\frac{\partial V}{\partial y} \tag{26}$$

In cases of plastic flow, the plastic action may be confined to a very narrow belt. As this belt shrinks to a curve, discontinuities in certain rates of displacement and strain may result. Because a discontinuity in W would correspond to infinite radial shearing strain in contradiction to the previous assumption that the radial shear does negligible work, such a discontinuity is W is not allowable. However, discontinuities in U and V and in the first derivatives of U, V, and W are permissible, provided that due account is taken of the energy dissipated at such discontinuities. This may be done by regarding the discontinuity as the limiting case of a continuous field, as will be illustrated in Section IV.

The physical conditions inherent in the simple support of the ends of the shell impose the requirement that

$$\text{at } y = \pm 1, \quad V = 0, \quad W = 0 . \tag{27}$$

Flow Rule

We consider the plastic strain rate vector defined by

$$\underline{E} = (\varepsilon_x, \varepsilon_\phi, HX, \gamma).$$

The Plastic Potential Flow Law then requires that during the plastic flow associated with a yield state of stress, the strain rate vector must be in the outward normal direction to the yield surface at a point on the surface corresponding to the given yield state of stress.[11,12,13,14,15] As was indicated previously, the yield surface is defined herein in terms of stress resultants by Eq. (17) and by Fig. 3. With the yield surfaces consisting of intersecting

planes, the flow rule states that if the stress point is on any one plane, then the strain rate vector must be outwardly normal to that plane. If the stress point is located at the intersection of two or more planes, the direction of the strain rate vector must lie between the outward normals to the several intersecting planes. The directions of the strain rate vectors associated with the various surfaces of the yield polyhedron are given in Table 1.

Limit Theorems

A complete development of the theoretical basis for Limit Analysis is given in Reference 9. A synopsis of the discussion applicable to this paper is given herein for purposes of continuity.

A statically admissible stress field is defined for the stress resultants of the shell as one which satisfies everywhere in the shell (a) the equations of equilibrium (21), (b) the stress resultant boundary conditions (22), and (c) the yield conditions (17). As previously noted certain discontinuities in the stress resultants are permissible.

A kinematically admissible velocity field, v^*, is defined for the displacement and strain rates of the shell as one which satisfies everywhere in the shell (a) the condition of incompressibility (b) the physical limitations on displacements involving continuity requirements and end constraints and (c) the condition that positive work must result from the external force, due to the radial pressure, acting through the displacement field when considering the shell as a whole. As previously noted, certain discontinuities in the displacement field are permissible. Also there corresponds to each kinematically admissible velocity field a plastic stress resultant field, n^*, associated with the former field by the flow rule. It is noted that although n^* is not necessarily unique, the work done by n^* in moving through the strain resultants of v^* is unique. Further, for each assumed kinematically admissible velocity there can be determined a value of the external radial pressure, p^{**}, for which the work done by these external forces in moving through the assumed displacements is equal to the internal work by the stress resultant field n^* in moving through the strain resultants of v^*.

Lower Bound Criterion.—Any value of the radial pressure on the shell for which a statically admissible stress field exists represents a lower bound for the collapse pressure, p^*.

Upper Bound Criterion.—Any value of the radial pressure, p^{**}, associated as previously described with a kinematically admissible velocity field represents an upper bound for the collapse pressure.

Statically Admissible Stress Fields and Lower Bounds

Statically Admissible Stress Field I

It is known that plastic action in ordinary beams occurs with the development of two zones of constant longitudinal stress, one on either side of the neutral axis. Since long shells can be expected to act principally as beams, in Stress Field I, the half shell $0 \leq \phi \leq \phi_0$ is considered in two longitudinal zones with the longitudinal stress resultant n_x independent of ϕ in each zone (Fig. 4). Thus we take

TABLE 1: YIELD POLYHEDRON

Face	Equation	Strain Rate Vector (ε_x, ε_φ, HX, γ)
A	$n_x - n_\varphi - m = 1$	λ (1, -1, -1, 0)
B	$-n_\varphi - m = 1$	λ (0, -1, -1, 0)
C	$-n_x + n_\varphi - m = 1$	λ (-1, 1, -1, 0)
D	$n_x - n_\varphi + m = 1$	λ (1, -1, 1, 0)
E	$-n_\varphi + m = 1$	λ (0, -1, 1, 0)
F	$-n_x + n_\varphi + m = 1$	λ (-1, 1, 1, 0)
G	$n_\varphi - m = 1$	λ (0, 1, -1, 0)
H	$n_\varphi + m = 1$	λ (0, 1, 1, 0)
J	$n_x = 1$	λ (1, 0, 0, 0)
K	$-n_x = 1$	λ (-1, 0, 0, 0)
L	$s = 1$	λ (0, 0, 0, 1)
M	$s = -1$	λ (0, 0, 0, -1)

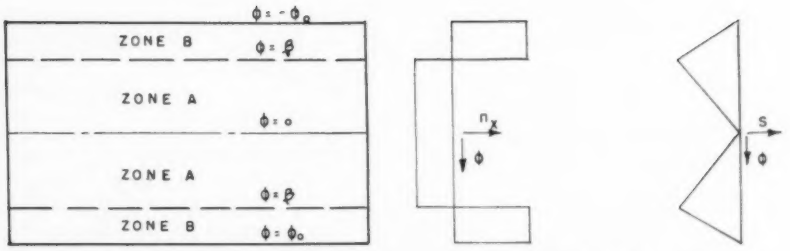

PLAN OF SHELL STRESS DISTRIBUTION

STRESS FIELD I

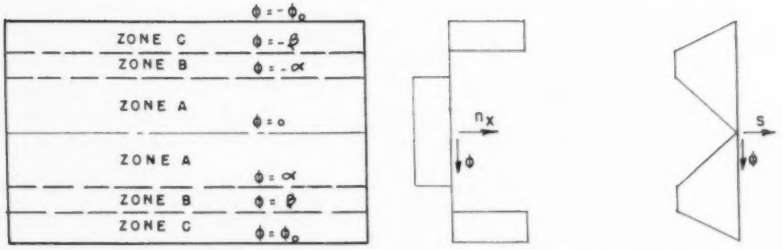

PLAN OF SHELL STRESS DISTRIBUTION

STRESS FIELD II

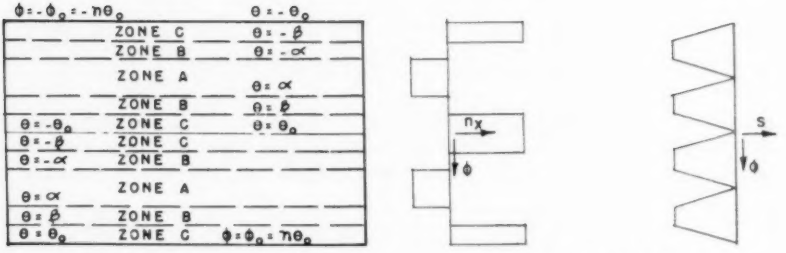

PLAN OF SHELL STRESS DISTRIBUTION

STRESS FIELD III

FIGURE 4

$$\text{zone A,}\quad 0 \le \varphi \le \beta \quad , \qquad n_x = n_{x_A}(y) \quad ,$$

$$\text{zone B,}\quad \beta \le \varphi \le \varphi_o \quad , \qquad n_x = n_{x_B}(y) \quad .$$

With these assumptions for n_x, the equilibrium equations are then solved subject to the stress boundary conditions and to continuity requirements on the stress resultants along $\phi = \beta$. The solutions for the stress resultants are for zone A, $0 \le \phi \le \beta$,

$$n_x = -\frac{P(\varphi_o - \beta)(\sin \varphi_o)(1 - y^2)}{2r^2 K} \qquad \text{(a)}$$

$$m = -\frac{P}{hK}\left[\varphi_o \sin(\varphi_o - \beta)\cos\varphi + \frac{(\varphi_o-\beta)}{2}(\sin\varphi_o)\varphi^2 - \varphi_o(\sin\varphi_o - \sin\beta) - \beta\varphi_o\frac{(\varphi_o-\beta)}{2}\sin\varphi_o\right] \qquad \text{(b)}$$

$$n_\varphi = -\frac{P}{K}\left[\varphi_o \sin(\varphi_o - \beta)\cos\varphi - \varphi_o(\sin\varphi_o - \sin\beta)\right] , \qquad \text{(c)} \qquad (31)$$

$$s = -\frac{\sqrt{3}P}{rK}(\varphi_o - \beta)(\sin\varphi_o)\varphi y \ , \qquad \text{(d)}$$

and for zone B, $\beta \le \varphi \le \varphi_o$,

$$n_x = \frac{P\beta(\sin\varphi_o)(1 - y^2)}{2r^2 K} \ , \qquad \text{(a)}$$

$$m = -\frac{P}{hK}\left\{\varphi_o \sin\beta[1 - \cos(\varphi - \varphi_o)] - \frac{\beta\sin\varphi_o}{2}(\varphi - \varphi_o)^2\right\} , \qquad \text{(b)}$$

$$n_\varphi = -\frac{P\varphi_o \sin\beta}{K}[1 - \cos(\varphi - \varphi_o)] \ , \qquad \text{(c)} \qquad (30)$$

$$s = -\frac{\sqrt{3}\,P\beta(\sin\varphi_o)(\varphi_o - \varphi)y}{rK} \ , \qquad \text{(d)}$$

where

$$K = \varphi_o \sin\beta - \beta\sin\varphi_o \ .$$

It will be observed that m and n_ϕ depend only upon ϕ, whereas n_x is a function of y only; the shear stress s depends upon both ϕ and y.

To permit application of the yield condition, information is required as to the location of the extrema of the stress resultants, individually and in combination. A summary of the pertinent characteristics for Stress Field I is given below for the typical quarter shell $0 \le \phi \le \phi_o$, $0 \le y \le 1$.

(1) n_x is invariant with ϕ in each zone. In the y-direction, n_x has its extrema at $y = 0$. It is negative in zone A and positive in zone B.

(2) s is negative or zero throughout. In the ϕ-direction, its absolute value increases linearly through zones A and B from zero to a maximum at $\phi = \beta$. In the y-direction, s had its extremum at $y = 1$.

(3) m is negative or zero throughout and is independent of y. The absolute value of m is a maximum at $\phi = 0$ and this absolute value decreases monotonically to the edge $\phi = \phi_o$. This applies for $0 \le \phi_o \le \pi$.

(4) n_ϕ is negative or zero throughout and is independent of y. Its absolute value is a maximum at $\phi = 0$ and this absolute value decreases monotonically to the edge $\phi = \phi_o$. This applies for $0 \le \phi_o \le \pi$.

(5) It turns out that the combination $m - n\phi$ needs to be considered in Zone A only. The largest value of $m - n\phi$ in the negative sense occurs at $\phi = 0$ provided that β, ϕ_o, and h comply with

$$\frac{\varphi_o \sin \beta}{\beta \sin \varphi_o} \geq \frac{\varphi_o - \beta}{(1 - h) \sin (\varphi_o - \beta)} \quad . \tag{42a}$$

In the following we will consider only those values of β which satisfy Inequality (42a). The above applies for $0 \leq \phi_o \leq \frac{\pi}{2}$.

The general yield conditions (17) can now be examined on the basis of the characteristics of Stress Fields I. With these characteristics, analysis of Fig. 3 shows that all twelve of the yield conditions are satisfied provided the following inequalities hold:

$$S(y, \varphi) = - s \leq 1 \quad , \tag{60}$$

$$\text{for } n_x > 0, \quad F(y, \varphi) = n_x - m - n_\varphi \leq 1 \quad ,$$

$$\text{for } n_x < 0, \quad G(y, \varphi) = - n_x - m + n_\varphi \leq 1 \quad ,$$

$$H(y, \varphi) = - m - n_\varphi \leq 1 \quad , \tag{62}$$

$$N(y) = - n_x \leq 1 \quad .$$

Let us denote the maximum values of each of these functions by the subscript C or A depending upon whether the maximum value occurs at $\phi = \beta$ or at $\phi = 0$. In view of the preceding remarks (1)-(5), the locations of these maxima are easily determined. Therefore, the yield condition will be satisfied provided that Inequality (42a) and all of

$$S_C = S(1, \beta) = - s(1, \beta) \leq 1 \quad ,$$

$$F_C = F(0, \beta) = n_{x_B}(0) - m(\beta) - n_\varphi(\beta) \leq 1 \quad ,$$

$$G_A = G(0, 0) = - n_{x_A}(0) - m(\beta) - n_\varphi(\beta)$$

$$H_A = H(0) = - m(0) - n_\varphi(0) \tag{63}$$

$$N_A = N(0) = - n_{x_A}(0)$$

are satisfied. Therefore, in order to determine the best lower bound, we determine β so as to maximize P satisfying (42a) and (63).

The procedure from here on depends upon the particular values of the parameters. If numerical values are assigned to r, h, and ϕ_o, then β and P can be determined so that at least two of Inequalities (42a) and (63) are equalities, and the rest are all satisfied. It turns out that $F_C = 1$ will usually be one of the equalities, and that the other one is either $S_C = 1$, $G_A = 1$, or $H_A = 1$.

Once a lower bound has been established, the next step is to determine an upper bound, using the methods of Section IV. If these bounds are reasonably close together, the problem is regarded as satisfactorily solved. However, if the bounds are far apart, improvements must be made in one or both of them. Generally Stress Field I yielded satisfactory lower bounds for long shells but these bounds become unsatisfactory as shorter shells were considered. In such cases, it was found that Stress Field I could be generalized as indicated in the sub-sections which follow.

Statically Admissible Stress Field II

For certain short, deep beams, the shearing stresses tend to become critical under increased loading. In Stress Field II shown in Fig. 4, the half shell $0 \le \phi \le \phi_0$ is considered in three longitudinal zones with the shear resultant in the middle zone taken independent of ϕ and the shear resultants in the other zones linear in ϕ. Thus we take

$$\text{zone A,}\quad 0 \le \varphi \le \alpha\,, \qquad s = \frac{\varphi}{\alpha}\, q(y)\,, \qquad \text{(a)} \tag{32}$$

$$\text{zone B,}\quad \alpha \le \varphi \le \beta\,, \qquad s = q(y)\,, \qquad \text{(b)}$$

$$\text{zone C,}\quad \beta \le \varphi \le \varphi_0, \qquad s = \frac{\varphi_0 - \varphi}{\varphi_0 - \beta}\, q(y). \qquad \text{(c)}$$

With these assumptions for s, the equilibrium equations are then solved subject to the stress boundary conditions and to continuity requirements on the stress resultants along $\phi = \alpha$ and $\phi = \beta$. The solutions for the stress resultants are for zone A, $0 \le \phi \le \alpha$,

$$n_x = -\frac{RP(1 - y^2)}{2r^2\alpha}\,, \qquad \text{(b)}$$

$$m = \frac{P}{h}\left[\left(1 + \frac{R}{\varphi_0 - \beta}\right)\cos(\varphi_0 - \varphi) - \frac{R\cos(\beta - \varphi)}{\varphi_0 - \beta} - \frac{R}{\alpha}\cos(\alpha - \varphi) - \frac{R\varphi^2}{2\alpha} + \frac{R}{\alpha} + \frac{R}{2}(\varphi_0 + \beta - \alpha) - 1\right], \qquad \text{(c)} \tag{38}$$

$$n_\varphi = P\left[\left(1 + \frac{R}{\varphi_0 - \beta}\right)\cos(\varphi_0 - \varphi) - \frac{R\cos(\beta - \varphi)}{\varphi_0 - \beta} - \frac{R}{\alpha}\cos(\alpha - \varphi) + \frac{R}{\alpha} - 1\right], \qquad \text{(d)}$$

$$s = -\frac{\sqrt{3}\,RP\varphi y}{r\alpha}\,, \qquad \text{(a)}$$

for zone B, $\alpha \le \varphi \le \beta$,

$$n_x = 0\,, \qquad \text{(b)}$$

$$m = \frac{P}{h}\left[\left(1 + \frac{R}{\varphi_0 - \beta}\right)\cos(\varphi_0 - \varphi) - \frac{R}{\varphi_0 - \beta}\cos(\beta - \varphi) - R\varphi + \frac{R(\varphi_0 + \beta)}{2} - 1\right], \qquad \text{(c)} \tag{37}$$

$$n_\varphi = P\left[\left(1 + \frac{R}{\varphi_0 - \beta}\right)\cos(\varphi_0 - \varphi) - \frac{R}{\varphi_0 - \varphi}\cos(\beta - \varphi) - 1\right], \qquad \text{(d)}$$

$$s = -\frac{3\,RPy}{r}\,, \qquad \text{(a)}$$

and for zone C, $\beta \leq \varphi \leq \varphi_o$,

$$n_x = \frac{RP(1 - y^2)}{2r^2(\varphi_o - \beta)} \quad , \tag{b}$$

$$m = \frac{P}{h}\left(1 - \frac{R}{\varphi_o - \beta}\right)\left[\cos(\varphi_o - \varphi) - 1\right] + \frac{R(\varphi_o - \varphi)^2}{2(\varphi_o - \beta)} \quad , \tag{c}$$

$$n_\varphi = P\left(1 + \frac{R}{\varphi_o - \beta}\right)\left[\cos(\varphi_o - \varphi) - 1\right] \quad , \tag{d}$$

$$s = -\frac{3RP(\varphi_o - \varphi)y}{r(\varphi_o - \beta)} \quad , \tag{a}$$

(36)

where

$$R = \frac{\alpha(\varphi_o - \beta)\sin\varphi_o}{(\varphi_o - \beta)\sin\alpha - \alpha(\sin\varphi_o - \sin\beta)} \quad .$$

If α is set equal to β, Stress Field II reduces to Stress Field I.

Similarly to the discussion of Stress Field I, the pertinent characteristics of Stress Field II must now be considered. A summary of the characteristics of Stress Field II follows.

(1) n_x is invariant with ϕ in each zone. In the y-direction, n_x has its extrema at y = 0. It is negative in zone A and positive in zone C.

(2) s is negative or zero throughout. In the ϕ-direction, its absolute value increases linearly through zones A and C from zero to the constant extremum over the entire interior zone B, $\alpha \leq \phi \leq \beta$. In the y-direction, s has its extremum at y = 1.

(3) m is negative or zero throughout and is independent of y. The absolute value of m is a maximum at $\phi = 0$ and this absolute value decreases montonically to the edge $\phi = \phi_o$. This applies for $o \leq \phi_o \leq \pi$.

(4) $n\phi$ is negative or zero throughout and is independent of y. Its absolute value is a maximum at $\phi = 0$ and this absolute value decreases monotonically to the edge $\phi = \phi_o$. This applies for $o \leq \phi_o \leq \pi$.

(5) The combination $m - n\phi$ needs to be considered in Zone A only. The largest value of $m - n\phi$ in the negative sense occurs at $\phi = 0$ provided that α, β, ϕ_o, and h comply with

$$1 + \frac{\varphi_o - \beta}{R} \geq \frac{\sin(\beta - \alpha) + \frac{\varphi_o - \beta}{1 - h}}{\sin(\varphi_o - \alpha)} \quad , o \leq \phi_o \leq \frac{\pi}{2} \tag{42}$$

With these stress resultant characteristics, the arguments previously advanced in the simplification of the yield condition for Stress Field I apply equally to Stress Field II except that Inequality (42) must be enforced in lieu of Inequality (42a). Hence Inequalities (63) replace the original yield condition, and we seek to determine both α and β so as to maximize P while satisfying (42) and (63). The best lower bound on P is thus obtained.

As previously the procedure now depends on the particular values of the parameters. After numerical values are assigned to r, h, and ϕ_o, α and β and consequently P can theoretically be evaluated so that at least three of the

Inequalities (42) and (63) are equalities and the rest are all satisfied. However, because of the rather complicated equations involved this method did not prove practical. Instead lower bounds were obtained by trial, assigning values to α and β on the basis of previous results and using the best resultant lower bound.

Again as previously, the lower bounds obtained by this method were judged to be satisfactory only if close enough to an upper bound determined by the methods of Section IV. In the procedure adopted for computing lower bounds, Stress Field II was tried only in those cases where the results of a previous trial using Stress Field I indicated S_C to be the controlling stress resultant. This was true of the shortest and thickest shells considered. In these cases the greater shear capacity of Stress Field II resulted in a higher and satisfactory lower bound. If the lower bound from Field I was judged to be too low and the controlling stress resultant combination was not S_C, Stress Field III, representing a further generalization of Stress Fields I and II was tried. This stress field is taken up in the succeeding sub-section.

Statically Admissible Stress Fields III

Stress Fields III are derivative from Stress Fields I and II previously considered which specified the stress resultants for the shell of subtended angle $2\phi_0$ with symmetry about the center line $\phi = 0$. Now taking a shell of subtended angle $2n\theta_0$ with n an integer we consider the shell as consisting of n adjoining sections, each of subtended angle $2\theta_0$, which extend from the near edge $\phi = n\theta_0$ to the far edge $\phi = -n\theta_0$. We assume that the stress field in each such section of subtended angle $2\theta_0$ is either Stress Field I or II as obtained for a shell of subtended angle $2\theta_0$. The near edge $\phi = n\theta_0$ will superimpose on the edge of a narrower shell $\phi = \theta_0$ and similarly the far edge $\phi = -n\theta_0$ will superimpose on the edge of a narrower shell $\phi = -\theta_0$. Since the boundary conditions at $\phi = \pm n\theta_0$ are the same as at $\phi = \pm\theta_0$ for the narrower shell, the boundary conditions at $\phi = \pm n\theta_0$ for the full shell are satisfied by the assumed stress fields. At all internal junctions between sections, $\phi = (n - 2K)\theta_0$, with K also an integer, the stress resultants, s, n_ϕ, m, and $\frac{\sigma m}{\sigma \phi}$ are each zero and thus necessary continuity conditions are complied with. Hence, subject to compliance with the yield condition, Stress Fields I and II developed for a shell of subtended angle $2\theta_0$ are statically admissible for shells of subtended angles $2n\theta_0$, n integral. Thus with the use of Inequalities (42), (42a) and (63), lower bounds can be developed as described in the preceding sub-sections. As previously indicated Stress Field III was considered only after previous use of Stress Field I gave an unsatisfactory lower bound with a controlling stress resultant combination other than S_C. In all such cases Stress Field III yielded a satisfactory lower bound. In general this stress field was found to give the controlling lower bound for the shorter, thinner shells.

Kinematically Admissible Velocity Fields and Upper Bounds

Kinematically Admissible Velocity Field I

The displacement pattern of this field is similar to that associated with collapse of a simple beam. As shown in Fig. 5, a plastic belt between $y = -y_1$ and $y = y_1$ is assumed with the remainder of the shell rigid. Displacement of each rigid section is taken to correspond to rotation about a horizontal axis in each end passing through the shell arc at $\phi = \pm\beta$. With displacements

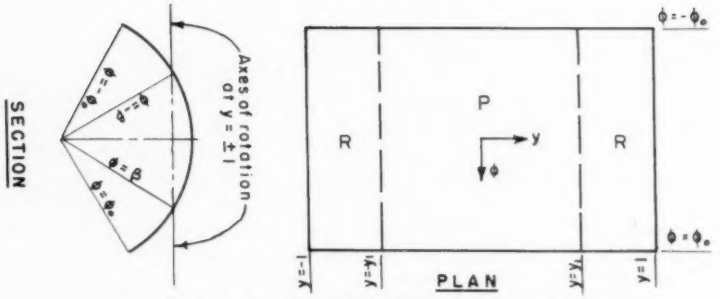

KINEMATICALLY ADMISSIBLE VELOCITY FIELD I

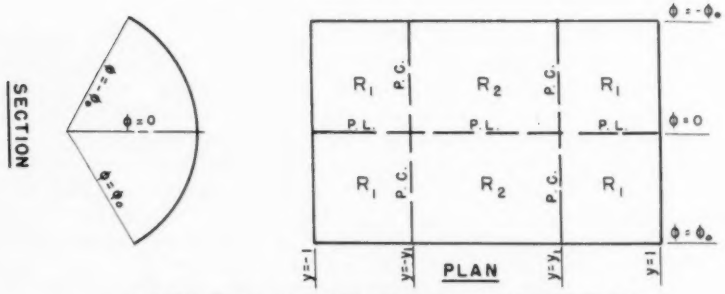

KINEMATICALLY ADMISSIBLE VELOCITY FIELD II

P.L.= Plastic Line
P.C.= Plastic Curve

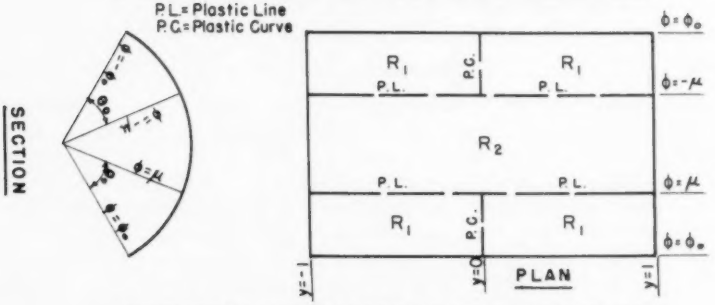

KINEMATICALLY ADMISSIBLE VELOCITY FIELD III

FIGURE 5

symmetrical about $\phi = 0$ and $y = 0$ the quarter shell $0 \le \phi \le \phi_0$, $0 \le y \le 1$ is typical and the expressions for dimensionless displacements are

$$\text{in R,} \quad y_1 \le y \le 1 \quad ,$$

$$U = \alpha r(\cos\beta - \cos\varphi),$$

$$V = \frac{\alpha}{r}(1 - y)\sin\varphi \, , \tag{44}$$

$$W = \frac{\alpha}{r}(1 - y)\cos\varphi \, ,$$

and in P, $0 \le y \le y_1$,

$$U = \alpha r(\cos\beta - \cos\varphi)\frac{y}{y_1} \quad ,$$

$$V = \frac{\alpha}{r}(\sin\varphi)\left(1 - \frac{y_1}{2} - \frac{y^2}{2y_1}\right) \quad , \tag{44}$$

$$W = \frac{\alpha}{r}(\cos\varphi)\left(1 - \frac{y_1}{2} - \frac{y^2}{2y_1}\right) \quad .$$

It is noted that these displacements obey the physical constraints of the simple supports with $V = W = 0$ at $y = 1$ and that W is continuous throughout the shell as required. The accompanying strains are derived from the displacements and the rigid body nature of the displacements in R is verified. Thus, in R,

$$\varepsilon_x = \varepsilon_\varphi = \gamma = HX = 0 \quad .$$

However, in P,

$$\varepsilon_\varphi = \gamma = HX = U \quad ,$$

$$\varepsilon_x = \frac{\alpha r}{y_1}(\cos\beta - \cos\varphi),$$

Then,

$$\varepsilon_x \le 0 \quad \text{for} \quad 0 \le \varphi \le \beta,$$

$$\varepsilon_x \ge 0 \quad \text{for} \quad \beta \le \varphi \le \varphi_0 \, .$$

With the above combinations of strains, the applicable plastic regimes for P are for $0 \le \phi \le \beta$, $n_x = -1$ and for $\beta \le \phi \le \phi_0$, $n_x = 1$. These regimes correspond to faces K and J respectively of the yield polyhedron, Fig. 3.

The internal work done in the quarter shell is designated I' and we define I by

$$I = \frac{I'}{2\sqrt{3}\,TK} \quad .$$

Then,

$$I = \oint_S (n_x \varepsilon_x + n_\varphi \varepsilon_\varphi + \frac{s\gamma}{\sqrt{3}} + mHX)dS. \tag{45}$$

We use the previous values of n_x and ϵ_x in P to obtain

$$I = \frac{\alpha r}{y_1}\left\{\int_0^{y_1}\int_0^{\beta} -(\cos\beta - \cos\varphi)\,L\,dy\,d\varphi + \int_0^{y_1}\int_\beta^{\varphi_0}(\cos\beta - \cos\varphi)L\,dy\,d\varphi\right\}$$

$$= L\alpha r\,[\varphi_0\cos\beta - \sin\varphi_0 - 2\beta\cos\beta + 2\sin\beta].$$

The work done by the external forces on the quarter shell is designated E' and we define E by

$$E = \frac{E'}{2\sqrt{3}\,T\chi} \quad .$$

Then

$$E = \oint_S PW \, dS \quad . \tag{46}$$

For Field I,

$$E = PL\alpha \left\{ \int_0^{y_1} \int_0^{\varphi_0} \frac{\alpha}{r} (\cos \varphi)\left(1 - \frac{y_1}{2} - \frac{y^2}{2y_1}\right) d\varphi dy + \int_{y_1}^{1} \int_0^{\varphi_0} \frac{\alpha}{r} (\cos\varphi)(1-y) d\varphi dy \right\}$$

$$= \frac{PL\alpha(3 - y_1^2) \sin \varphi_0}{6r}$$

For P to be an upper bound, E = I, from which we obtain

$$P = \frac{6r^2(\varphi_0 \cos\beta - \sin\varphi_0 - 2\beta\cos\beta + 2\sin\beta)}{(3 - y_1^2)\sin\varphi_0}$$

Minimum values of P with respect to y_1 and β result for $y_1 = 0$ and $\beta = \frac{\phi_0}{2}$. These values of y_1 and β are used to give the expression for an upper bound on P,

$$P^{**} = \frac{2r^2(2\sin\frac{\varphi_0}{2} - \sin\varphi_0)}{\sin\varphi_0} \quad . \tag{47}$$

It is noted that by taking $y_1 = 0$, the plastic belt has been shrunk to a curve. This results in a discontinuity in U which is permissible. Although ϵ_x becomes infinite, the internal work remains finite.

If the upper bounds obtained from (47) are reasonably close to the lower bounds obtained in Section III for a particular value of the shape parameters, no further effort towards a better upper bound is made. In general, Velocity Field I gives satisfactory upper bounds for the longer shells considered. However for shorter, thinner shells of larger central angle, the departure of the upper bound from known satisfactory lower bounds tends to become unreasonably large and additional velocity fields must be investigated. Such fields are taken up in the succeeding subsections.

Kinematically Admissible Velocity Field II

In the displacement pattern of Field II, the complete shell is divided directly into 6 rigid sections separated by plastic curves as shown in Fig. 5. Region R_2 rotates as a rigid body about a plastic line at $\phi = 0$ and undergoes a simultaneous tangential displacement. Region R_1 rotates as a rigid body about an axis at the end y = 1 which is parallel to the normal to the shell at $\phi = 0$ but which is displaced laterally therefrom. In addition region R_1 undergoes a rigid body twisting motion. Although the chosen displacement field was set up originally on the above physical basis it suffices now to verify the rigid body nature of the displacement pattern and the satisfaction of continuity and boundary requirements. Again we consider the quarter shell $0 \le \phi \le \phi_0$ and $0 \le y \le 1$. The displacement pattern in R_2, $0 \le \phi \le \phi_0$, $0 \le y \le y_1$ is chosen as

$$U = 0, \quad V = \frac{\alpha}{r}(A - \cos\varphi), \quad W = \frac{\alpha}{r}\sin\varphi, \tag{48}$$

and it is evident that $\epsilon_x = \epsilon_\phi = \gamma = HX = 0$ in R_2 as required for a rigid body motion. The displacement pattern in R_1, $0 \leq \phi \leq \phi_0$, $y_1 \leq y \leq 1$ is chosen as

$$U = \frac{\alpha r}{1 - y_1}(A\varphi - \sin\varphi + B) \quad ,$$

$$V = \frac{\alpha(1 - y)}{r(1 - y_1)}(A - \cos\varphi) \quad , \tag{49}$$

$$W = \frac{\alpha(1 - y)}{r(1 - y_1)}\sin\varphi \quad .$$

The internal strains with this displacement field are all zero. With regard to W, it is noted that W is continuous in each of the regions R_1 and R_2 and at all junctions between regions as required. At $y = 1$, the physical constraints are satisfied as $V = W = 0$.

With the displacement pattern of Field II, internal work is done along the plastic curves. The discontinuities along these curves are investigated for consequent internal work as noted below.

Discontinuities Along $\phi = 0$, $0 \leq y \leq y_1$.—Pertinent discontinuities applicable to the quarter shell are*

$$\frac{\partial W}{\partial \varphi}\Big] = \frac{\alpha}{r} \quad , \quad V\Big] = \frac{\alpha}{r}(A - 1).$$

I_1, the internal work expression (45) corresponding to these discontinuities, is minimized by setting

$$A = \frac{1}{1 + h} \quad . \tag{50}$$

Then,

$$I_1 = \frac{La\alpha hy_1}{r(1 + h)} \quad .$$

Discontinuities Along $\phi = 0$, $y_1 \leq y \leq 1$.—Pertinent discontinuities applicable to the quarter shell are

$$\frac{\partial W}{\partial \varphi}\Big] = \frac{\alpha(1 - y)}{r(1 - y_1)} \quad , \quad V\Big] = \frac{\alpha(1 - y)(A - 1)}{r(1 - y_1)} \quad .$$

I_2, the internal work expression corresponding to these discontinuities is again minimized by evaluating A as in (50) and we obtain

$$I_2 = \frac{La\alpha h(1 - y_1)}{2r(1 + h)}$$

Discontinuity Along $y = y_1$, $0 \leq \phi \leq \phi_0$.—A discontinuity in U exists, namely

$$U\Big] = \frac{\alpha r}{1 - y_1}(A\varphi - \sin\varphi + B).$$

The value of B is selected so as to minimize I_3, the internal work expression corresponding to the discontinuity in U. The form of the expression I_3 is dependent on the value of ϕ_0. Thus, for

*The symbol] denotes a discontinuity in the quantity immediately preceding.

$$2\gamma \le \varphi_o, \quad I_3 = \frac{La\alpha r}{1 - y_1}\left[1 - 2\cos\frac{\varphi_o}{2} + \cos\varphi_o + \frac{\varphi_o^2}{4(1+h)}\right],$$

$$2\delta \le \varphi_o < 2\gamma, \quad I_3 = \frac{La\alpha r}{1 - y_1}\left[2(\cos\varphi_1 + \cos\varphi_2) - \frac{(\varphi_2^2 - \varphi_1^2 - \frac{\varphi_o^2}{2})}{1+h} + \cos\varphi_o - 1\right],$$

$$0 \le \varphi_o \le 2\delta, \quad I_3 = -\frac{La\alpha r}{1 - y_1}\left[1 - 2\cos\frac{\varphi_o}{2} + \cos\varphi_o + \frac{\varphi_o^2}{4(1+h)}\right].$$

The expressions defining γ, δ, ϕ_1, ϕ_2 are

$$\frac{\gamma}{1+h} - \sin\gamma = 0, \tag{51}$$

$$\varphi_2 - \varphi_1 = \frac{\varphi_o}{2}, \tag{52}$$

$$\frac{\varphi_2 - \varphi_1}{1+h} - \sin\varphi_2 + \sin\varphi_1 = 0, \tag{53}$$

$$\frac{\delta}{1+h} - \sin 2\delta + \sin\delta = 0. \tag{54}$$

The expression for the external work associated with Velocity Field II is

$$E = \frac{Pla\alpha}{r}\left\{\int_0^{\gamma_1}\int_0^{\varphi_o} \sin\varphi\, d\varphi\, dy + \int_{y_1}^{1}\int_0^{\varphi_o} \frac{1-y}{1-y_1}\sin\varphi\, d\varphi\right\},$$

$$= \frac{Pla\alpha(1 - \cos\varphi_o)(1 + y_1)}{2r}.$$

For P to be an upper bound, $E = I_1 + I_2 + I_3$. We can write P in terms of y_1 and three constants which are independent of y_1. Thus

$$P = \frac{C_2}{C_1} + \frac{C_3}{C_1(1 - y_1^2)}.$$

Then, P will have its lowest value with respect to y_1 when $y_1 = 0$. The resultant expressions for the upper bound P^{**} are

$$2\gamma \le \varphi_o, \quad P^{**} = \frac{2r^2(1 - 2\cos\frac{\varphi_o}{2} + \cos\varphi_o + \frac{A\varphi_o^2}{4}) + Ah}{1 - \cos\varphi_o},$$

$$2\delta \le \varphi_o \le 2\gamma, \quad P^{**} = \frac{2r^2[2(\cos\varphi_1 - \cos\varphi_2) - A(\varphi_2^2 - \varphi_1^2 - \frac{\varphi_o^2}{2}) + \cos\varphi_o - 1] + Ah}{1 - \cos\varphi_o}, \tag{55}$$

$$0 \le \varphi_o \le 2\delta, \quad P^{**} = \frac{-2r^2(1 - 2\cos\frac{\varphi_o}{2} + \cos\varphi_o + \frac{A\varphi_o^2}{4}) + Ah}{1 - \cos\varphi_o},$$

where $A = \frac{1}{1 \quad h}$.

As noted in the preceding subsection, Velocity Field II has been investigated in an effort to obtain better upper bounds than those yielded by Field I particularly in the area of the shorter, thinner shells of larger central angle. It is found that Field II does give better upper bounds than Field I in this region of the shape parameters and in an isolated instance does give the controlling value of the upper bound. However, generally the upper bounds from Field II are still not considered satisfactorily close to known lower bounds, and it is necessary to investigate Velocity Field III, a generalization of Field II taken up in the subsection directly following.

Kinematically Admissible Velocity Field III

This field is derivative from Velocity Field II in which it was found that minimizing of the resultant upper bound enforced the shrinkage of a central rigid section $-y_1 < y < y_1$ to a curve at $y = 0$. In Field III, the shell is divided into 5 rigid sections separated by plastic curves as shown in Fig. 5. However, the rigid section R_2, $-\mu \leq \phi \leq \mu$, is completely motionless and only the sections R_1, $-\phi_0 \leq \phi \leq -\mu$ and $\mu \leq \phi \leq \phi_0$, are in motion. Plastic lines occur at $\phi = \pm\mu$ and plastic curves at $y = 0$ in the ranges $-\phi_0 \leq \phi \leq -\mu$ and $\mu \leq \phi \leq \phi_0$. We consider the quarter shell in the first quadrant and select for the displacement pattern in R_2, $0 \leq \phi \leq \mu$ and $0 \leq y \leq 1$,

$$U = V = W = 0 \quad , \tag{56}$$

and in R_1, $\mu \leq \phi \leq \phi_0$ and $0 \leq y \leq 1$,

$$\begin{aligned} U &= \alpha r \left[A(\varphi - \mu) - \sin(\varphi - \mu) + B\right] , \\ V &= \frac{\alpha(1 - y)}{r} \left[A - \cos(\varphi - \mu)\right] , \\ W &= \frac{\alpha(1 - y)}{r} \sin(\varphi - \mu) . \end{aligned} \tag{57}$$

Investigation readily reveals that the derived strains are zero in each of regions R_1 and R_2, that V and W vanish at the ends, and that W is continuous throughout.

We now set $\phi - \mu$ equal to θ and $\phi_0 - \mu$ equal to θ_0 and compare Fields II and III using $y_1 = 0$ in Field II. It is apparent that the expressions for the discontinuities and the external and internal work in Field II are identical with those previously obtained for Field II except θ and θ_0 replace ϕ and ϕ_0. Expressions can therefore be written for the upper bound P** analogous to (55) as

$$\begin{aligned} 2\gamma \leq \vartheta_0,\ P^{**} &= \frac{2r^2\left(1 - 2\cos\frac{\vartheta_0}{2} + \cos\vartheta_0 - \frac{A\vartheta_0^2}{4}\right) + Ah}{1 - \cos\vartheta_0} , \\ 2\delta \leq \vartheta_0 \leq 2\gamma,\ P^{**} &= \frac{2r^2\left[2(\cos\vartheta_1 - \cos\vartheta_2) - A\left(\vartheta_2^2 - \vartheta_1^2 - \frac{\vartheta_0^2}{2}\right) + \cos\vartheta_0 - 1\right] + Ah}{1 - \cos\vartheta_0} , \\ 0 \leq \vartheta_0 \leq 2\delta,\ P^{**} &= \frac{-2r^2\left(1 - 2\cos\frac{\vartheta_0}{2} + \cos\vartheta_0 + \frac{A\vartheta_0^2}{4}\right) + Ah}{1 - \cos\vartheta_0} . \end{aligned} \tag{58}$$

The expressions defining γ, δ, θ_1, θ_2, and A are

$$\begin{aligned} A\gamma - \sin\gamma &= 0 , \\ A\delta - \sin 2\delta + \sin\delta &= 0 , \\ \vartheta_2 - \vartheta_1 &= \frac{\vartheta_0}{2} , \\ A(\vartheta_2 - \vartheta_1) - \sin\vartheta_2 + \sin\vartheta_1 &= 0 , \\ A &= \frac{1}{1 + h} . \end{aligned} \tag{59}$$

By the use of equations (58), P can be minimized with respect to θ_0 for particular values of the parameters r and h and the minimizing values of θ_0 established. By this procedure, collapse modes involving collapse of only portions of the shell are developed.

Solutions for Bounds

Computations were carried out to give upper and lower bounds for the collapse pressure parameter P with a wide range of values for the parameters ϕ_0, r, and h. With ϕ_0 taken first as 30° and then as 90° and h taken in turn equal to .02, .005, and .00125, r was varied from 0.2 to 4.0 in 5 steps. The results are plotted as 6 pairs of curves in Figs. 6 to 11. Tabulation of the results with associated pertinent developmental data is given in Tables 2-7.

With regard to Velocity Field III, the defining ranges of θ_0, $2\gamma \leq \theta_0$, $2\delta \leq \theta_0 \leq 2\gamma$, $0 \leq \theta_0 \leq 2\delta$, have been designated Cases 1, 2, and 3 for purposes of tabulation. Special data developed for Field III are tabulated in Table 8.

CONCLUSIONS

1. For the case of a simply supported cylindrical shell without edge beams, collapse pressures and collapse modes have been obtained.

   a. By the use of methods of Limit Analysis for a plastic-rigid structure, lower and upper bounds for the collapse pressure parameter, P*, and P**, have been developed. Subject to the validity of the basic assumptions, if $\bar{P} = \frac{1}{2}(P^* + P^{**})$ is adopted as the solution for the collapse pressure parameter, the results indicate this solution to be accurate to within $\pm$ 2 to 25 per cent for the wide range of the shape parameters, ϕ_0, r, h considered.

   b. It is realized that the results obtained herein for P* and P** do not define precisely the collapse modes. However, review of the controlling stress and velocity fields as tabulated in Tables 2-7 indicates that when the controlling lower bound is defined by Stress Field I the controlling upper bound is usually defined by Velocity Field I and that when the controlling lower bound is defined by Stress Field III, the controlling upper bound is usually defined by Velocity Field III. Now Stress Field I and Velocity Field I have been based on characteristics associated with the collapse of simple beams. Since the results for lower and upper bounds obtained from these fields for long shells are in close proximity it seems reasonable to conclude that collapse of long shells will approximate that of simple beams. Similarly Stress and Velocity Fields III each appear to be associated with partial collapse of the shell along the edges. Hence Velocity Field III is considered to be a reasonably close approximation to the collapse mode of those shells for which the controlling value of the upper bound P** was obtained from Field III.

2. Considered assumptions made in the development of this paper are now reconsidered to assess their possible effect on an extension of the results to real shells.

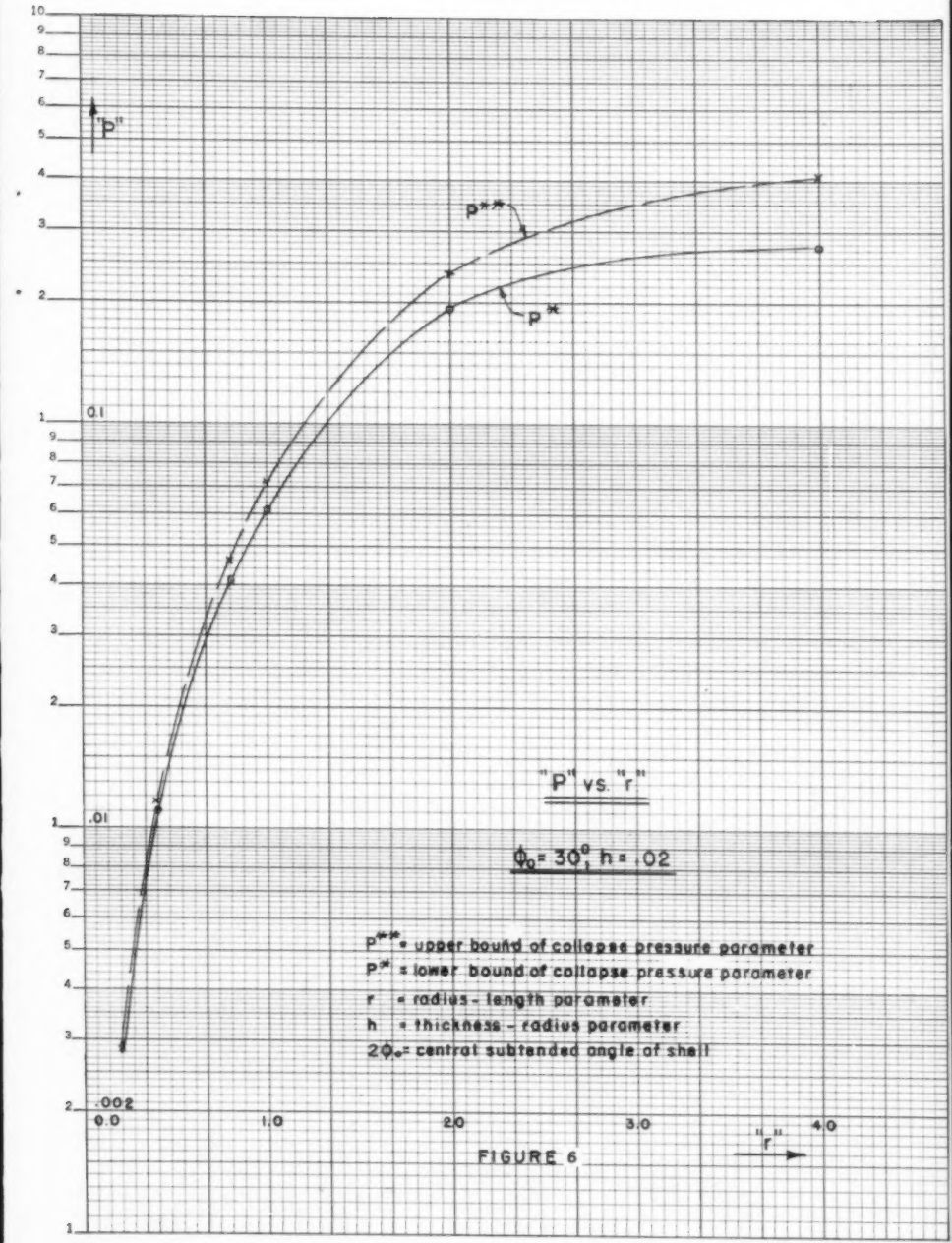
"P"
P**
P*
.1
.01
.002
0.0
1.0
2.0
3.0
4.0
"r"
"P" vs. "r"
$\phi_0 = 30^0$, h = .02
P** = upper bound of collapse pressure parameter
P* = lower bound of collapse pressure parameter
r = radius - length parameter
h = thickness - radius parameter
$2\phi_0$ = central subtended angle of shell

FIGURE 6

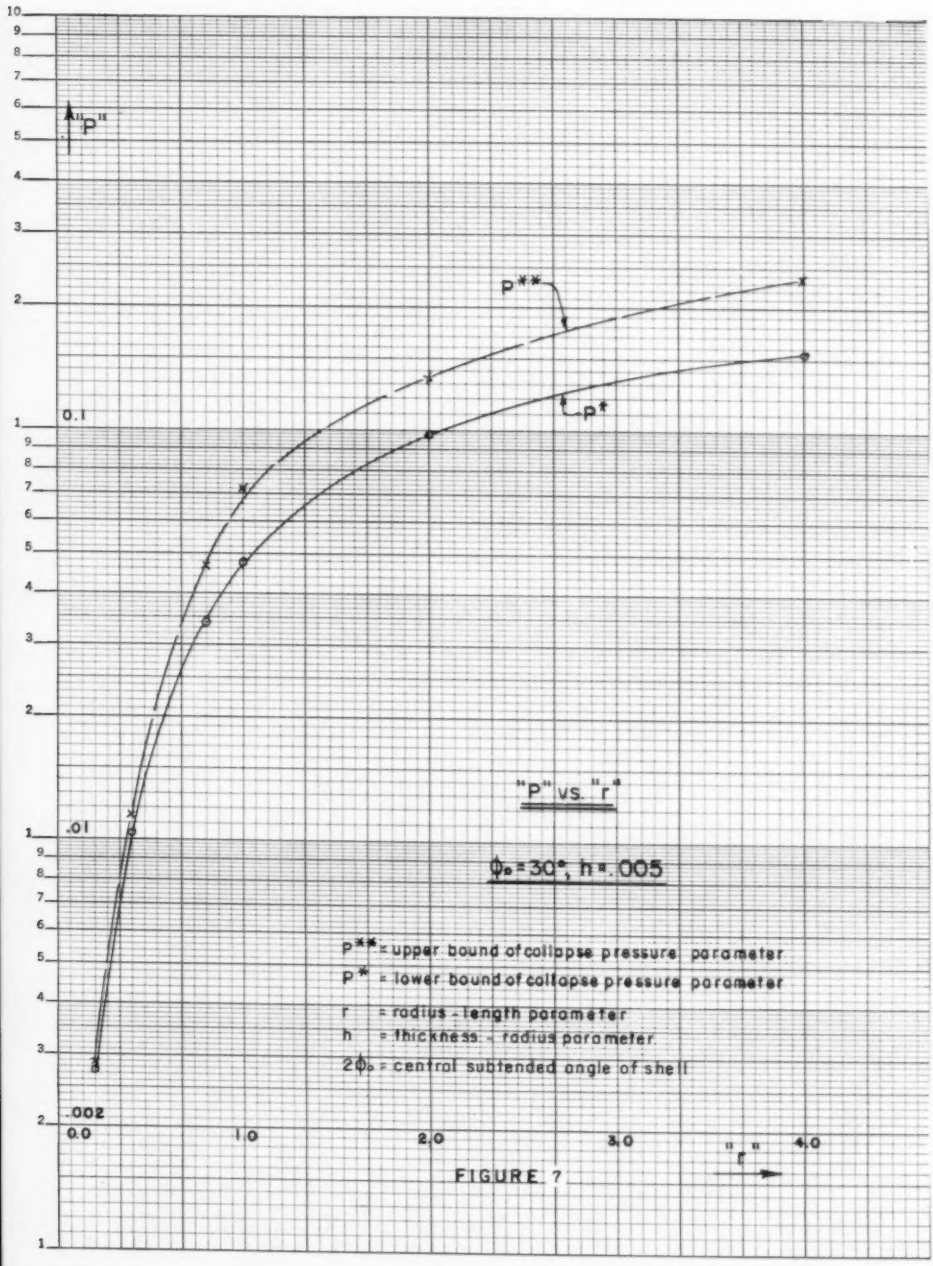
"P"
P**
P*
0.1
.01
.002
"P" vs. "r"
ϕ_o = 30°, h = .005
P** = upper bound of collapse pressure parameter
P* = lower bound of collapse pressure parameter
r = radius - length parameter
h = thickness - radius parameter
$2\phi_o$ = central subtended angle of shell
0.0
1.0
2.0
3.0
4.0
"r"

FIGURE 7

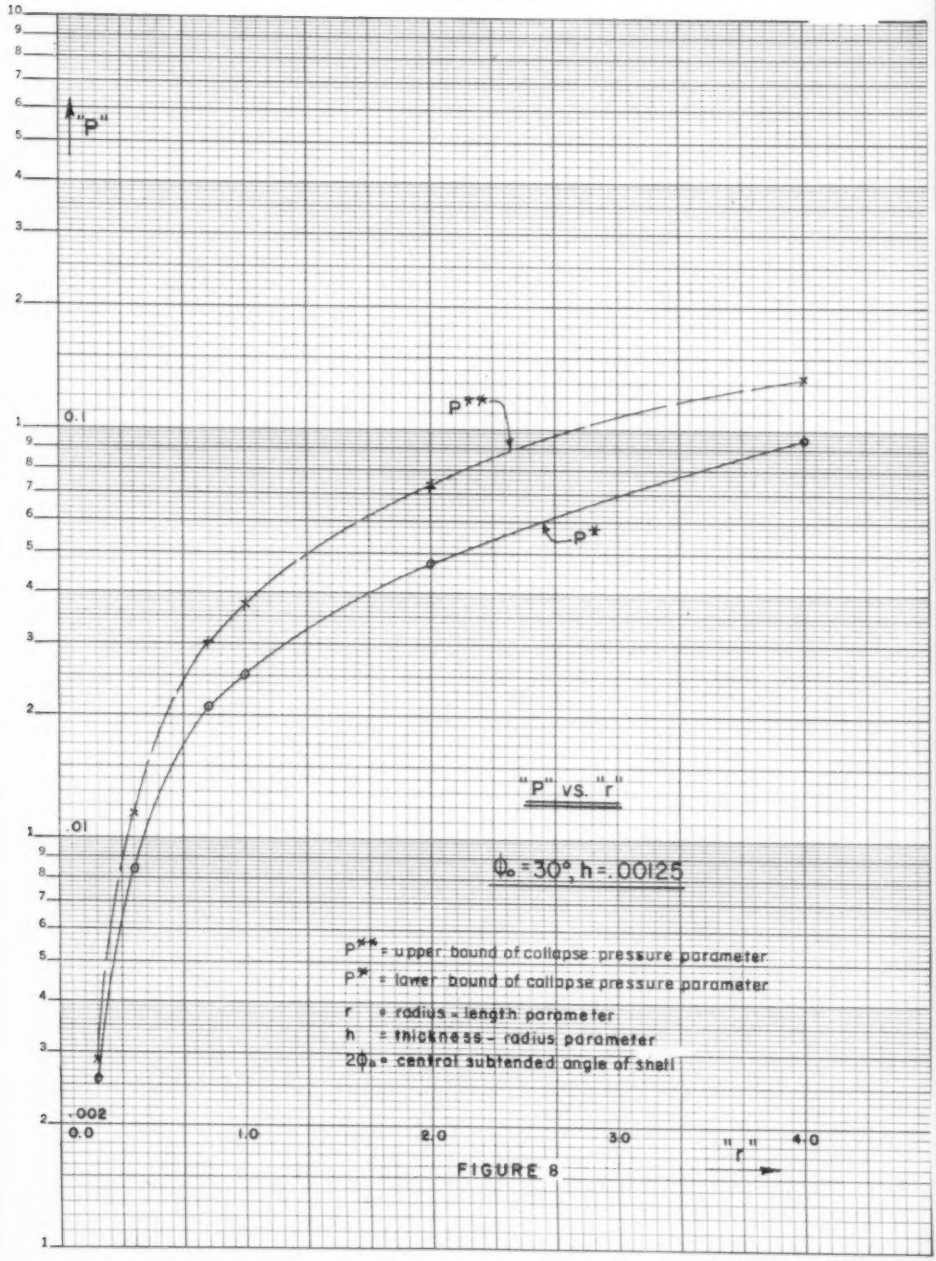
"P"
P**
P*
0.1
.01
.002
0.0
1.0
2.0
3.0
4.0
"r"
"P" vs. "r"
$\phi_o = 30°, h = .00125$
P** = upper bound of collapse pressure parameter
P* = lower bound of collapse pressure parameter
r = radius - length parameter
h = thickness - radius parameter
$2\phi_o$ = central subtended angle of shell

FIGURE 8

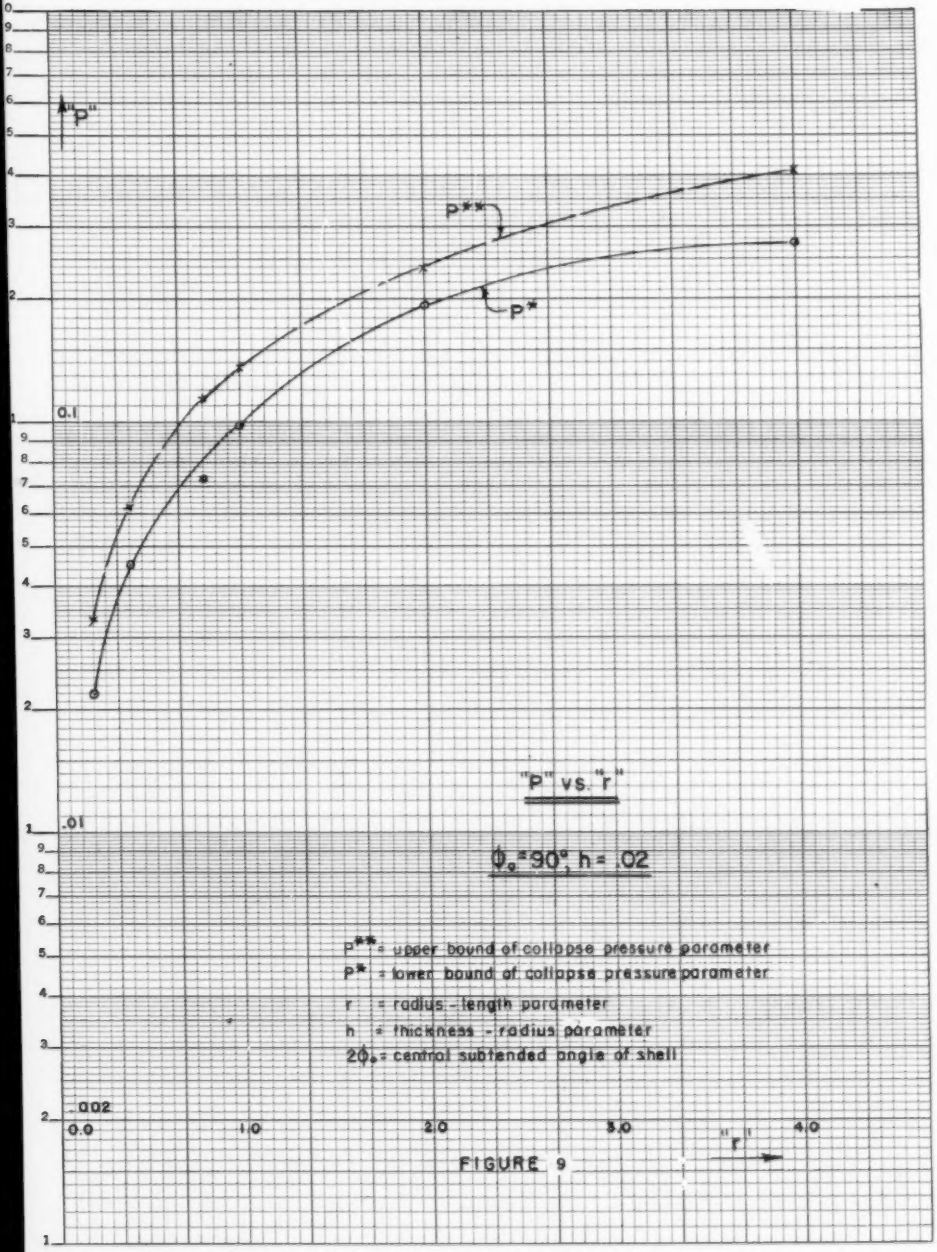
"P"
P**
P*
0.1
.01
.002
0.0
1.0
2.0
3.0
4.0
"r"
"P" vs. "r"
$\phi_o = 90°$; h = .02
P** = upper bound of collapse pressure parameter
P* = lower bound of collapse pressure parameter
r = radius - length parameter
h = thickness - radius parameter
$2\phi_o$ = central subtended angle of shell

FIGURE 9

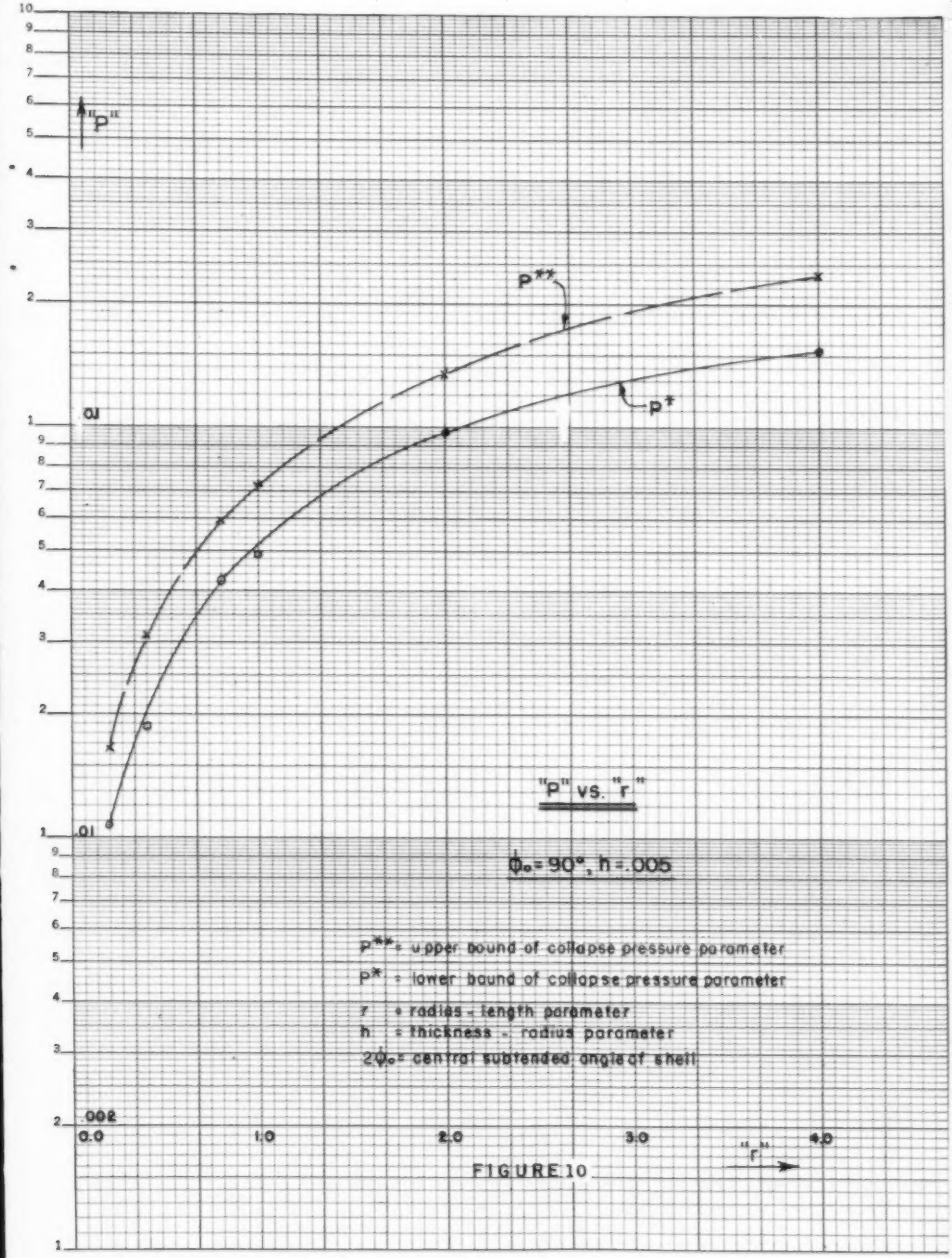
"P"
P**
P*
"P" vs. "r"
Φ₀ = 90°, h = .005
P** = upper bound of collapse pressure parameter
P* = lower bound of collapse pressure parameter
r = radius - length parameter
h = thickness - radius parameter
2Φ₀ = central subtended angle of shell
0.0
1.0
2.0
3.0
4.0
"r"

FIGURE 10

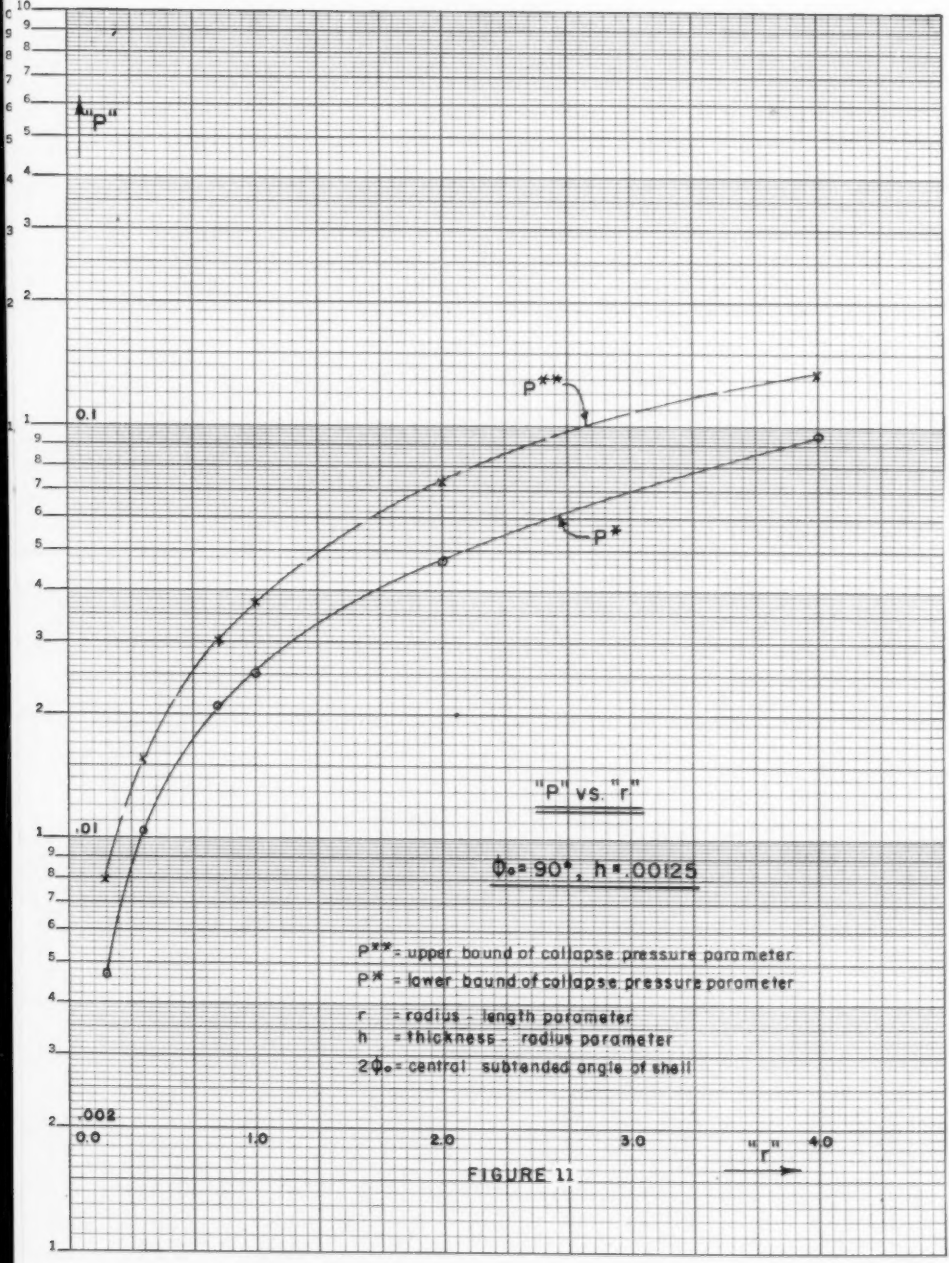
"P"
P**
P*
0.1
.01
.002
0.0
1.0
2.0
3.0
4.0
"r"
"P" vs "r"
Φ₀ = 90°, h = .00125
P** = upper bound of collapse pressure parameter
P* = lower bound of collapse pressure parameter
r = radius - length parameter
h = thickness - radius parameter
2Φ₀ = central subtended angle of shell

FIGURE 11

TABLE 2: $\varphi_o = 30^\circ$, h = .02

LOWER BOUNDS						
r	.2	.4	.8	1.0	2.0	4.0
P*	.0028	.011	.041	.061	.193	.272
S.A. Field	I	I	I	I	II	II
β-α Criterion	$F_C = G_A$	$F_C = G_A$	$F_C = G_A$	$F_C \approx G_A$	$F_C \approx G_A \approx H_A$	$F_C \approx H_A$
β	15°	15°	14° 30'	14°00'	20°	27°
α	-	-	-	-	10°	22°
ϑ_o	-	-	-	-	-	-

UPPER BOUNDS						
r	.2	.4	.8	1.0	2.0	4.0
P*	.00288	.0115	.046	.072	.236	.410
K. A. Field	I	I	I	I	III	III
Case	-	-	-	-	2	2
ϑ_o	-	-	-	-	30°	24°
ϑ_2	-	-	-	-	18°	16° 50'
ϑ_1					3°	4° 50

TABLE 3: $\varphi_o = 30^\circ$, $h = .005$

LOWER BOUNDS						
r	.2	.4	.8	1.0	2.0	4.0
P^*	.00275	.0103	.0339	.0477	.097	.153
S. A. Field	I	I	I	I	I	III
β-α Criterion	$F_C = G_A$	$F_C = G_A$	$F_C = G_A$	$F_C = G_A$	$F_C \approx H_A$	S_C
β	15°	15°	16°	17°	24°40'	7°30'
α	-	-	-	-	-	-
ϑ_o	-	-	-	-	-	15°

UPPER BOUNDS						
r	.2	.4	.8	1.0	2.0	4.0
P^{**}	.00288	.0115	.0461	.072	.134	.235
K. A. Field	I	I	I	I	III	III
Case	-	-	-	-	1	2
ϑ_o	-	-	-	-	20°30'	16°
ϑ_2	-	-	-	-	-	9°13'
ϑ_1	-	-	-	-	-	1°13'

TABLE 4: $\varphi_o = 30^o$ $h = .00125$

LOWER BOUNDS						
r	.2	.4	.8	1.0	2.0	4.0
P^*	.00259	.00840	.0210	.0250	.047	.095
S. A. Field	I	I	I	I	III	III
β-α Criterion	$F_C = G_A$	$F_C = G_A$	$F_C = G_A$	$F_C = G_A$	$F_C = G_A$	$F_C = H_A$
β	15°24'	17°00'	23°20'	25°20'	8°29'	12°42'
α	-	-	-	-	-	-
ϑ_o	-	-	-	-	15°00'	15°00'

UPPER BOUNDS						
r	.2	.4	.8	1.0	2.0	4.0
P^{**}	.00288	.0115	.0300	.0372	.0730	.133
K. A. Field	I	I	III	III	III	III
Case	-	-	1	1	1	1
ϑ_o	-	-	23°00'	21°00'	13°20'	10°30'
ϑ_2	-	-	-	-	-	-
ϑ_1	-	-	-	-	-	-

TABLE 5: $\varphi_o = 90^\circ$ $h = .02$

LOWER BOUNDS						
r	.2	.4	.8	1.0	2.0	4.0
P^*	.0219	.0453	.0728	.0980	.193	.272
S. A. Field	I	I	III	III	III	III
α-β Criterion	$F_C = G_A$	$F_C = G_A$	$F_C = G_A$	$F_C = G_A$	$F_C \simeq G_A \simeq H_A$	$F_C \simeq H_A$
β	$54^\circ 40'$	$76^\circ 00'$	$22^\circ 30'$	$23^\circ 10'$	20°	27°
α	-	-	-	-	10°	22°
ϑ_o	-	-	45°	45°	30°	30°
UPPER BOUNDS						
r	.2	.4	.8	1.0	2.0	4.0
P^{**}	.0331	.0623	.113	.136	.236	.410
K. A. Field	I	III	III	III	III	III
Case	-	1	1	1	2	2
ϑ_o	-	$64^\circ 10'$	$45^\circ 20'$	$41^\circ 10'$	30°	24°
ϑ_2	-	-	-	-	18°	$16^\circ 50'$
ϑ_1	-	-	-	-	3°	$4^\circ 50'$

TABLE 6: $\varphi_o = 90^\circ$ $h = .005$

LOWER BOUNDS						
r	.2	.4	.8	1.0	2.0	4.0
P^*	.0107	.0187	.0422	.0493	.097	.153
S. A. Field	I	III	III	III	III	III
α-β Criterion	$F_C \simeq G_A$	$F_C = G_A$	$F_C \simeq H_A$	$F_C = H_A$	$F_C \simeq H_A$	S_C
β	76°	26°10'	35°30'	39°10'	24°40'	7°30'
α	-	-	-	-	-	-
ϑ_o	-	45°	45°	45°	30°	15°
UPPER BOUNDS						
r	.2	.4	.8	1.0	2.0	4.0
P^{**}	.0164	.0310	.0591	.0724	.134	.235
K. A. Field	III	III	III	III	III	III
Case	1	1	1	1	1	2
ϑ_o	63°	45°40'	33°30'	28°40'	20°30'	16°00'
ϑ_2	-	-	-	-	-	9°13'
ϑ_1	-	-	-	-	-	1°13'

TABLE 7: $\varphi_o = 90^o$ $h = .00125$

LOWER BOUNDS						
r	.2	.4	.8	1.0	2.0	4.0
P^*	.00469	.0103	.0210	.0250	.047	.095
S. A. Field	III	III	III	III	III	III
β-α Criterion	$F_C = G_A$	$F_C = G_A$	$F_C = G_A$	$F_C = G_A$	$F_C = G_A$	$F_C = H_A$
β	26°56'	37°04'	23°20'	25°20'	8°29'	12°42'
α	-	-	-	-	-	-
ϑ_o	45°	45°	30°	30°	15°	15°
UPPER BOUNDS						
r	.2	.4	.8	1.0	2.0	4.0
P^{**}	.00791	.0154	.0300	.0372	.0730	.133
K. A. Field	III	III	III	III	III	III
Case	1	1	1	1	1	1
ϑ_o	45°30'	33°40'	23°00'	21°00'	13°20'	10°30'
ϑ_2	-	-	-	-	-	-
ϑ_1	-	-	-	-	-	-

TABLE 8

Date for Velocity Field III

h	A	γ	δ	Case 1	Case 2	Case 3
.02	.980392	$19^{\circ}50'$	6°	$39^{\circ}40' \leq \theta_0$	$12^{\circ} \leq \theta_0 \leq 39^{\circ}40'$	$\theta_0 \leq 12^{\circ}$
.005	.995025	$9^{\circ}50'$	$3^{\circ}45'$	$19^{\circ}40' \leq \theta_0$	$7^{\circ}30' \leq \theta_0 \leq 19^{\circ}40'$	$\theta_0 \leq 7^{\circ}30'$
.00125	.998752	$4^{\circ}58'$	$1^{\circ}57.'5$	$9^{\circ}56' \leq \theta_0$	$3^{\circ}55' \leq \theta_0 \leq 9^{\circ}56'$	$\theta_0 \leq 3^{\circ}55'$

a. As we have dealt with a rigid-perfectly-plastic material, we have assumed no deflections prior to the onset of plastic action. While this approximation may be close for short shells the elastic deflection of long shells up to the onset of plastic flow may be so large as to make the shell non-usable for its intended purpose. The assumption of perfect plasticity which assumes no strain hardening is not believed to offer serious objections for ductile materials such as soft steel which undergo substantial plastic flow prior to onset of strain hardening.

b. The yield condition used herein represents a linear approximation to the Mises yield condition. However, since the Mises condition also represents the behavior of actual materials only approximately, it does not appear unreasonable to use this linear yield condition for ductile metals. The linear condition used is closest to the Mises condition where the shear is small and its validity is therefore believed to be greatest for small shear. Of course the linear condition can be readily revised to approximate the Mises condition more closely for larger shears, but this would complicate the work of attaining solutions.

c. In the development of equilibrium equations, certain stress resultants were neglected. For very short shells, the omission of the longitudinal bending moment from equilibrium considerations appears to require critical evaluation. Thus very short shells of small curvature could be expected to act as plates supported on the ends. However the effects of shortness and curvature tend to magnify and lessen respectively the importance of this longitudinal bending moment and no conclusions are drawn at this time as to the effect of this omission.

d. The expressions used for strains and the equilibrium equations presupposed small deflections. Although this is not in accord with the deflections associated with collapse no conclusions are drawn as to the resultant effect on the accuracy of the solutions.

e. With regard to the applicability of the results obtained herein to shells built of reinforced concrete, it is considered that present information on yielding of this material under the three dimensional stress system of the shell is insufficient to permit assessment of the extent of the approximation involved. However, it is believed that with the development of necessary yield criteria for reinforced concrete, the methods of limit analysis as used herein can be utilized to advantage to develop the desired data on plastic collapse.

f. Extension of the methods of this article to cover other end and edge conditions of the shell is suggested.

ACKNOWLEDGEMENTS

This paper is based on a dissertation submitted in June 1957 to the Polytechnic Institute of Brooklyn in partial fulfillment of the requirements for the degree of Doctor of Philosophy in Applied Mechanics. The author wishes to express his appreciation and gratitude to Professor Philip G. Hodge, Jr., Chairman of the dissertation Guidance Committee for his many helpful suggestions during the development of the dissertation.

List of Symbols

a = radius of shell

$h = \frac{H}{a}$ = dimensionless thickness-radius parameter = $\frac{t}{2a}$

$m = \frac{M}{M_o}$ = circumferential bending moment in non-dimensional form

n = any integer

$n_x = \frac{N_x}{N_o}$ = longitudinal direct stress resultant in non-dimensional form

$n_\phi = \frac{N_\phi}{N_o}$ = circumferential direct stress resultant in non-dimensional form

p = uniform radial pressure on shell

p^*, p^{**} = lower and upper bounds on p

$r = \frac{a}{L}$ = dimensionless radius-length parameter

$s = \frac{S}{S_o}$ = membrane shearing stress resultant in non-dimensional form

$2t$ = thickness of shell

u, v, w = displacements in longitudinal, circumferential, and radial directions

x = longitudinal coordinate

$y = \frac{x}{L}$ = longitudinal coordinate in non-dimensional form

z = radial coordinate

A, B = constants defining Velocity Fields

D = total internal plastic work in shell

E = reduced expression for work done by external forces

$\underline{E}$ = displacement vector

F_C, G_A, H_A, N_A, S_C = critical combinations of stress resultants relative to yield condition

G, H, R, K = functions of $_o, \alpha, \beta$ defining the stress resultants

$2H$ = distance between centers of faces of the equivalent ideal sandwich shell = t

I = reduced expression for internal plastic work

K = constant of Mises yield condition

$2L$ = length of shell

$M = M\phi$ = circumferential bending moment per unit length

M_o = limit bending moment per unit length = $2\sqrt{3}THK = \sqrt{3}\, t^2K$

N_x, N_ϕ = membrane direct stress resultants per unit length

N_o = limit direct stress resultant per unit length = $2\sqrt{3}\,TK = 2\sqrt{3}\,tK$

$P = \frac{pa}{2\sqrt{3}\,KT}$ = dimensionless pressure parameter

$\bar{P}$ = value of P at collapse

P^*, P^{**} = lower and upper bounds of $\bar{P}$

Q = radial shearing force per unit length

S = membrane shearing force per unit length

S_o = limit membrane shearing force per unit length = 2TK = 2tK

T = thickness of one face of the equivalent ideal sandwich shell = t

$U = \frac{u}{L}$ = longitudinal displacement in non-dimensional form

$V = \frac{v}{a}$ = circumferential displacement in non-dimensional form

$W = \frac{w}{a}$ = radial displacement in non-dimensional form

α = constant associated with rigid body rotations in Velocity Fields

α, β, μ = values of ϕ defining boundaries between longitudinal zones

γ, δ, ϕ_1, ϕ_2 = values of ϕ_o used with Velocity Field II

γ, δ, θ_1, θ_2 = values of ϕ_o used with Velocity Field III

ϕ = angular coordinate in circumferential direction

$2\phi_o$ = central angle subtended by the shell arc

$\theta = \phi - \mu$

ϵ_x, ϵ_ϕ = unit elongations

$\gamma = \gamma_{x\phi}$ = shearing strain

$X = X_\phi$ = rate of change of curvature in circumferential direction

σ_x, σ_ϕ, σ_z = normal components of stress

$\tau_{x\phi}$, $\tau_{\phi z}$, τ_{zx} = shearing components of stress

$\tau = \tau_{x\phi}$

REFERENCES

1. Flügge, W., Statik und dynamik der schalen, Julius Springer, Berlin, 1934.
2. Donnell, L. H., Stability of thin walled tubes under torsion, NACA Technical Report No. 479, Washington, D. C., 1933.
3. Timoshenko, S., Theory of plates and shells, McGraw-Hill Book Company, Inc., New York and London,1940.
4. ASCE Manual No. 31, Design of cylindrical concrete shell roofs, New York, 1952.

5. Drucker, D. C., Limit analysis of cylindrical shells under axially-symmetric loading, Proceedings of First Midwest Conference on Solid Mechanics (Urbana) 1952, Engineering Experiment Station, University of Illinois, 1953.

6. Hodge, P. G., Jr., The rigid-plastic analysis of symmetrically loaded cylindrical shells, Journal of Applied Mechanics, Vol. 21, No. 4, Dec. 1954.

7. Onat, E. T., Plastic collapse of cylindrical shells under axially symmetric loading, Quarterly of Applied Mathematics, Vol. 13, 1955.

8. Onat, E. T. and Prager, W., Limit analysis of shells of revolution, Proceedings Royal Netherlands Academy of Science, B57, 1954.

9. Prager, W. and Hodge, P. G., Jr., Theory of perfectly plastic solids, John Wiley and Sons, Inc., New York 1951.

10. Hill, R., A variational principle of maximum plastic work in classical plasticity, Quarterly Journal Mechanics and Applied Mathematics, Vol. 1, 1948.

11. Prager, W., The general theory of limit design, Proceedings of the Eighth International Congress of Applied Mechanics (Istanbul) 1952, Vol. 2, 1956.

12. Mises, R. v., Mechanik der plastischen formaenderung von Kristallen, Zeitschrift fuer angewandte Mathemetik und Mechanik. Vol. 8, 1928.

13. Drucker, D. C., Some implications of work hardening and ideal plasticity, Quarterly of Applied Mathematics, Vol. 7, 1950.

14. Drucker, D. C., A more fundamental approach to plastic stress-strain relations, Proceedings First U. S. National Congress of Applied Mechanics (Chicago) 1951, J. W. Edwards, Ann Arbor, Michigan, 1952.

15. Hill, R., Plastic distortion of nonuniform sheets, Philosophical Magazine, Vol. 309 (1949).

Paper 1718 July, 1958 EM 3

Journal of the
ENGINEERING MECHANICS DIVISION
Proceedings of the American Society of Civil Engineers

EFFECTIVE WIDTH OF THIN RECTANGULAR PLATES

Morris Ojalvo,* A.M. ASCE and Frederick H. Hull**
(Proc. Paper 1718)

SUMMARY

The behavior of simply supported rectangular plates subjected to edge compression in one direction is investigated by means of load-shortening tests. The data are presented by non-dimensional curves and compared with the theoretic results of Levy(1) and Coan(2) and the experimental data of Sechler,(3) Winter,(4) and Lahde and Wagner.(5)

INTRODUCTION

Edge supported rectangular plates are subject to buckling when compressed by edge forces in the middle plane of the plate. The theoretic buckling stress when the load is parallel to a pair of opposite edges is given by:

$$\sigma_{CR.} = K \frac{E}{(1-\mu^2)} \frac{t^2}{b^2} \quad \mu, \neq \qquad (1)$$

The constant K depends upon the length ratio of the sides of the plate and the degree of rotational restraint at the edges. In actual tests buckles develop at stresses smaller than those given by equation (1) because of the deviations from flatness found in all real plates.

The buckling of a plate does not signify the limit of its load carrying capacity. After buckling the plate continues to carry increased loads but at reduced stiffness. That is, for any additional load increment the plate shortens at an increased rate. Meanwhile the average stress distribution over the thickness of the plate becomes non-uniform on any section

Note: Discussion open until December 1, 1958. To extend the closing date one month, a written request must be filed with the Executive Secretary, ASCE. Paper 1718 is part of the copyrighted Journal of the Engineering Mechanics Division, Proceedings of the American Society of Civil Engineers, Vol. 84, No. EM 3, July, 1958.

* Asst. Prof., Dept. of Civ. Eng., Princeton Univ.
** Asst. in Instruction, Dept. of Civ. Eng., Princeton Univ.

≠ All symbols are defined at the end of the paper.

transverse to the load with the larger compressive stresses at the edges of the plate. This has given rise to the effective width concept.[7] A useful definition for the effective width is given by equation (2):

$$b_e = \frac{P}{teE} \tag{2}$$

P is the load carried by the plate at a unit shortening of e.

The effective width is always smaller than the total width, b. Its significance may be seen if equation (2) is multiplied by $\frac{1}{b}$ and rearranged:

$$\frac{P/bt}{eE} = \frac{\sigma_{ave}/e}{E} = \frac{b_e}{b} \tag{3}$$

The ratio b_e to b equals the ratio of the secant modulus of the average stress-unit shortening curve of the plate to the modulus of the plate material. With this ratio known, it is possible to evaluate closely the contribution of compressed plate elements when they are part of semi-monocoque structures or occur in members formed of thin sheet metal. Theoretical analysis[1,2] shows that the unit longitudinal strain at the edges parallel to the compressive load is variable. "e" is the average value of the longitudinal unit strain over the length of one buckle. It may be evaluated by computing the unit shortening for a long plate having several buckles.

The plates tested were supported along the edges in a manner providing little rotational restraint. The longitudinal edges were allowed to move in the plane of the plate.

Description of the Test Procedure

Each of the two jigs used in the tests consisted of a six-inch I-beam with two guide bars (figure 1). Two of the I-beam flange edges, a, were carefully machined so that the surfaces were smooth and lay in the same plane. The outer surfaces of the I-beam flanges, b, were partly machined to provide a smooth surface for the guide bars, A, to bear upon. The surfaces, c, of the guide bars were carefully made plane so that the surfaces c and a could form the parallel sides of a groove along which the longitudinal edges of the plate slide. The bolts, B, clamp the guide bars in position to accommodate the different thicknesses of plate tested. A 1/4 inch base plate with a shallow slot cut in it keeps the lower edge of the plate in its plane while a 3/8 inch bar with a similar slot is used at the top of the plate (figure 2). The clearance with the jig at each end of this top bar was made as small as possible, it being about 1/32 of an inch for the thinnest (.025 inch) plates.

The plate material in all of the tests was 24S-T3 aluminum. The mechanical properties in compression were obtained from stress-strain curves of small coupons restrained from buckling. Some of the plate tests were conducted with the load parallel to the grain and some with load transverse to the grain. All of the plates were 5.80 inches wide. They were inserted into the

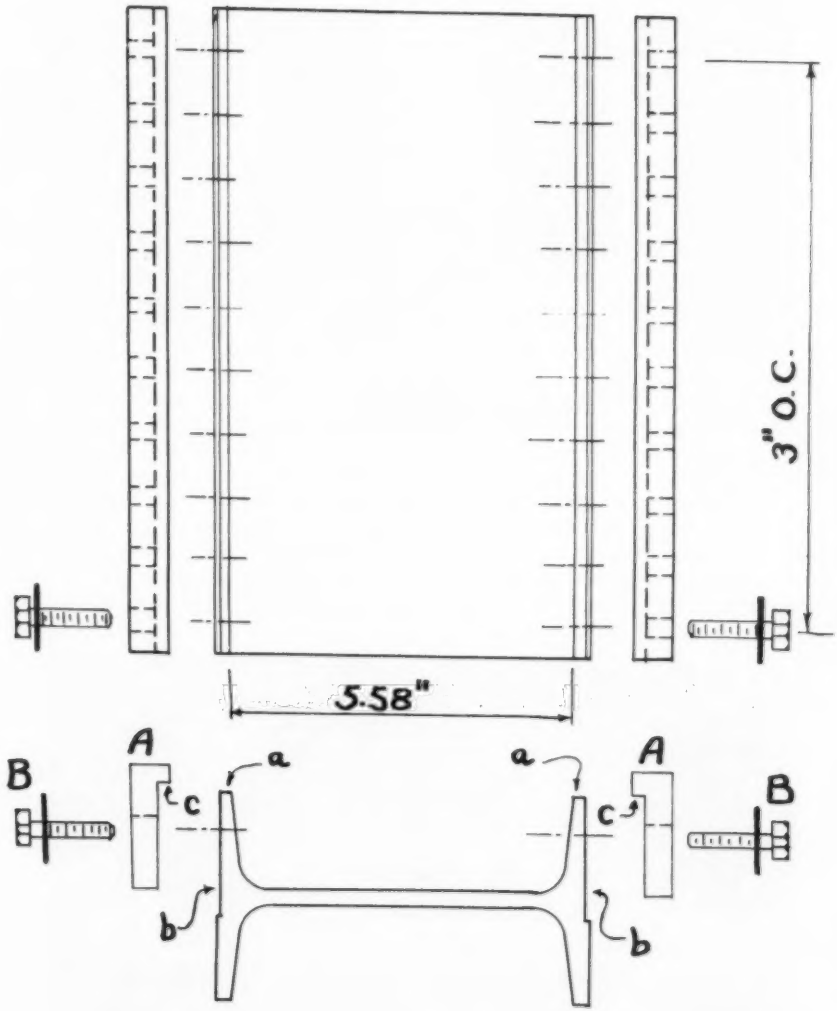

FIGURE 1

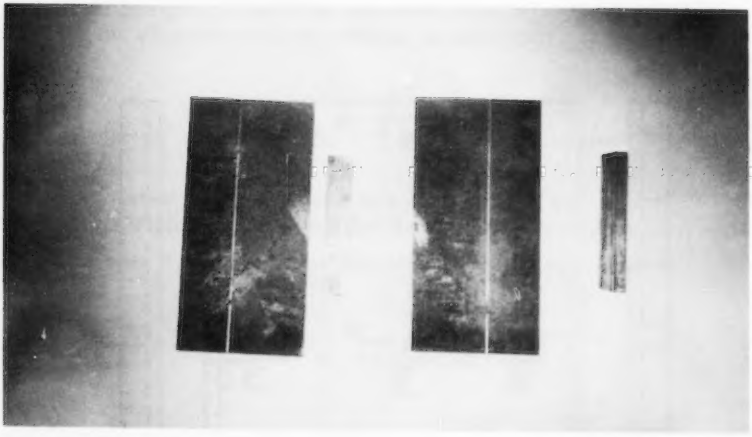

FIGURE 2

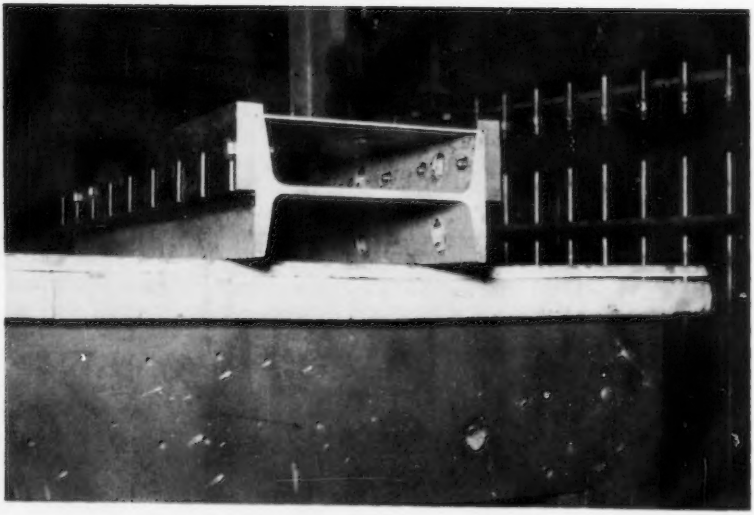

FIGURE 3

jig as shown in figure 3. Table 1 summarizes the dimensions of the test specimens and the mechanical properties as determined from the stress-strain curves of the coupon tests. In machining the plates special care was taken to make the ends parallel.

Figure 4 shows one of the long plates being tested. Dial gages reading directly to the nearest 1/10000 of an inch are placed in the plane of the plate to measure the shortening. A rigid bar, C, is placed between the loading head of the testing machine and the slotted top bar to fascilitate this measurement. In practically all cases the dial readings were in close agreement. The average was used to give the shortening. The testing machine was of 400,000 lb. capacity operating in the 0-16,000 lb. range. The least count on the load dial was 20 lbs.

Consideration was given to the possibility that a substantial portion of the load transferred to the jig by means of friction between the longitudinal edges of the beam and the grooves of the jig. This would mean that the load supported by the plate is greater at the top and that as a consequence the stiffness of the plate would appear greater than its true value. To minimize this effect the longitudinal edges were lubricated with Molykote type G thinned with a fine grease. To test the effectiveness of this procedure SR-4 type A-12 strain gages were attached to the front and back of a .082 inch thick plate at the locations shown in figure 5. These were wired to give the longitudinal strain in the middle plane of the plate. The proximity of the gages to the edges meant that the normal stresses in the transverse direction were small and that therefore the strain reading was a good measure of the longitudinal normal stresses. Before buckling took place the strain readings indicated practically no strain variation along the edges. For higher loads the strains in micro-inches are plotted against the load on the plate (figure 5). The maximum load of 4800 lbs. applied in this test was about half the load at failure. There is no indication that the readings obtained from the bottom gages are generally lower. The spread in readings is expected from the theory(2) which predicts variations in the longitudinal stress after buckling. The theory predicts much higher edge stresses at the center of a buckle as compared with edge stresses at a nodal line. The best indication that the frictional transfer was not large is found by comparison of the performance of the long (46.40 inches) plates with the short (23.85 inches) plates. In figures 6, 7, 8, and 9 where b_e/b is plotted against e/e_{cr}, the results for the long plates usually fall within the band of scatter established for all plates of the same width to thickness ratio.

Observed Behavior of the Loaded Plates

All of the plates showed buckles at loads smaller than the critical buckling load (figure 10). The buckles initially numbered 8 for the long plates and 4 for the short ones. As the load was further increased the amplitudes of the buckles increased and also the lengths of some of the buckles increased while others decreased. This behavior was followed by an increase in the number of buckles. Sometimes the increase in the number of buckles occurred with an audible snap.

In the case of one .025 inch thick plate, buckles near the edge were noticed in addition to the primary ones when the critical strain had been greatly exceeded. Figures 11 and 12 are photographs of this kind of buckling as viewed from two different angles.

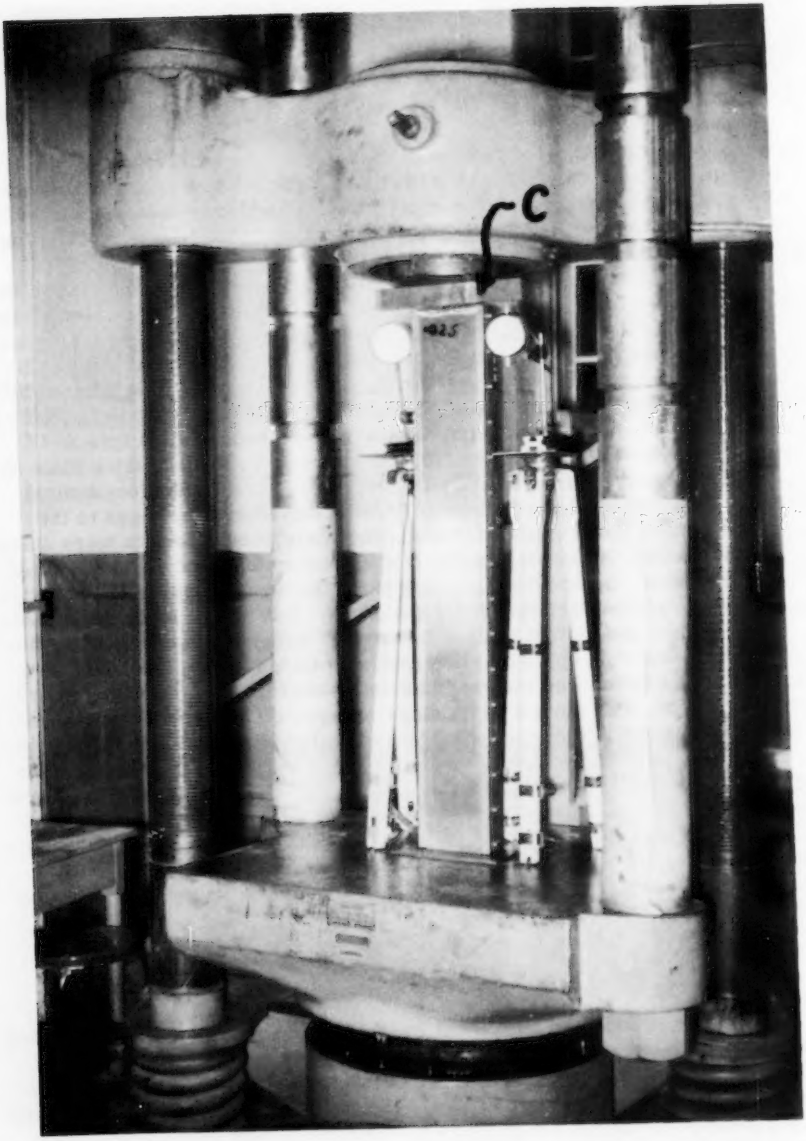

FIGURE 4

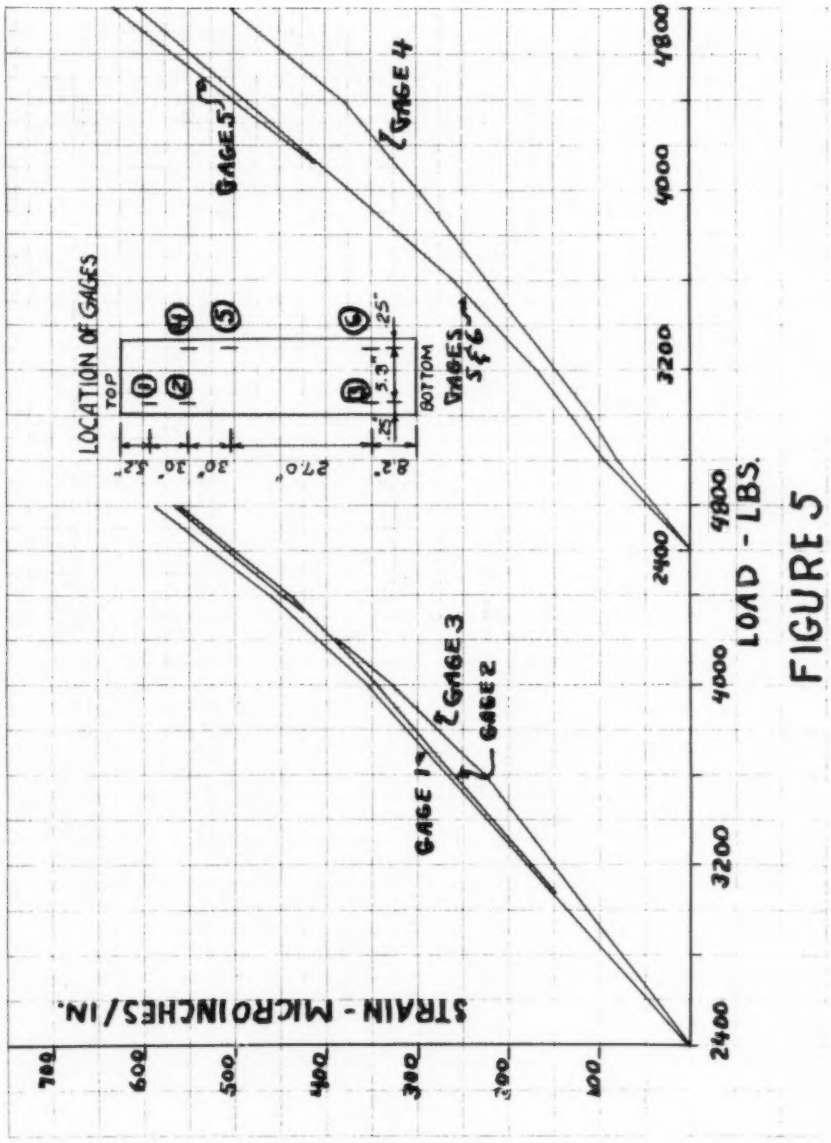
STRAIN - MICROINCHES/IN.
LOAD - LBS.
GAGE 1
GAGE 2
GAGE 3
GAGE 4
GAGE 5
GAGES 5 & 6
LOCATION OF GAGES
TOP
BOTTOM
82"
270"
30"
30"
82"
5.3"
25"
25"

FIGURE 5

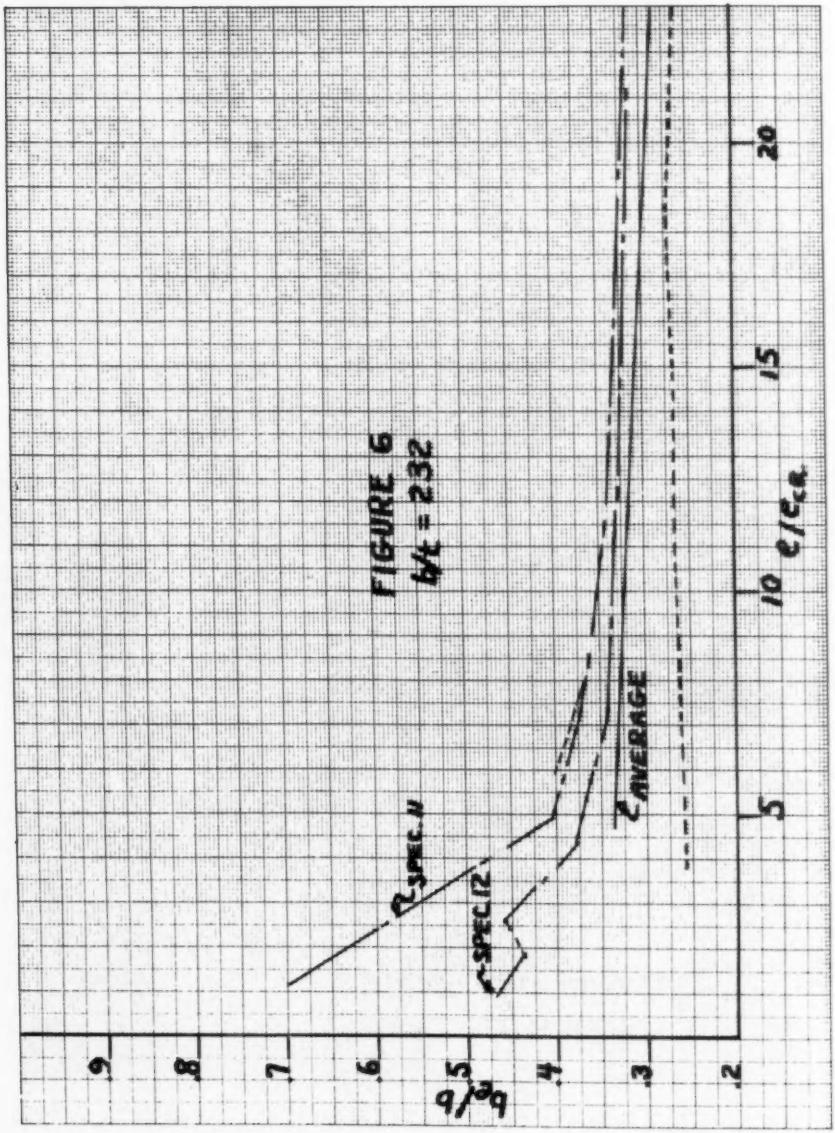
FIGURE 6
b/t = 232
SPEC. 11
SPEC. 12
AVERAGE
.9
.8
.7
.6
.5
.4
.3
.2
5
10
15
20
c/c.c.

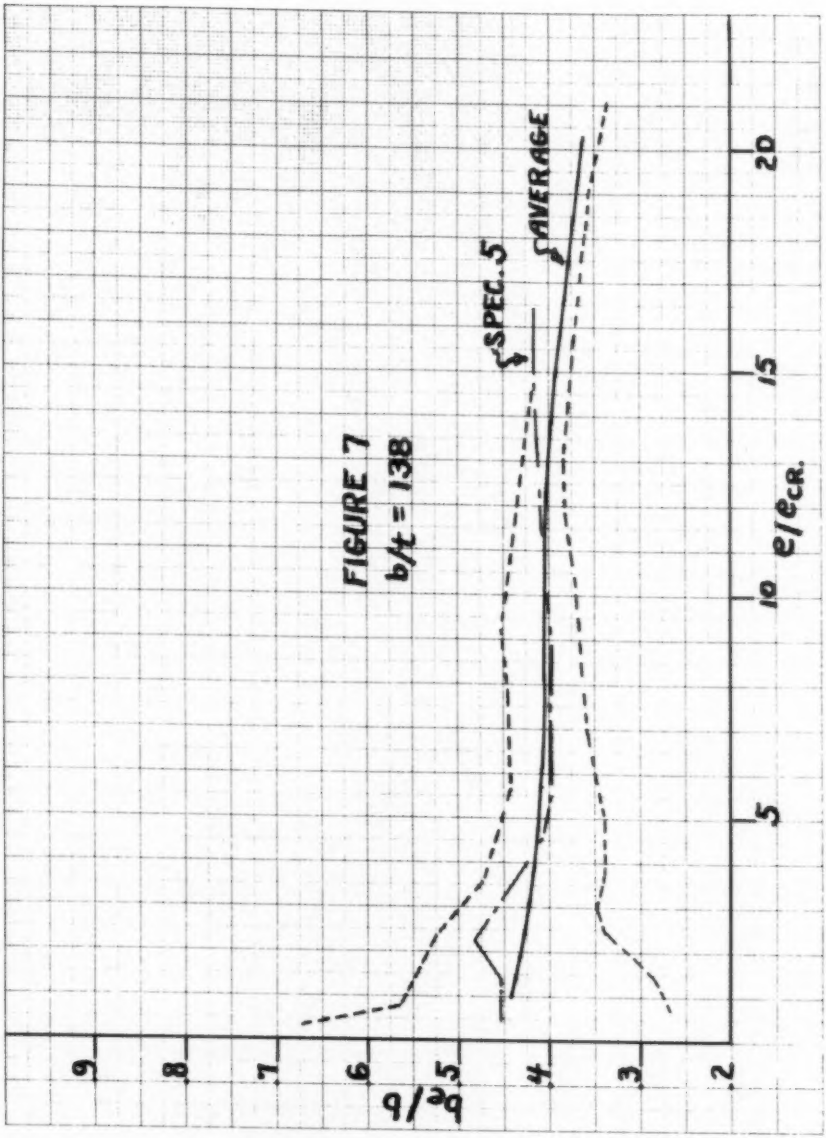
FIGURE 7
b/t = 138
SPEC. 5
AVERAGE
9
8
7
6
5
4
3
2
σ/σ0.5
5
10
15
20
e/eCR.

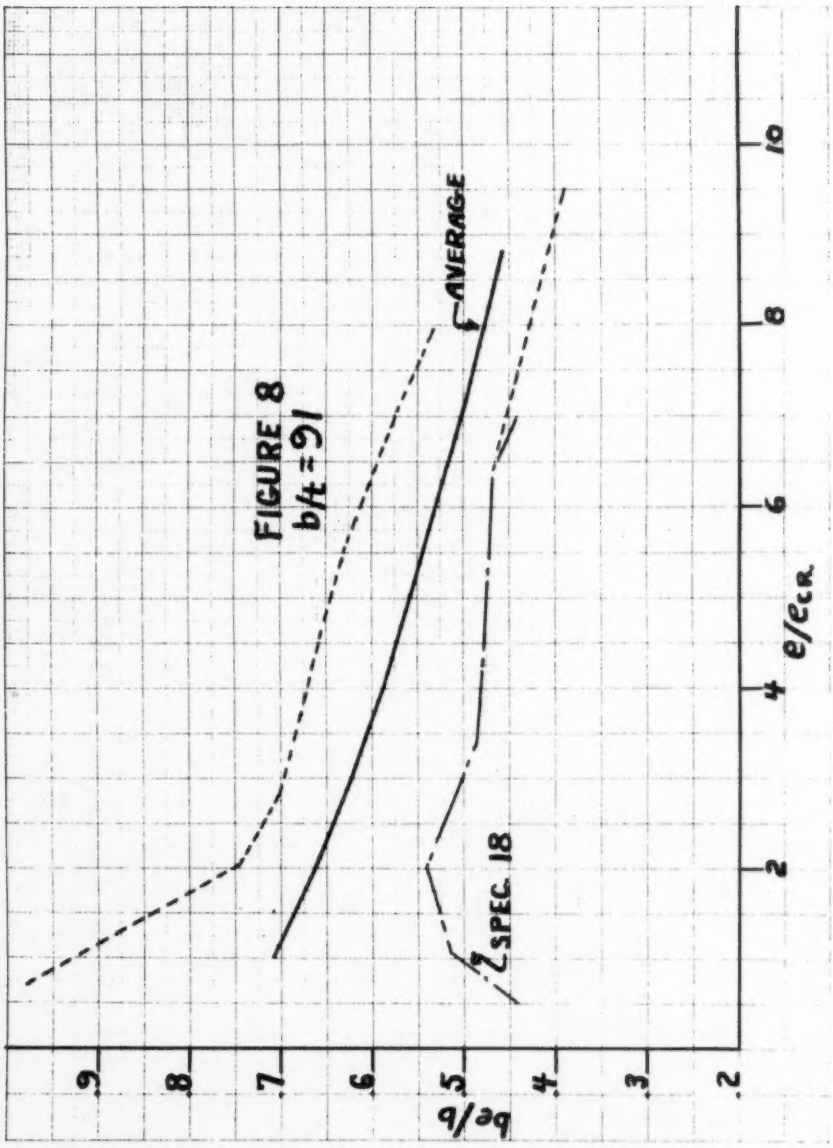
FIGURE 8
b/t = 91
AVERAGE
SPEC. 18
σ_e/σ_y
e/e_{cr}
.2
.3
.4
.5
.6
.7
.8
.9
2
4
6
8
10

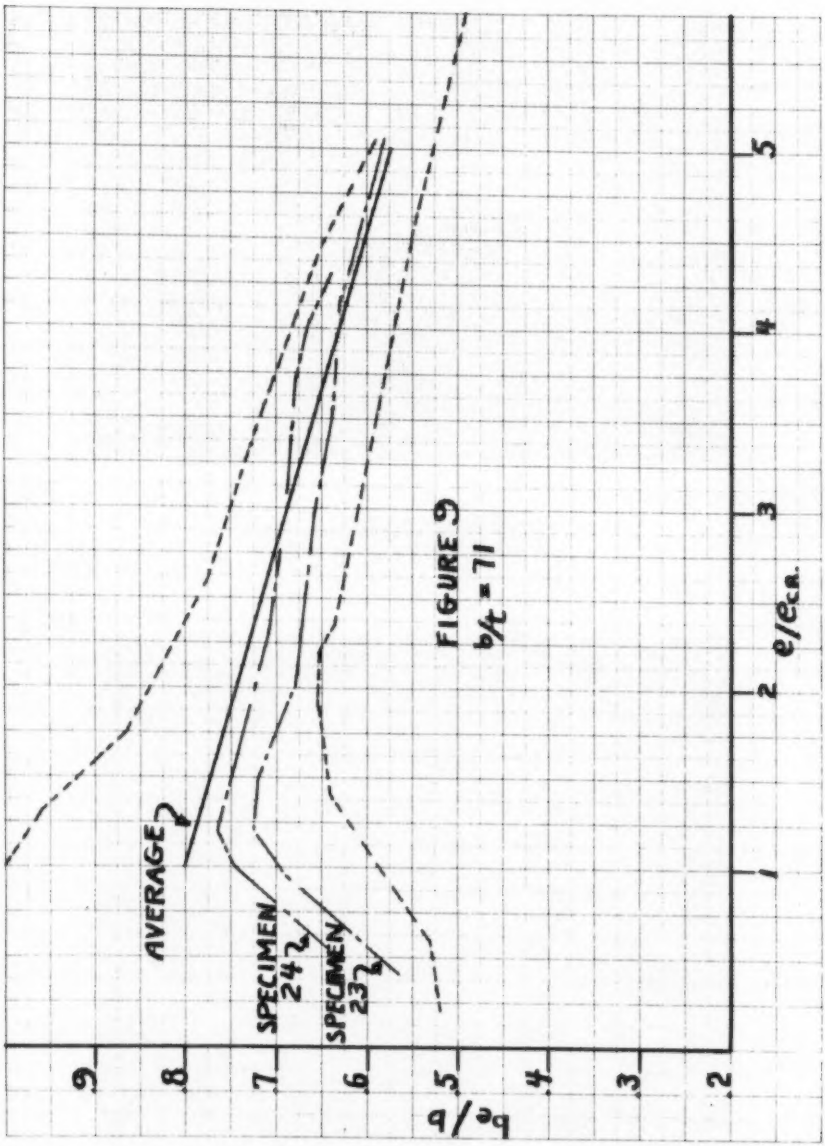
FIGURE 9
b/t = 71
AVERAGE
SPECIMEN 24
SPECIMEN 23
q/q_cr
e/e_cr
.2
.3
.4
.5
.6
.7
.8
.9
1
2
3
4
5

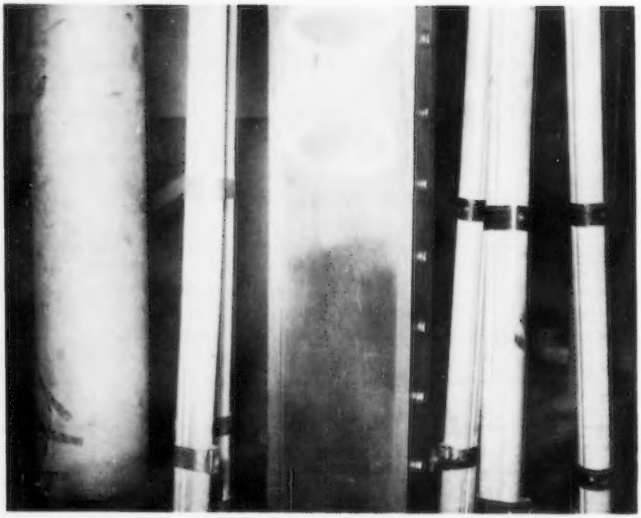

FIGURE 10

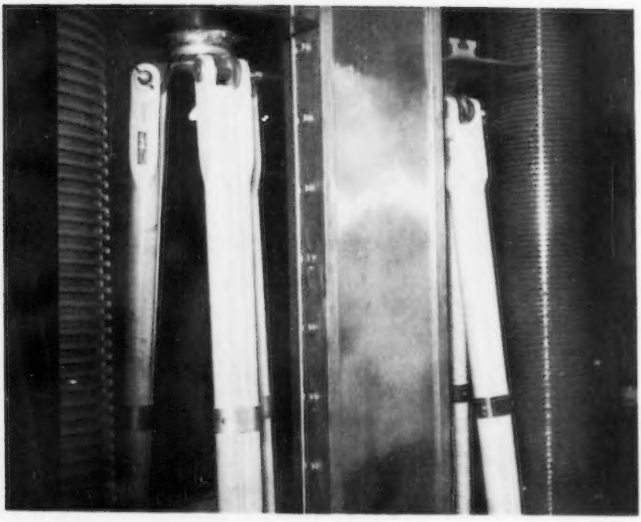

FIGURE 11

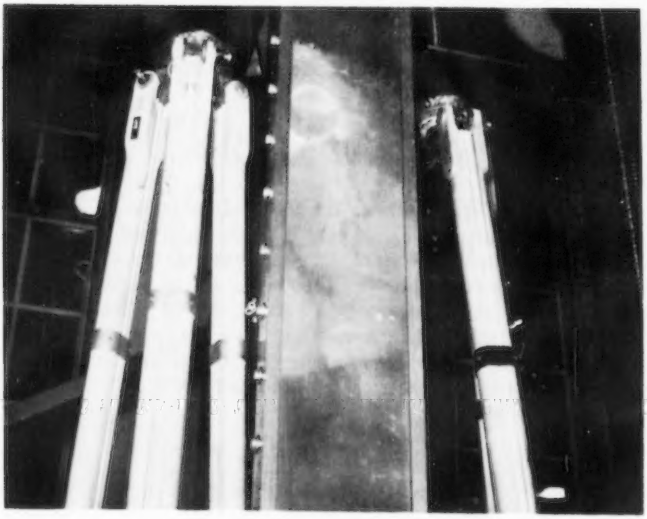

FIGURE 12

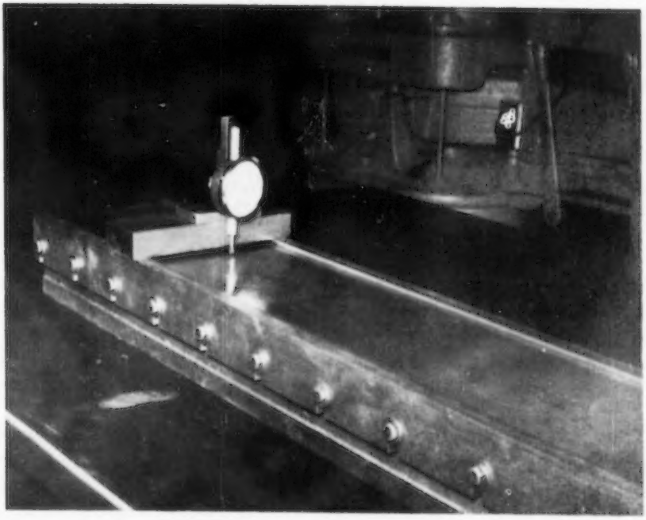

FIGURE 13

Failure was always due to a tearing at the top along longitudinal lines between the top bar and the grooves. The thicker plates showed a little of the buckled shape remaining throughout the length after removal of the specimen from the jig, thus indicating some plastic flow under combined stress at the higher values of the load.

Discussion of the Test Data

To determine the average stress the load was divided by the area based upon the full width (5.80 inches). It was felt that this was preferable to estimating the portion of the load carried by the edge strips within the grooves and basing the average stress on the free width of the plate. The portion of the width in the grooves is just under 4% of the entire plate width.

The critical buckling stress (theoretical) was taken as the buckling stress for a square plate simply supported along the edges. In the formula for it given below the full width (5.80 inches) was used for b:

$$\sigma_{CR.} = \frac{\pi^2 E}{3(1-\mu^2)} \frac{t^2}{b^2} \qquad (4)$$

Poissons ratio was taken as .32. The critical strain is determined by dividing the critical stress by the modulus of elasticity.

The test data are presented in figures 6, 7, 8 and 9 in non-dimensional form by plotting b_e/b against $e/e_{cr.}$. The solid lines represent an average curve while the band of scatter within the dotted lines includes the results of 5 to 7 load-shortening tests. The results of the tests on the long plates are indicated by dot-dash lines within the band of scatter. These are similar to the curves obtained from the tests on the shorter plates.

The wide band of scatter at low values of $e/e_{cr.}$ shows the influence of initial deviations of the plate from flatness. Theoretic work considering small, regular deflections of square plates(2,8) indicates that this is to be expected. Deflection measurements made in the manner shown by figure 13 were taken on one of the .025 inch plates and on one of the .082 inch plates. Maximum deflections were about 60% of the thickness for the .025 inch plate and 20% of the thickness for the .082 inch plate. The initial deflections were entirely on one side for the .082 inch plate. The .025 inch plate had deflections below the plate parallel to one longitudinal edge and above the plate parallel to the other edge.

Figure 14 compares the results of the present investigation (dotted curves) with other theoretical and experimental results. The tests of this paper give evidence of an additional dependence of the data on the b/t value. This effect does not manifest itself in the theoretical solutions and is not indicated in the results of other investigations.

At this point it is profitable to revue the boundary conditions assumed for obtaining the theoretical results and the methods used to obtain the experimental results of figure 14.

Levy's solution is for a square plate with the edges free of rotational restraint. All edges are constrained to remain straight, there are no shears on the edges, and there is no resultant transverse force on the longitudinal boundaries. He has obtained solutions for the displacement normal to the

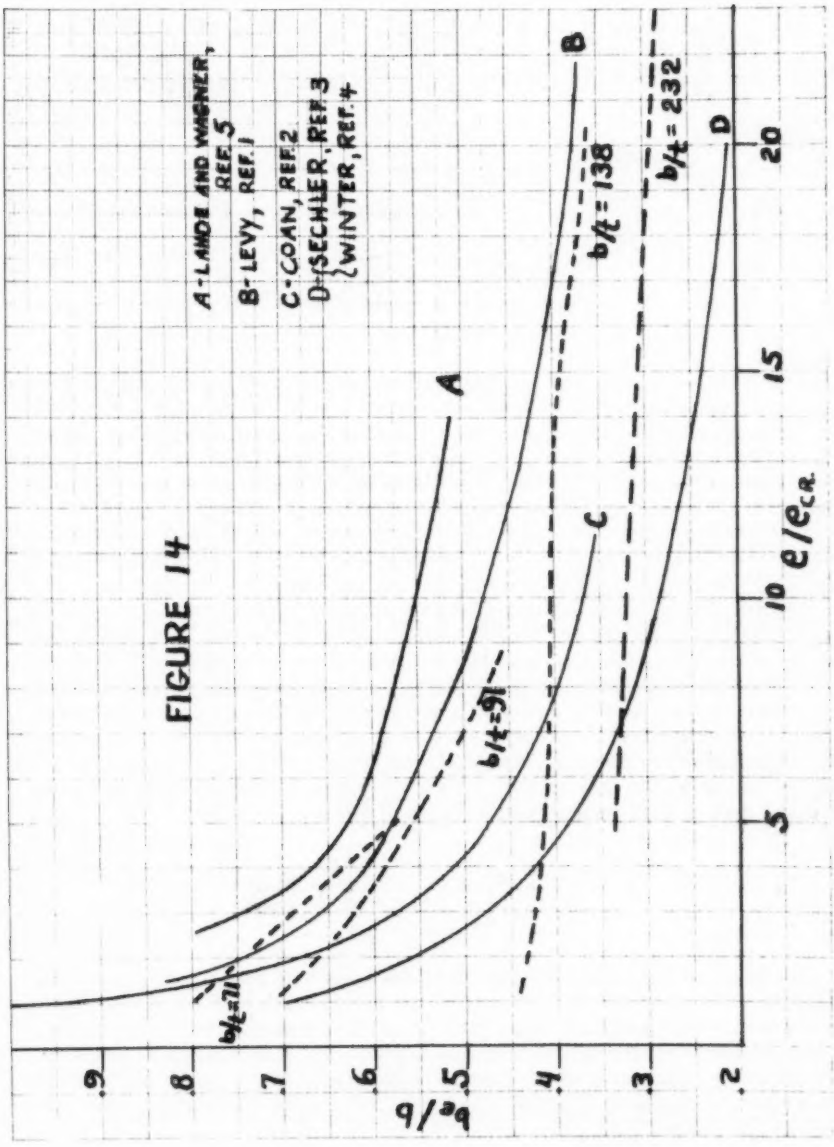
A-LANDIS AND WAGNER, REF. 5
B-LEVY, REF. 1
C-COAN, REF. 2
D-SECHLER, REF. 3
WINTER, REF. 4
A
B
C
D
b/t=11
b/t=91
b/t=138
b/t=232
.9
.8
.7
.6
.5
.4
.3
.2
σ/σ
5
10
15
20
e/e_cr

FIGURE 14

plate in terms of doubly infinite series for a number of different compressive loads. These satisfy the boundary conditions and Von Karman's two differential equations for the large deflection of plates:(9)

$$\left.\begin{aligned} \frac{\partial^4 F}{\partial x^4} + 2\frac{\partial^4 F}{\partial x^2 \partial y^2} + \frac{\partial^4 F}{\partial y^4} &= E\left(\frac{\partial^2 w}{\partial x\,\partial y}\right)^2 - \frac{\partial^2 w}{\partial x^2}\frac{\partial^2 w}{\partial y^2} \\ \frac{\partial^4 w}{\partial x^4} + 2\frac{\partial^4 w}{\partial x^2 \partial y^2} + \frac{\partial^4 w}{\partial y^4} &= \frac{t}{D}\left[\frac{\partial^2 F}{\partial y^2}\frac{\partial^2 w}{\partial x^2} + \frac{\partial^2 F}{\partial x^2}\frac{\partial^2 w}{\partial y^2} - 2\frac{\partial^2 F}{\partial x\,\partial y}\frac{\partial^2 w}{\partial x\,\partial y}\right] \end{aligned}\right\} \quad (5)$$

The results were obtained by assuming all but the most significant six terms of the series to be equal to zero. The error due to this is quite insignificant.

Coan's solution differs from Levy's in that the longitudinal edges are not constrained to remain straight. This corresponds most closely to the present tests. In this solution only three terms of the series are assumed to be different from zero. This too is believed to introduce only minor errors.

Sechler's results were obtained by compressing simply supported plates to failure. The effective width was determined by dividing the load at failure by the product of the yield strength and the thickness.

Winter evaluated the effective width by testing beams made of thin gage sheet metal. In the elastic range the location of the neutral axis was determined from the assumption that the strain is linear over the depth of the beam. The effective width of the compression flange was then evaluated from the condition that the neutral axis was also the centroidal axis of the section. In the plastic range a stress distribution as in a plastic hinge was assumed and the effective width was computed from the condition that the resultant of horizontal forces on the transverse section disappears. The equation that best fits the data of both Sechler's and Winter's tests is given by:

$$\frac{b_e}{b} = \frac{e_{cr.}}{e} - .298\,\frac{e_{cr.}}{e} \quad (6)$$

The tests of Lahde and Wagner were made on long plates with the edges fixed against rotation. The changes in the plate length in the longitudinal and in the transverse direction were measured. The load carried by the plate on a transverse section was computed from numerous slope measurements on the surface of the plate. Since there are shearing forces on the edges of the plate the computations give the average values for the longitudinal load carried by the plate.

CONCLUSIONS

1. Initial deflections of plates having the same width to thickness ratios cause large variations in the effective widths at low values of $e/e_{cr.}$. As $e/e_{cr.}$ becomes larger the variation in the effective width grows smaller.

2. In general, for any value of $e/e_{cr.}$ the value of b_e/b will be larger the lower the width to thickness ratio of the plate.

3. The results of Sechler's and Winter's tests are conservative for design purposes except when b/t is large and $e/e_{cr.}$ is small.

4. It is desirable that further tests include:

   a) extensive determinations of the initial deflections for the purpose of correlating the behavior of the plate with the magnitude and shape of the initial deflections;

   b) specimens having the same b/t ratios as in these tests but different widths and thicknesses.

Symbols

b - width of the plate normal to the direction of the load.

b_e - effective width of plate.

D - plate constant equal to $\frac{E\,t^3}{12(1-u^2)}$.

E - modulus of elasticity.

e - unit shortening of the plate in the longitudinal direction over a length of one buckle.

$e_{cr.}$ - $\sigma_{cr.}$ divided by the modulus of elasticity.

F - stress function.

K - constant.

P - compressive load carried by the plate.

t - plate thickness.

w - displacement of the middle surface of a plate perpendicular to its plane.

x - coordinate.

y - coordinate.

u - poissons ratio.

σ_{ave} - average compressive stress over entire width of plate, b.

$\sigma_{cr.}$ - the critical stress at buckling (theoretical) for a square flat plate simply supported at the edges and under uniaxial edge compression.

REFERENCES

1. Levy, Samuel: Bending of Rectangular Plates with Large Deflections NACA TN No. 846, 1942.

2. Coan, J. M.: Large - Deflection Theory for Plates with Small Initial Curvature Loaded in Edge Compression. Journal of Applied Mechanics, Vol. 18, 1951.

3. Sechler, E. E.: The Ultimate Strength of Thin Flat Sheet in Compression, Publication 27, Guggenheim Aeronautics Laboratory, Calif. Inst. of Tech., 1933.

4. Winter, G.: Strength of Thin Steel Compression Flanges, Transactions of the American Society of Civil Engineers, Vol. 112, 1947.

5. Lahde, R. and Wagner, H.: Experimental Studies of the Effective Width of Buckled Sheets, NACA TM No. 814, Translation from Luftfahrtforschung Vol. 13, 1936.

6. Roark, R. J.: Formulas for Stress and Strain, Third Edition, p. 312, McGraw Hill Book Co., 1954.

7. Von Karman, T., Sechler, E. E., and Donnell, L. H.: The Strength of Thin Plates in Compression, ASME Trans., APM-54-5, Vol. 54, 1932.

8. Hu, P. C., Lundquist, E. E., and Batsdorf, S. B.: Effect of Small Deviations from Flatness on Effective Width and Buckling of Plates in Compression, NACA TN No. 1124, 1946.

9. Timoshenko, S.: Theory of Elastic Stability, McGraw Hill Book Co., pp. 321-323, 1936.

BIBLIOGRAPHY

Schuman, L. and Back, G.: Strength of Rectangular Flat Plates Under Edge Compression, NACA Report No. 356, 16th Annual Report, 1930.

Cox, H. L.: Buckling of Thin Plates in Compression, Air Ministry R&M No. 1554, 1933.

Marguerre, K.: The Apparent Width of the Plate in Compression, NACA TM No. 833, Translation from Luftfahrtforschung Vol. 14, 1937.

Jackson, K. B. and Hall, A. H.: Curved Plates in Compression, National Research Council of Canada AR-1, 1947.

Jackson, K. B. and Hall, A. H.: Experimental Diagrams of Deformation and Strain Distribution in Curved Plates under Compression, National Research Council of Canada AR-9, 1951.

TABLE I

Specimen	Length (inches)	Width (inches)	Thickness (inches)	Young's Modulus x 10^{-6} P.S.I.	Proportional Limit x 10^{-3} P.S.I.	Yield Strength .2% Offset x 10^{-3} P.S.I.	Load to Grain Direction
1	23.85	5.80	.042	10.8	31.5	45.3	Parallel
2	23.85	"	.042	"	31.5	45.3	Parallel
3	23.85	"	.042	"	31.5	45.3	Parallel
4	23.85	"	.042	"	31.5	45.3	Parallel
5	46.40	"	.042	"	31.5	45.3	Parallel
6	23.85	"	.025	10.7*			Parallel
7	23.85	"	.025	" *			Perpendicular
8	23.85	"	.025	" *			Parallel
9	23.85	"	.025	" *			Perpendicular
10	23.85	"	.025	" *			Parallel
11	46.40	"	.025	" *			Parallel
12	46.40	"	.025	" *			Parallel

* No stress-strain test conducted. Value assumed.

TABLE I (Continued)

Specimen	Length (inches)	Width (inches)	Thickness (inches)	Young's Modulus x 10^{-6} P.S.I.	Proportional Limit x 10^{-3} P.S.I.	Yield Strength .2% Offset x 10^{-3} P.S.I.	Load to Grain Direction
13	23.85	5.80	.064	11.1	29.5	43.8	Parallel
14	23.85	"	.064	11.1	29.5	43.8	Parallel
15	23.85	"	.064	11.0	33.2	49.7	Perpendicular
16	23.85	"	.064	11.1	29.5	43.8	Parallel
17	23.85	"	.064	11.0	33.2	49.7	Perpendicular
18	46.40	"	.064	11.1	29.5	43.8	Parallel
19	23.85	"	.082	10.7	29.0	42.5	Parallel
20	23.85	"	.082	10.7	29.0	42.5	Parallel
21	23.85	"	.082	10.5	31.4	46.4	Perpendicular
22	23.85	"	.082	10.7	29.0	42.5	Parallel
23	46.40	"	.082	10.7	29.0	42.5	Parallel
24	46.40	"	.082	10.7	29.0	42.5	Parallel

Paper 1719 July, 1958 EM 3

Journal of the
ENGINEERING MECHANICS DIVISION
Proceedings of the American Society of Civil Engineers

BENDING OF ELASTICALLY SUPPORTED RECTANGULAR PLATES

Melvin Zaid and Marvin Forray*
(Proc. Paper 1719)

NOMENCLATURE

$B_{Km}^{(1)} = \dfrac{2(1-\nu)\gamma_K^3}{\left[1+\left(\frac{\gamma_K}{g_m}\right)^2\right]^2} \sinh \gamma_K a$

$B_{Km}^{(2)} = \dfrac{2(1-\nu)g_K^3}{\left[1+\left(\frac{g_K}{\gamma_m}\right)^2\right]^2} \sinh g_K b$

$D = \dfrac{Eh^3}{12(1-\nu^2)}$

E = Modulus of Elasticity in Tension and Compression

$F_m = -\dfrac{A'_m}{r_m D}$

$g_m = \dfrac{m\pi}{a}$

h = Plate Thickness

$K_m^i = \dfrac{(EI)_o^i}{D}\Gamma_m^i(\gamma_m^i)^4$ (i. A, B, C, D)

$M = \dfrac{4D\alpha t}{ah}(1-\nu^2)$

Note: Discussion open until December 1, 1958. To extend the closing date one month, a written request must be filed with the Executive Secretary, ASCE. Paper 1719 is part of the copyrighted Journal of the Engineering Mechanics Division, Proceedings of the American Society of Civil Engineers, Vol. 84, No. EM 3, July, 1958.

* Scientific Research Staff, Republic Aviation Corporation, Farmingdale, N. Y.

$$r_m = \gamma_m^3 \left\{ (3+\nu)\cosh \gamma_m a + \frac{(1-\nu)\gamma_m a}{\sinh \gamma_m a} \right\}$$

$$R_m = g_m b \coth g_m b + \frac{2}{1-\nu}$$

$$\Delta_m = [(1+\nu) + \rho_m (1-\nu)]\, \gamma_m^3$$

t = TEMPERATURE DIFFERENCE $= t\left(\frac{h}{2}\right) - t\left(-\frac{h}{2}\right)$

$$t_m = g_m^3 \left\{ (3+\nu)\cosh g_m b + \frac{(1-\nu)\, g_m b}{\sinh g_m b} \right\}$$

W = DEFLECTION

$$W_m = [(1+\nu) + R_m (1-\nu)]\, g_m^3$$

α = COEFFICIENT OF LINEAR EXPANSION

$$\alpha_m = \frac{m\pi b}{2a}$$

$$\gamma_m = \frac{m\pi}{b}$$

ν = POISSON'S RATIO

$$\rho_m = \frac{2}{1-\nu} + \gamma_m a \coth \gamma_m a$$

ABSTRACT

The problem of bending of a rectangular plate, elastically supported on variable rigidity beams, subjected to a transverse loading or temperature gradient is solved in this paper.

Specific combinations of support are examined and, in addition, a detailed solution is given for a square plate with one edge free.

INTRODUCTION

The problem of the bending of an elastically supported rectangular plate subjected to transverse loading or to temperatures varying linearly through the thickness will be considered in this paper. The plate is assumed to be supported on beams which in turn are simply supported at their ends. The four beams may have variable rigidity along their length, and this rigidity may vary from beam to beam. The deflection is determined and from this the

moments and stresses can be readily calculated according to the classical theory[1] of thin plates. The plane stress problem, associated with the symmetric component of the thermal gradient will not be considered here.

The method of solution is to consider the superposition of deflections of the following:

1. Rectangular plate, simply supported on all four edges, subjected to the given temperature distribution or loading system.

2. Rectangular plate, subjected to an arbitrary line load on one edge and simply supported on the other three edges.

3. Simply supported beam of variable rigidity, subjected to an arbitrary load distribution.

The satisfaction of equilibrium and compatibility along the plate edges yields the unknown line loads, from which the complete solution can be obtained.

Solutions have been previously obtained[1, 2, 3, 4, 5] for the plate under transverse loading and supported by constant cross section beams arranged either in grid like fashion, or paired in such a manner as to have equal rigidities on opposite plate edges. This paper represents a generalization of the edge supported plate to include thermal gradients and arbitrarily assigned variable cross section supports.

The technique of superposition of various elementary problem types leads to an understanding of the nature of the support reaction, which in turn points up and allows detailed investigation of certain difficulties inherent in the thermal problem. In addition this technique is useful in the establishment and evaluation of the accuracy of approximations, and in obtaining separate checks of the numerical calculations. Alternatively, the boundary conditions may be written in terms of the total deflection and its associated derivatives. The latter approach was used in some of the references indicated above and involves no essential difference in solution techniques.

Theory

A. Fundamental Solutions

1. Simply Supported Plate

The plate is referred to a cartesian coordinate system (Figure 1). The positive z-direction is assumed to be taken into the plane of the paper.

a) General Loading

This problem has been completely explored[1] and need not be considered here. It is only important to note that the stress, deflection and edge reactions can be found for this case.

b) Temperature Gradient

The problem of a simply supported rectangular plate subjected to a temperature distribution varying linearly through the thickness has been solved.[1] If the plate is referred to the coordinates of Figure 1, the solution takes the form

$$w_{s.s.} = \frac{\alpha t (1+\nu)}{h}\left\{\frac{(a-x)x}{2} - \frac{4a^2}{\pi^3}\sum_{m=1,3,\cdots}^{\infty} \frac{\sin g_m x \cosh g_m (y-\frac{b}{2})}{m^3 \cosh \alpha_m}\right\} \quad (1)$$

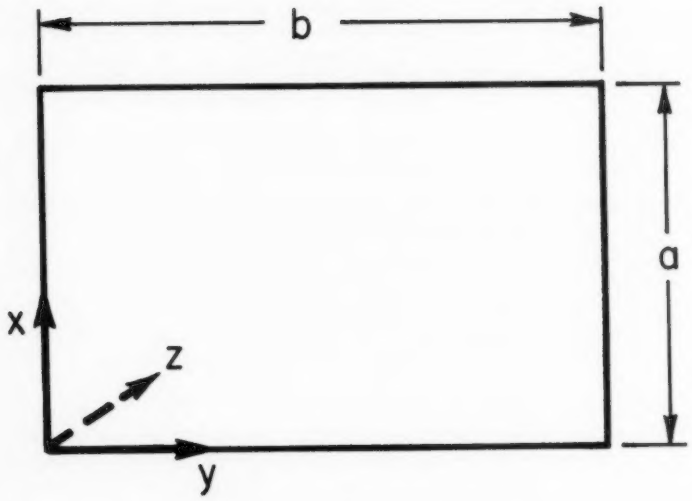

Fig. 1. Simply Supported Plate

$t > 0$ implies that the deflection will be in the positive z direction.

Using the deflection function given by equation (1), the distributed line reactions can be determined.(1) This will be done only for $V_x\big]_{x=a}$ but can be generalized for each line loading. Thus

$$V_x\big]_{x=a} = -D\left[W_{xxx} + (2-\nu)W_{xyy}\right]_{x=a} \tag{2}$$

Differentiation of each infinite series can be performed termwise since each successive resulting series converges uniformly(6) in any chosen closed subinterval of the interval $o<y<b$. Thus

$$V_x\big]_{x=a} = -M\sum_{m=1,3\cdots}^{\infty} \frac{\cosh g_m\left(y-\frac{b}{2}\right)}{\cosh \alpha_m} \tag{3}$$

The expression (3) represents the line reactions at all points except at the corners. The corner reactions can be determined from equilibrium considerations along each edge, and will not be discussed further here.

The Fourier sine expansion of the line reactions along the edges will be obtained for future use. Due to the non-uniform convergence(6) of the series representing this reaction V over $o\leq y\leq b$ the coefficients of the Fourier sine series cannot be determined by interchanging the order of summation and integration. To by-pass this difficulty, use is made of the fact that the series (3) converges uniformly in any closed subinterval of the region $o<y<b$.

Therefore the function $[V_x]_{x=a}$ may be approximated to any prescribed degree of accuracy over a given sub-interval by replacing the right hand side of equation (3) by a finite series (see Appendix A). All of the ensuing steps for the determination of the coefficients of the Fourier series are then valid. Thus equation (3) can be replaced by

$$V_x]_{x=a} = -M\sum_{m=1,3,\cdots}^{2N-1} \frac{\cosh g_m(y-\frac{b}{2})}{\cosh \alpha_m} \tag{4}$$

This can be represented in the open interval $o<y<b$ in the terms of the sine series as,

$$V_x]_{x=a} = \sum_{m=1,2,\cdots}^{\infty} A_m \sin \gamma_m y \tag{5}$$

where the A_m are determined from

$$A_m = \frac{2}{b}\int_o^b V_x]_{x=a} \sin \gamma_m y \, dy \tag{6}$$

Combining equations (5) and (6) and interchanging the order of the finite summation and integration there results,

$$A_m = -\frac{4M}{b\gamma_m}\sum_{m=1,3,\cdots}^{2N-1} \frac{1}{1+\left(\frac{g_m}{\gamma_m}\right)^2} \qquad (m = 1,3,5,\cdots) \tag{7}$$

$$A_m = 0 \qquad (m = 2,4,6,\cdots) \tag{8}$$

2. Edge Loaded Rectangular Plate

The deflection of a rectangular plate (Fig. 2) loaded along one edge and simply supported along the other three edges will now be discussed.

Subject to the basic differential equation and the boundary conditions of zero moment everywhere and zero deflection along the supported edges, and in addition

$$V_x]_{x=a} = -D\left[W_{xxx} + (2-\nu)W_{xyy}\right]_{x=a} = \sum_{m=1,2,\cdots}^{\infty} A'_m \sin \gamma_m y \tag{9}$$

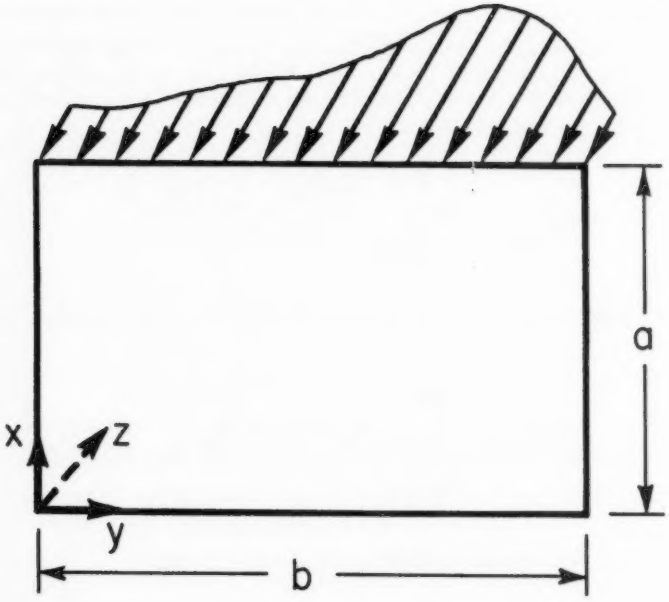

Fig. 2. Edge Loaded Rectangular Plate.

along the loaded edge (x=a), where A_m' are the Fourier coefficients associated with the line loadings there results,

$$w = \sum_{m=1,2,\cdots}^{\infty} F_m \left(\gamma_m x \cosh \gamma_m x - \rho_m \sinh \gamma_m x \right) \sin \gamma_m y \quad (10)$$

From equations (9) and the definition of F_m the distributed line force along the edge A (x=a) is

$$V_x\Big]_{x=a} = V_A^A = -D \sum F_m r_m \sin \gamma_m y \quad (11)$$

Let V_j^i represent the line load along edge j due to a line load along i, where positive V implies the loading in the direction of positive z on each edge. Then, with this convention,(1)

$$V_B^A = -D\left[W_{yyy} + (2-\nu)\, W_{yxx}\right]_{y=b}$$

$$V_C^A = +D\left[W_{xxx} + (2-\nu)\, W_{xyy}\right]_{x=0} \qquad (12)$$

$$V_D^A = +D\left[W_{yyy} + (2-\nu)\, W_{yxx}\right]_{y=0}$$

By direct calculation, from equations (10) and (12)

$$V_B^A = -D\sum_m (-1)^{m+1} \gamma_m^3 F_m \left\{\left[\rho_m(1-\nu) - 2(2-\nu)\right]\sinh \gamma_m x - (1-\nu)\gamma_m x \cosh \gamma_m x\right\}$$

$$V_C^A = D\sum_m F_m \delta_m \sin \gamma_m y \qquad (13)$$

$$V_D^A = -D\sum_m \gamma_m^3 F_m \left\{\left[\rho_m(1-\nu) - 2(2-\nu)\right]\sinh \gamma_m x - (1-\nu)\gamma_m x \cosh \gamma_m x\right\}$$

B. General Solution-Elastically Supported Plate

The general problem of a rectangular plate with four edges elastically supported, subjected to an arbitrary load or thermal gradient, will not be investigated. This is solved by the successive superposition of the three types of structures shown in Figures 3(a), to 3(c) inclusive. Two conditions must be met at each edge of the plate. These are:

1. The deflection of the edge of the plate must be identical with the deflection of the supporting beam (condition of compatibility).

2. The distributed line reaction along each edge must be supplied by the beam, so that the corresponding load on the supporting beam must be equal and opposite (condition of equilibrium).

These conditions are satisfied in equations (14) and (15) below,
Compatibility:

$$(W_{Plate})_i = (W_{Beam})_i \qquad (i = A, B, C, D) \qquad (14)$$

Equilibrium:

$$(V_{s.s.})_i + V_i^A + V_i^B + V_i^C + V_i^D + (V_{Beam})_i = 0 \qquad (15)$$

Where all loads are considered positive in the direction of positive z.

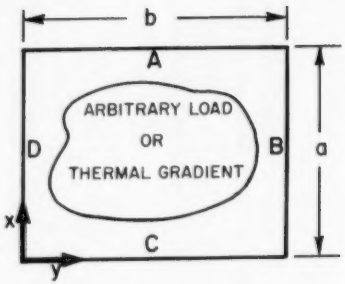

(a) Simply Supported Plate

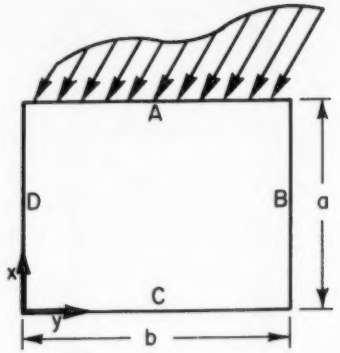

(b) Line Loaded Plate–
Other Edges Simply Supported

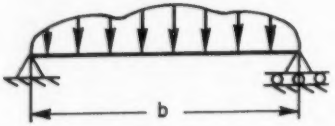

(c) Simply Supported Beam–Transversely Loaded

Fundamental Problems to be Superposed

Fig. 3

The subscript i refers to the edge being considered and the superscript refers to the loaded edge which defines the structure associated with figure 3(b).

The effects of a line load along edge A can be obtained from equations (10), (11) and (13).

The effect of a line load along B may be obtained most directly from Figure 3(b) and the associated equations (11), and (13), if (x, y) and (a, b) are replaced respectively by (y, x) and (b, a).

With reference to Figures 3(b) and 4, the reactions and displacements due to a line load along C [x', y coordinates] will be identical in form to those obtained for the plate loaded along A [x, y coordinates . The x' coordinate may be eliminated through the transformation x' = a - x.

The effect of a line load along D may be obtained from the result for a line load along C in exactly the same manner as B was obtained from A.

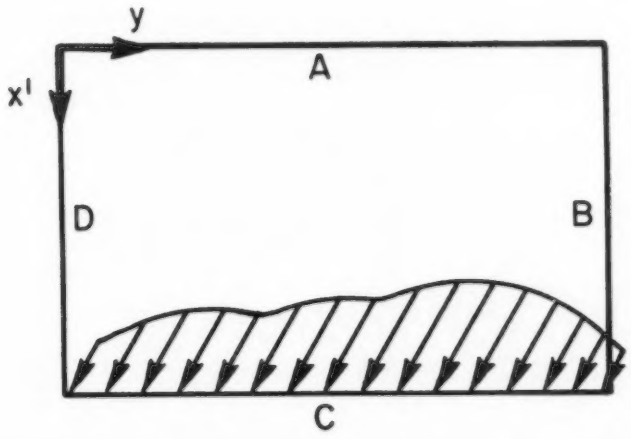

Fig. 4. Line Loaded Plate Referred to x' y Coordinate System.

This leads to

$$W^A = \sum_m F_m^A \left\{ \gamma_m x \cosh \gamma_m x - \rho_m \sinh \gamma_m x \right\} \sin \gamma_m y$$

$$W^B = \sum_m F_m^B \left\{ g_m y \cosh g_m y - R_m \sinh g_m y \right\} \sin g_m x \qquad (16)$$

$$W^C = \sum_m F_m^C \left\{ \gamma_m (a-x) \cosh \gamma_m (a-x) - \rho_m \sinh \gamma_m (a-x) \right\} \sin \gamma_m y$$

$$W^D = \sum_m F_m^D \left\{ g_m (b-y) \cosh g_m (b-y) - R_m \sinh g_m (b-y) \right\} \sin g_m x$$

$$V_A^A = -D\sum_m F_m^A r_m \sin \gamma_m y$$

$$V_B^B = -D\sum_m F_m^B t_m \sin q_m x$$

$$V_c^C = -D\sum_m F_m^C r_m \sin \gamma_m y$$

$$V_D^D = -D\sum_m F_m^D t_m \sin q_m x$$

$$V_C^A = D\sum_m F_m^A s_m \sin \gamma_m y \qquad (17)$$

$$V_D^B = D\sum_m F_m^B w_m \sin q_m x$$

$$V_A^C = D\sum_m F_m^C s_m \sin \gamma_m y$$

$$V_B^D = D\sum_m F_m^D w_m \sin q_m x$$

$$V_B^A = -D\sum_m (-1)^{m+1} \gamma_m^3 F_m^A \left\{[\rho_m(1-\nu)-2(2-\nu)]\sinh \gamma_m x - (1-\nu)\gamma_m x \cosh \gamma_m x\right\}$$

$$V_D^A = -D\sum_m \gamma_m^3 F_m^A \left\{[\rho_m(1-\nu)-2(2-\nu)]\sinh \gamma_m x - (1-\nu)\gamma_m x \cosh \gamma_m x\right\}$$

$$V_B^C = -D\sum_m (-1)^{m+1} \gamma_m^3 F_m^C \left\{[\rho_m(1-\nu)-2(2-\nu)]\sinh \gamma_m(a-x) - (1-\nu)\gamma_m(a-x)\cosh \gamma_m(a-x)\right\} \qquad (18)$$

$$V_D^C = -D\sum_m \gamma_m^3 F_m^C \left\{[\rho_m(1-\nu)-2(2-\nu)]\sinh \gamma_m(a-x) - (1-\nu)\gamma_m(a-x)\cosh \gamma_m(a-x)\right\}$$

$$V_A^B = -D\sum_m (-1)^{m+1} q_m^3 F_m^B \left\{[R_m(1-\nu)-2(2-\nu)]\sinh q_m y - (1-\nu) q_m y \cosh q_m y\right\}$$

$$V_c^B = -D\sum_m g_m^3 F_m^B \left\{\left[R_m(1-\nu) - 2(2-\nu)\right]\sinh g_m y - (1-\nu) g_m y \cosh g_m y\right\}$$

$$V_A^D = -D\sum_m (-1)^{m+1} g_m^3 F_m^D \left\{\left[R_m(1-\nu) - 2(2-\nu)\right]\sinh g_m (b-y) - (1-\nu) g_m (b-y) \cosh g_m (b-y)\right\}$$

$$V_c^D = -D\sum_m g_m^3 F_m^D \left\{\left[R_m(1-\nu) - 2(2-\nu)\right]\sinh g_m (b-y) - (1-\nu) g_m (b-y) \cosh g_m (b-y)\right\}$$

where

W^i = Deflection of plate due to a line load along edge i

F_m^i = Coefficients to be determined

In determining the Fourier sine expansion for the line reactions given by equation (18), it is assumed that the order of summation and integration can be interchanged. After simplification, there results

$$\begin{aligned}
V_B^A &= D\sum_m \frac{2}{m\pi}(-1)^m \sin g_m x \sum_K (-1)^K F_K^A B_{Km}^{(1)} \\
V_D^A &= D\sum_m \frac{2}{m\pi}(-1)^{m+1} \sin g_m x \sum_K F_K^A B_{Km}^{(1)} \\
V_B^C &= D\sum_m (-)\frac{2}{m\pi} \sin g_m x \sum_K (-1)^K F_K^C B_{Km}^{(1)} \\
V_D^C &= D\sum_m \frac{2}{m\pi} \sin g_m x \sum_K F_K^C B_{Km}^{(1)} \\
V_A^B &= D\sum_m \frac{2}{m\pi}(-1)^m \sin \gamma_m y \sum_K (-1)^K F_K^B B_{Km}^{(2)} \\
V_c^B &= D\sum_m \frac{2}{m\pi}(-1)^{m+1} \sin \gamma_m y \sum_K F_K^B B_{Km}^{(2)} \\
V_A^D &= D\sum_m -\frac{2}{m\pi} \sin \gamma_m y \sum_K (-1)^K F_K^D B_{Km}^{(2)} \\
V_c^D &= D\sum_m \frac{2}{m\pi} \sin \gamma_m y \sum_K F_K^D B_{Km}^{(2)}
\end{aligned} \qquad (19)$$

As indicated in section A, the downward positive line loads along the edges of the arbitrarily loaded simply supported plate can be determined and expressed in terms of a Fourier sine series,

$$
\begin{aligned}
V_{s.s.A} &= \sum_m A_m \sin \gamma_m y \\
V_{s.s.B} &= \sum_m B_m \sin g_m x \\
V_{s.s.C} &= \sum_m C_m \sin \gamma_m y \\
V_{s.s.D} &= \sum_m D_m \sin g_m x
\end{aligned}
\tag{20}
$$

As an example, the quantities A_m are determined from equation (7) for the simply supported plate subjected to a thermal gradient. The quantities B_m, C_m, D_m, may be determined analogously for this problem.

From equation (14), considering the problem types being superposed, the beam deflection can be written as

$$
[W_{Beam}]_i = w_i^i \qquad (i = A, B, C, D) \tag{21}
$$

where the quantities on the right hand side represent the i^{th} edge deflection for a plate simply supported on three sides, and edge loaded on the i^{th} side. The values of w_i^i can be obtained from equations (16) and written as

$$
W_i^i = -\sum_m F_m^i \Gamma_m^i \sin \gamma_m^i \eta \tag{22}
$$

where

$$
\Gamma_m^i = \frac{2}{1-\nu} \sinh \gamma_m^i a^i \tag{23}
$$

For i = A, C

$$
\begin{aligned}
a^i &= a \\
\eta &= y \\
\gamma_m^i &= \gamma_m
\end{aligned}
$$

and for i = B, D

$$a^i = b$$
$$\eta = x$$
$$\gamma_m^i = g_m$$

The beam deflection and loading are related by,

$$V_{Beam} = \frac{d^2}{d\eta^2}\left[EI \frac{d^2 W_{Beam}}{d\eta^2}\right] \tag{24}$$

From equation (22), the bracketed term in equation (24) becomes

$$EI \frac{d^2 W_{Beam}}{d\eta^2} = \sum_m F_m^i \Gamma_m^i (\gamma_m^i)^2 (EI)^i \sin \gamma_m^i \eta \tag{25}$$

Expressing $(EI)^i = (EI)_o^i \left[1 + g(\eta)\right]$, and assuming that the order of integration and summation can be interchanged, equation (25) can be written as the Fourier series

$$EI \frac{d^2 W_{Beam}}{d\eta^2} = (EI)_o^i \sum_m \frac{C_m^i}{\gamma_m^{i2}} \sin \gamma_m^i \eta \tag{26}$$

where

$$\frac{C_m^i}{(\gamma_m^i)^2} = F_m^i \Gamma_m^i (\gamma_m^i)^2 + \frac{2}{a^i} \sum_n F_n^i \Gamma_n^i (\gamma_n^i)^2 C_{nm}^i \tag{27}$$

and

$$C_{nm}^i = \int_o^{a^i} g(\eta) \sin \gamma_m^i \eta \sin \gamma_n^i \eta \, d\eta$$

For a beam of constant cross-section, the infinite summation in equation (27), is identically zero since $g(\eta) = 0$.

Combining equations (24) and (26) there results

$$V_{beam} = -(EI)_o^i \sum_m C_m^i \sin \gamma_m^i \eta \tag{28}$$

Substituting equations (17), (19), (20) and (28) into equation (15) and replacing the quantities C_n^i by their definitions, the basic equations for the determination of the unknown coefficients F_n^i become,

$$F_m^A(r_m + K_m^A) + \frac{2}{a}\sum_m \left(\frac{m}{m}\right)^2 K_m^A C_{mm}^A F_m^A - \frac{2}{m\pi}\sum_m (-1)^{m+m} F_m^B B_{mn}^{(2)} - F_n^C A_m + \frac{2}{m\pi}\sum_m (-1)^m F_m^D B_{mn}^{(2)} = \frac{A_m}{D} \tag{29a}$$

$$-\frac{2}{n\pi}\sum_m (-1)^{m+n} F_m^A B_{mn}^{(1)} + F_n^B(t_n + K_n^B) + \frac{2}{b}\sum_m \left(\frac{m}{m}\right)^2 K_m^B C_{mn}^B F_m^B + \frac{2}{m\pi}\sum_m (-1)^m F_m^C B_{mn}^{(1)} - F_n^D W_n = \frac{B_n}{D} \tag{29b}$$

$$-F_n^A A_m + \frac{2}{n\pi}\sum_m (-1)^n F_m^B B_{mn}^{(2)} + F_m^C(r_n + K_m^C) + \frac{2}{a}\sum_m \left(\frac{m}{m}\right)^2 K_m^C C_{mn}^C F_m^C - \frac{2}{m\pi}\sum_m F_m^D B_{mn}^{(2)} = \frac{C_m}{D} \tag{29c}$$

$$\frac{2}{n\pi}\sum_m (-1)^m F_m^A B_{mn}^{(1)} - F_n^B W_n - \frac{2}{m\pi}\sum_m F_m^C B_{mn}^{(1)} + F_n^D(t_n + K_n^D) + \frac{2}{b}\sum_m \left(\frac{m}{m}\right)^2 K_m^D C_{mn}^D F_m^D = \frac{D_m}{D} \tag{29d}$$

Once these coefficients are determined, the deflection can be evaluated by superposition as

$$W = W_{s.s.} + W^A + W^B + W^C + W^D \tag{30}$$

where the w^i are obtained from equation (16).

In the special case of constant $(EI)^i$, the coefficients C_{mn}^i are zero so that the associated summations disappear in equations (29a) to (29d) inclusive.

C. Summary of Method for Obtaining Solution

The following steps are suggested for the solution of the elastically supported rectangular plate subject to mechanical or thermal loads.

1. Calculate the reactive force along each of the supports for the simply supported plate acted upon by the particular mechanical loading or thermal gradient in question.

2. Expand these functions in a Fourier sine series in order to determine A_m, B_m, C_m, D_m in equation (20).

3. Evaluate $B_{m,n}(1)$, $B_{m,n}(2)$, K_n^i, C_{mn}^i, r_n, s_n, w_n, and t_n.

4. Solve equations (29) for F_m^A, F_m^B, F_m^C, and F_m^D.

5. Substitute these coefficients into equations (16) and then evaluate w(x, y) using equation (30).

6. Evaluate all required stresses by using the proper combinations of the derivatives of the deflection.(1)

D. Special Cases

Several of the possible combinations are discussed to illustrate the details of the solution technique.

1. Two Opposite Edges Simply Supported and the Other Edges Elastically Supported on Constant Rigidity Beams

Edges B and D become simply supported by letting the associated beam rigidities and hence K_n^B and K_n^D approach infinity. Using these values in equation (29b) and (29d) it follows that $F_n{}^B = F_n{}^D = 0$. Equations (29a) and (29c) then reduce to,

$$F_m^A(r_m + K_m^A) - F_m^C \Delta_m = \frac{A_m}{D}$$
$$F_m^C(r_m + K_m^C) - F_m^A \Delta_m = \frac{C_m}{D} \tag{31}$$

Solving for F_n^A and F_n^C there results

$$F_m^A = \frac{\begin{vmatrix} A_m & -\Delta_m \\ C_m & r_n + K_m^C \end{vmatrix}}{\Delta}$$
$$F_n^C = \frac{\begin{vmatrix} r_m + K_m^A & A_m \\ -\Delta_m & C_m \end{vmatrix}}{\Delta} \tag{32}$$

where

$$\Delta = D[(r_m + K_m^A)(r_n + K_m^C) - \Delta_n^2] \tag{33}$$

Equation (30) then reduces to

$$W = W_{s.s.} + W^A + W^C \tag{34}$$

where these separate deflections w^A and w^C can be obtained from $F_n{}^A$ and $F_n{}^C$ together with equation (16).

2. Two Opposite Edges Simply Supported on Constant Rigidity Beam and the Other Two Edges Free

The equations (31) to (34) inclusive apply for this case where

$$E_A I_A = E_c I_c = 0 \tag{35}$$

so that

$$K_m^A = K_m^c = 0 \tag{36}$$

therefore

$$\begin{aligned} F_m^A &= \frac{1}{\Delta}\left[A_m r_m + C_m \Delta_m\right] \\ F_m^c &= \frac{1}{\Delta}\left[A_m \Delta_m + C_m r_m\right] \end{aligned} \tag{37}$$

where

$$\Delta = D\left[r_m^2 - \Delta_m^2\right] \tag{38}$$

3. Three Edges Simply Supported and the Fourth Edge Elastically Supported on a Beam of Constant Rigidity

Let the edge A be the elastically supported edge, then K_n^B, K_n^C, and K_n^D approach infinity. From equations (29b), (29c) and (29d), there results

$$F_m^B = F_m^c = F_m^D = 0 \tag{39}$$

Equation (29a) then yields

$$F_m^A = \frac{A_m}{D(r_m + K_m^A)} \tag{40}$$

Thus

$$W = W_{s.s.} + W^A \tag{41}$$

4. Three Edges Simply Supported and the Fourth Edge Free

For this case $E_A I_A = 0$, so that $K_n^A = 0$. Therefore

$$F_m^A = \frac{A_m}{D r_m} \tag{42}$$

5. Square Plate, Subjected to a Thermal Gradient, Three Edges Simply Supported and the Fourth Edge Free

This is a special case of 4. The deflection of a simply supported plate is given by equation (1). The deflection w^A is obtained from equation (16), using F_n^A from equation (42). From equation (41) the stresses can be evaluated[1] to be

$$\frac{h}{M}\sigma_x\Big]_{Max.} = \frac{6a}{h}\left(\frac{M_x}{Ma}\right) \tag{43}$$

$$\frac{h}{M}\sigma_y\Big]_{Max.} = \frac{6a}{h}\left(\frac{M_y}{Ma}\right) \tag{44}$$

$$\frac{h}{M}\tau_{xz}\Big]_{Max.} = \sum_{m=1,3,\cdots}^{\infty} 3\left(-\frac{A_m}{M}\right)\frac{\cosh g_m x \sin g_m y}{(3+\nu)\cosh m\pi + \frac{(1-\nu)\, m\pi}{\sinh m\pi}} \tag{45}$$

$$\frac{h}{M}\tau_{yz}\Big]_{Max.} = \sum_{m=1,3,\cdots}^{\infty} 3\left(-\frac{A_m}{M}\right)\frac{\sinh g_m x \cos g_m y}{(3+\nu)\cosh m\pi + \frac{(1-\nu)\, m\pi}{\sinh m\pi}} \tag{46}$$

where

$$-\left(\frac{M_x}{Ma}\right) = \sum_{m=\text{odd}} \frac{1}{m\pi}\left\{\frac{\sin g_m x \cosh(g_m y - \alpha_m)}{\cosh \alpha_m}\right. \tag{47}$$
$$\left. + \frac{A_m}{M}(1-\nu)\left[\frac{g_m x \cosh g_m x - m\pi \coth m\pi \sinh g_m x}{(3+\nu)\cosh m\pi + \frac{(1-\nu)\, m\pi}{\sinh m\pi}}\right]\sin g_m y\right\}$$

$$-\left(\frac{M_y}{Ma}\right) = \frac{1}{4} + \sum_{m=\text{odd}} \frac{1}{m\pi}\left\{-\frac{\sin g_m x \cosh(g_m y - \alpha_m)}{\cosh \alpha_m}\right. \tag{48}$$
$$\left. + \frac{A_m}{M}(1-\nu)\left[\frac{-g_m x \cosh g_m x + \left\{\frac{2(1+\nu)}{1-\nu} + m\pi \coth m\pi\right\}\sinh g_m x}{(3+\nu)\cosh m\pi + \frac{(1-\nu)\, m\pi}{\sinh m\pi}}\right]\sin g_m y\right\}$$

The results for deflection and bending moments are plotted nondimensionally in Figures 5 to 7 inclusive. The plate with four sides simply supported

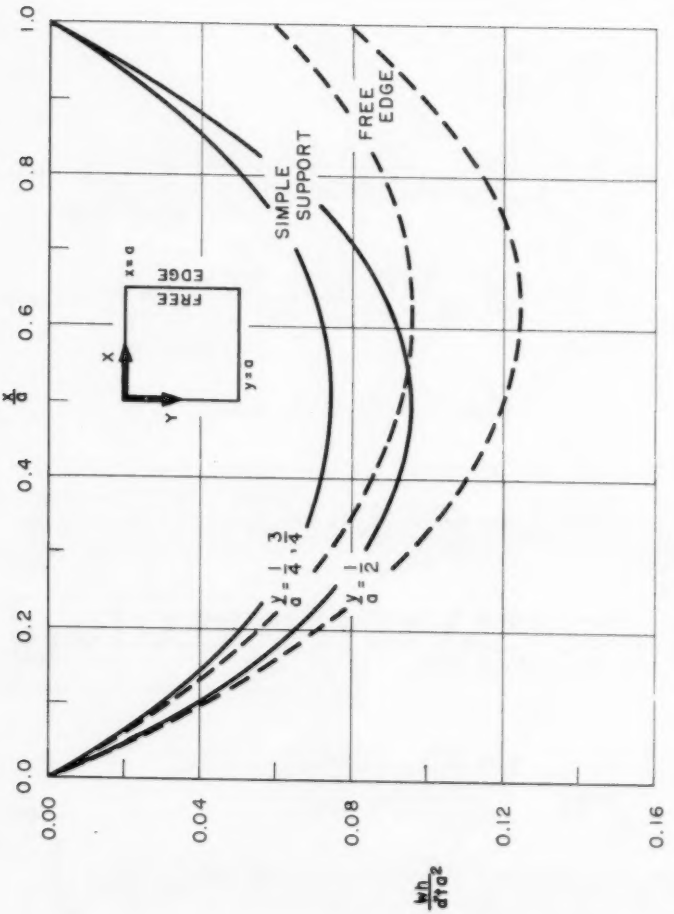

DEFLECTION (w) VS. POSITION (x) FOR y PARAMETERS

FIG. 5

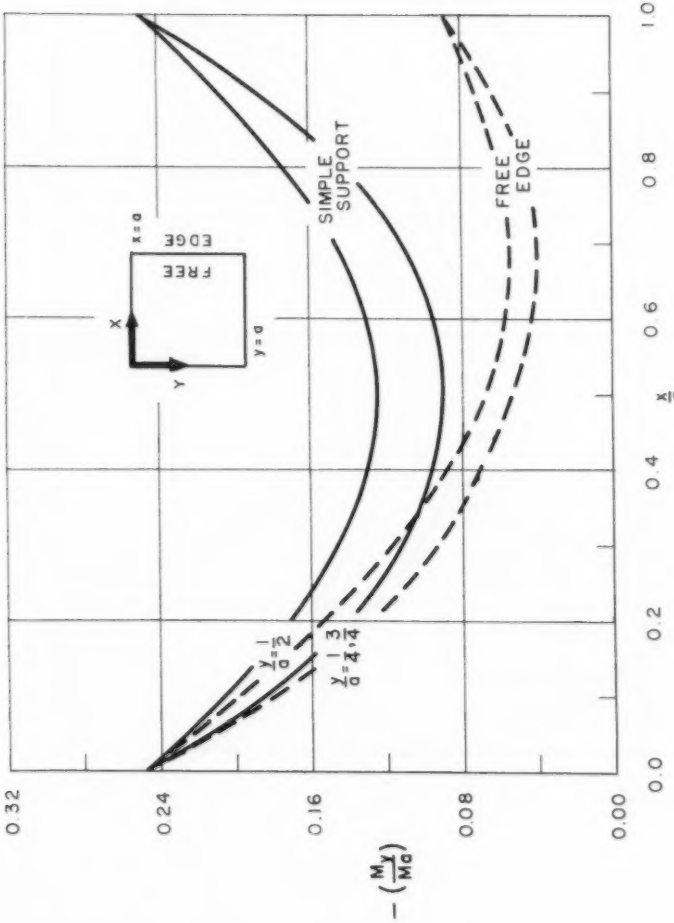

BENDING MOMENT (M_y) VS. POSITION (x) FOR y PARAMETERS

FIG. 6

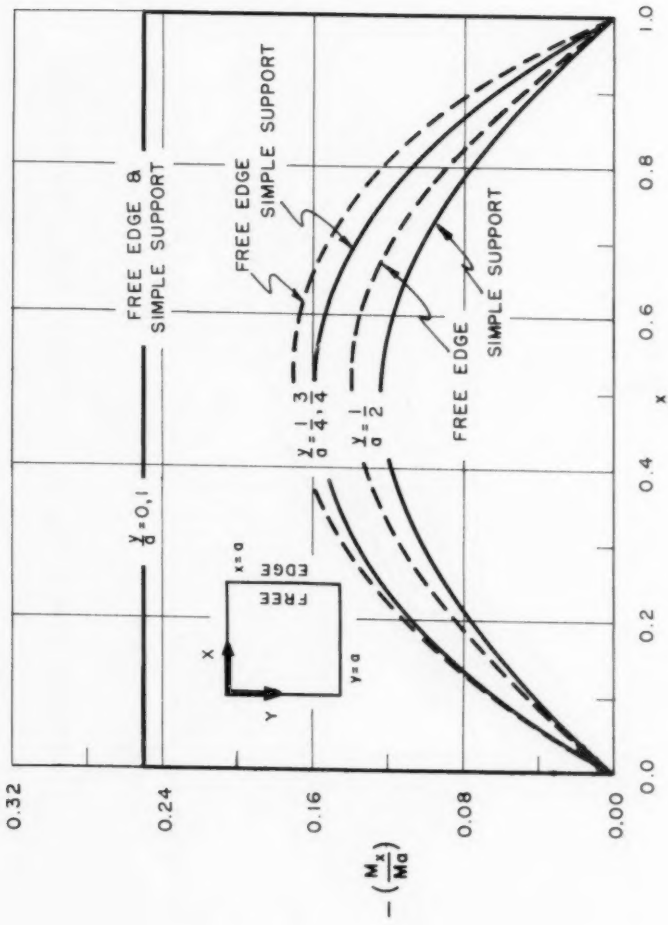

BENDING MOMENT (M_x) VS. POSITION (x) FOR y PARAMETERS

FIG. 7

is designated by "Simple Support" and that with the one free edge by "Free Edge." Both are included for purposes of comparison.

As is well known,(1) the value of τ along the free edge, as determined from shear force Q, need not vanish. This results from the use of the elementary theory and the necessary combining of the shear force and twisting moment boundary condition. The largest shear stress occurs at the free edge, and for the square plate it can be shown, by calculation, to be related to the largest bending stress by

$$|\tau_{max}| < \frac{2}{3}\frac{h}{a}|\sigma_{max}|$$

Thus even relatively thick plates with a thickness to length ratio of 1/10 would give a maximum shear stress amounting to, at most, 7% of the direct stress. For thinner plates this shear stress is correspondingly less. In addition these maximum stresses do not occur at the same location, so that the shear stress becomes negligible in design considerations.

Appendix A: Finite Series Approximation

Consider a rectangular plate subjected to a loading q(x,y) and reactions as shown in Figure A-1.

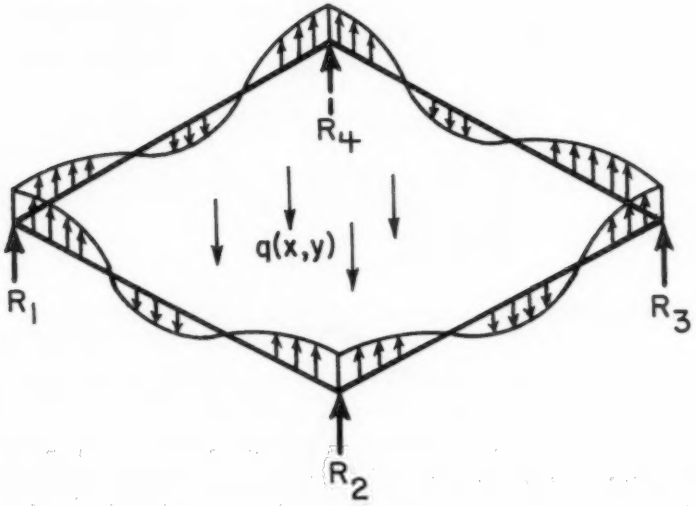

Fig. A-1.

The deflection solution for this general problem can be obtained from the solutions for the three superposeable loadings shown in Figures A-2a to A-2c. Figure A-2 (a) illustrates the loaded plate with corner reactions only. Figure A-2 (b) illustrates the symmetrical component of the line load.

FIG. A-2(a)

FIG. A-2(b)

FIG. A-2(c)

Figure A-2 (c) illustrates the anti-symmetrical component of the line load. It is necessary to investigate the error introduced by finite series approximation to the line load. This error will affect the plate of Figures A-2(b) and A-2(c) only. The symmetrical case will be discussed and the anti-symmetrical situation follows analogously.

Consider the distributed symmetrical line load on a representative edge together with its equilibrating reactions at the corners, Fig. A-3. Divide the load and associated reactions into 2 parts as shown in Fig. A-4, where $T = T' + T''$, and each sub-system is in equilibrium.

The loads acting over the central region in Figure A-4 (a) can be replaced by the statically equivalent system (Fig. A-5). The moment

$$M' < \delta T'$$

can be made as small as desirable by decreasing δ. Furthermore, from St. Venant's principle, the effect of the self equilibrating force system associated with T' is negligible except in the neighborhood of the corners.

By taking a sufficiently large number of terms, the actual line load may be approximated uniformly well in the central sub-region, Figure A-4 (b), and the interval of error (δ) correspondingly approaches zero. The associated Fourier sine series expansion should always include enough terms to represent the exact line loading well, except possibly in the subregion of Fig. A-4 (a) of width δ. This can be always ascertained in advance of obtaining the complete solution. Therefore the use of the finite series will lead to stresses and displacements which agree sufficiently well with that obtained for the exact line loading except possibly in the neighborhood of the corners.

ACKNOWLEDGMENT

The authors wish to acknowledge the aid of Mrs. Sidnie Holbrook in diligently performing the calculations for this paper.

REFERENCES

1. "Theory of Plates and Shells" by S. Timoshenko, McGraw-Hill Book Company, Inc., New York, N. Y., 1940.
2. "On Rectangular Elastically Supported Plates." Pierro Pozzati, Boll, Un. mat. ital. 3, pp. 236-248, Dec. 1948.
3. "Die Berechnung rechteckiger, gleichformig belasteter Platten, die an Zwei gegenuber liegenden Randern durch elastiche Trager unterstutzt Sind.," by E. Muller. Ingenieur - Archiv II. Band 1932 pp. 606 to 621.
4. "Uber elasticher Tragern durchlaufende Platten" by Wilhelm Ihlenburg, Der Sthul Bau 22, No. 8 Aug. 1953, pp. 169 to 171; No. 9, Sept. 1953 pp. 209 to 214.
5. "Plates with Boundary Conditions of Elastic Support" by S. J. Fuchs, Trans. ASCE, Vol. 119, 1954 pp. 935 to 968. (This, together with the Discussion, includes many other references.)

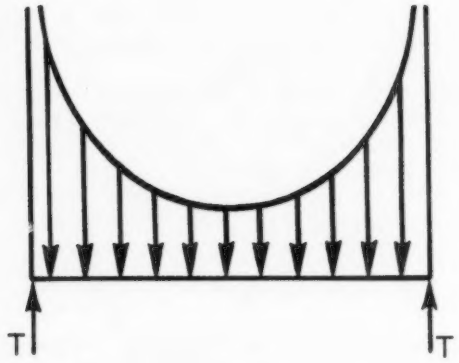

FIG. A-3

LINE LOADED EDGE

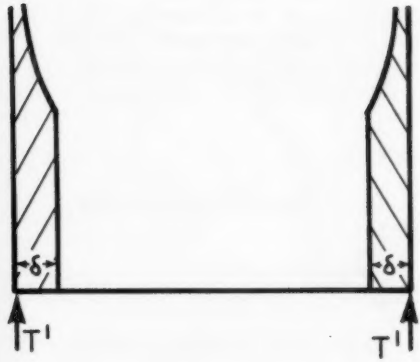

FIG. A-4(a)

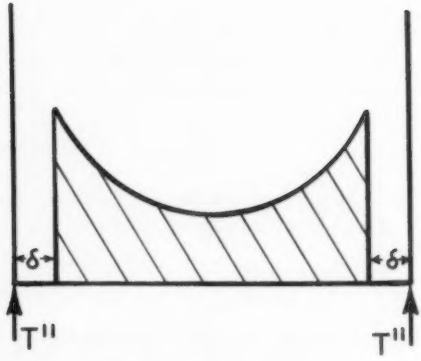

FIG. A-4(b)

FIG. A-5

6. "Differential and Integral Calculus" Vol. I by R. Courant, Nordeman Publishing Company, Inc., New York, N. Y., 1940.

7. Reports on "Elastically Supported Rectangular Plates" by M. Zaid, Sperry Gyroscope Corp. Report Nos. 5284 - 2342, 5284 - 2343, 5284 -, 1951, Great Neck, N. Y.

Paper 1724 July, 1958 EM 3

Journal of the
ENGINEERING MECHANICS DIVISION
Proceedings of the American Society of Civil Engineers

CONTENTS

DISCUSSION
(Proc. Paper 1724)

INCREMENTAL COMPRESSION TEST FOR CEMENT RESEARCH[a]

Corrections by A. Hrennikoff

CORRECTIONS.—The following illustrations were inadvertently reproduced in Proc. Paper 1604 in a size too small for clarity. To facilitate study of these figures, they are reproduced herewith.

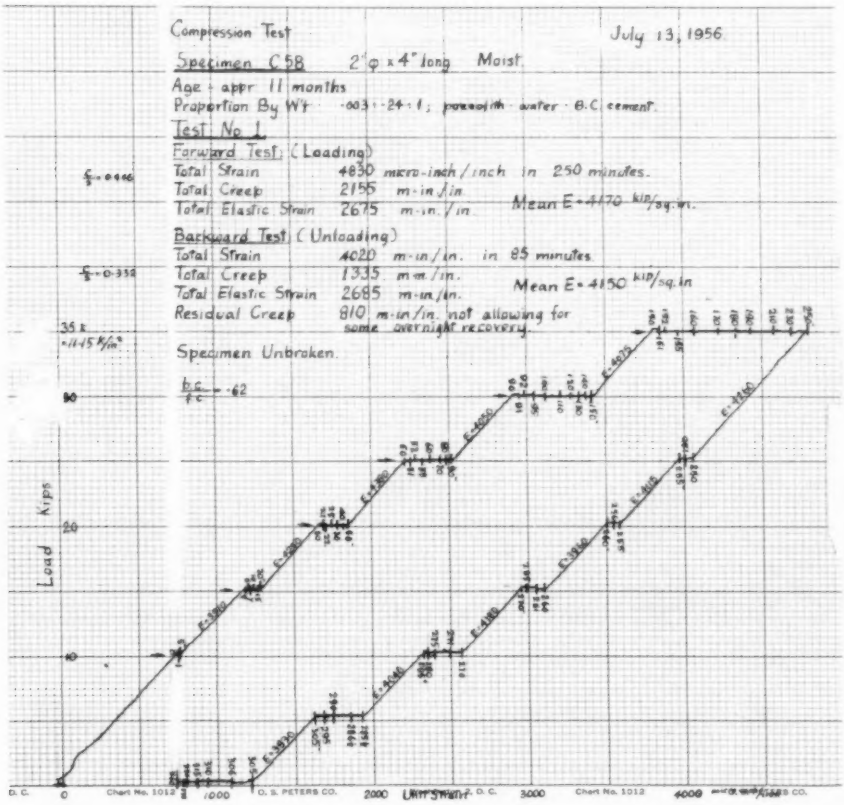

Fig. 9

Note: Paper 1724 is part of the copyrighted Journal of the Engineering Mechanics Division, Proceedings of the American Society of Civil Engineers, Vol. 84, No. EM 3, July, 1958.

a. Proc. Paper 1604, April, 1958, by A. Hrennikoff.

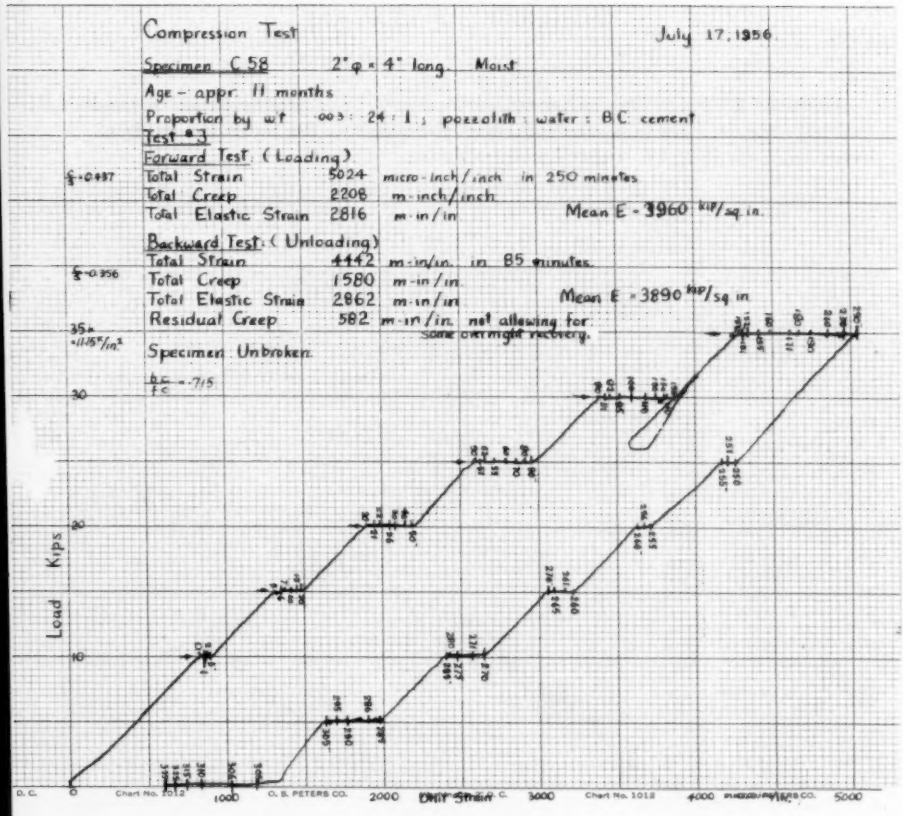
Compression Test
July 17, 1956
Specimen C 58 2" φ × 4" long. Moist
Age - appr. 11 months
Proportion by wt 00 : 24 : 1 ; pozzolith : water : B.C. cement
Test #3
Forward Test (Loading)
Total Strain 5024 micro-inch/inch in 250 minutes
Total Creep 2208 m-inch/inch
Total Elastic Strain 2816 m-in/in
Mean E = 3960 kip/sq in.
Backward Test (Unloading)
Total Strain 4442 m-in/in. in 85 minutes
Total Creep 1580 m-in/in
Total Elastic Strain 2862 m-in/in
Mean E = 3890 kip/sq in.
Residual Creep 582 m-in/in. not allowing for some overnight recovery.
Specimen Unbroken.
Load Kips
Unit Strain
O. B. PETERS CO.
Chart No. 1012

Fig. 10.

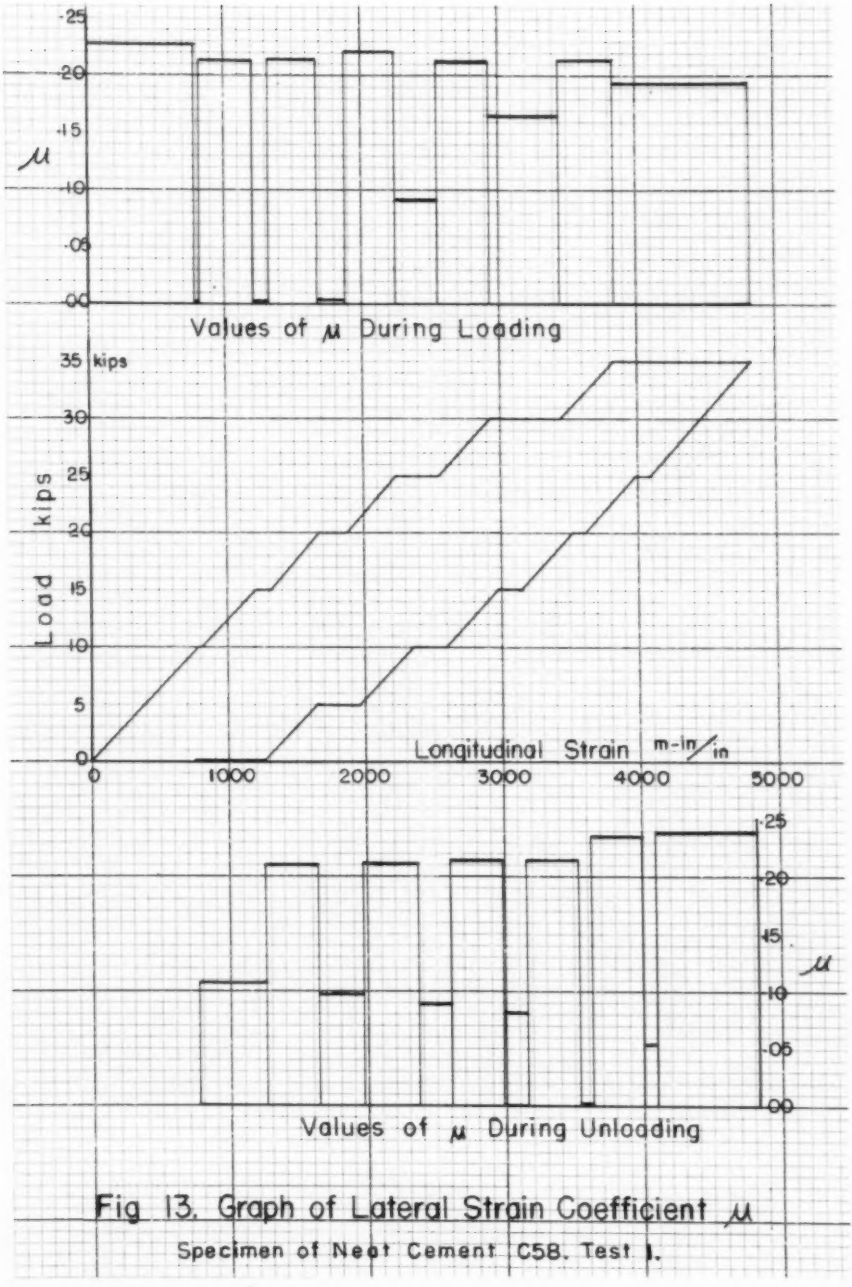

Fig. 13. Graph of Lateral Strain Coefficient μ
Specimen of Neat Cement C58, Test 1.

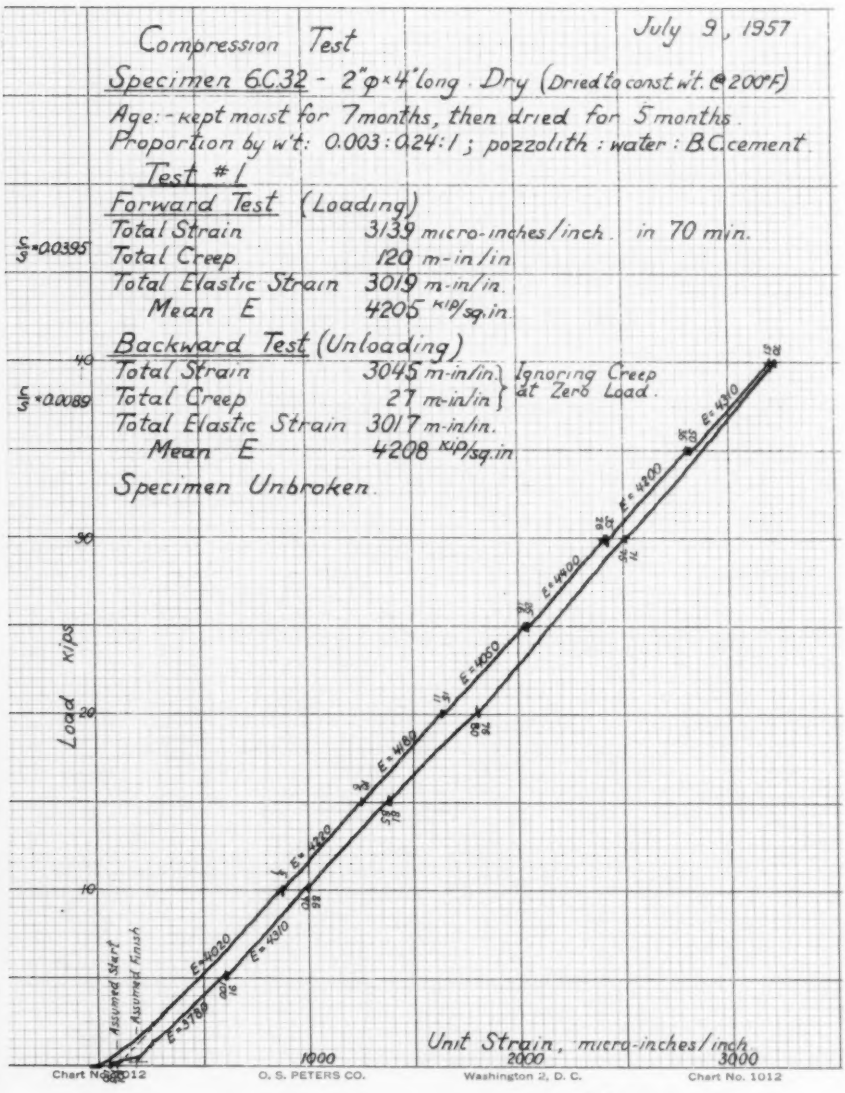
Compression Test
July 9, 1957
Specimen 6C32 - 2"φ×4" long. Dry (Dried to const. wt. @ 200°F)
Age:- kept moist for 7 months, then dried for 5 months.
Proportion by w't: 0.003 : 0.24 : 1 ; pozzolith : water : B.C. cement.
Test #1
Forward Test (Loading)
Total Strain 3139 micro-inches/inch. in 70 min.
Total Creep 120 m-in/in
Total Elastic Strain 3019 m-in/in.
Mean E 4205 kip/sq.in.
Backward Test (Unloading)
Total Strain 3045 m-in/in. Ignoring Creep
Total Creep 27 m-in/in } at Zero Load.
Total Elastic Strain 3017 m-in/in.
Mean E 4208 kip/sq.in.
Specimen Unbroken.
S/3 = .00395
S/3 = .00089
Load kips
40
30
20
10
Assumed Start
Assumed Finish
E = 4020
E = 3760
E = 4210
E = 4200
E = 4160
E = 4050
E = 4000
E = 4210
1000
2000
3000
Unit Strain, micro-inches/inch
Chart No. 1012
O. S. PETERS CO.
Washington 2, D. C.
Chart No. 1012

Fig. 14.

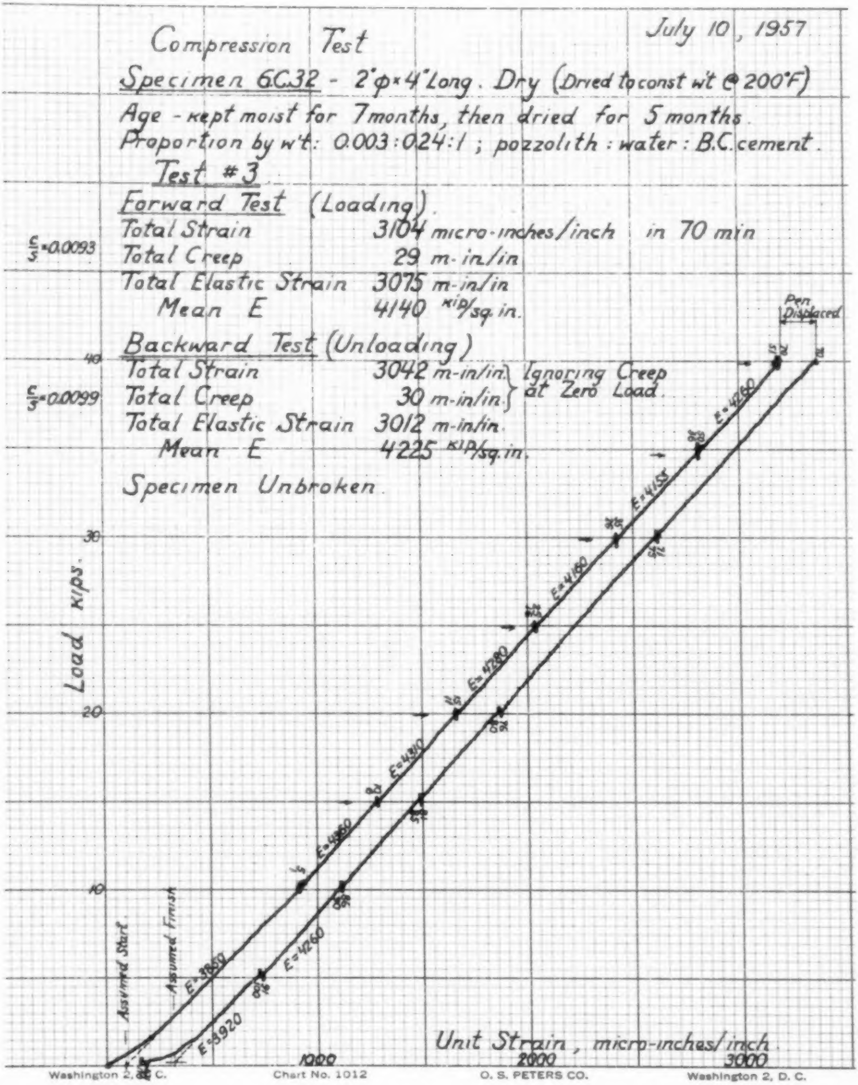
Compression Test
July 10, 1957
Specimen 6C32 - 2"φ × 4" Long. Dry (Dried to const wt @ 200°F)
Age - kept moist for 7 months, then dried for 5 months.
Proportion by wt: 0.003 : 0.24 : 1 ; pozzolith : water : B.C. cement.
Test #3
Forward Test (Loading)
Total Strain 3104 micro-inches/inch in 70 min
c/s = 0.0093
Total Creep 29 m-in/in
Total Elastic Strain 3075 m-in/in
Mean E 4140 kip/sq. in.
Backward Test (Unloading)
Total Strain 3042 m-in/in
c/s = 0.0099
Total Creep 30 m-in/in
Ignoring Creep at Zero Load
Total Elastic Strain 3012 m-in/in
Mean E 4225 kip/sq. in.
Specimen Unbroken
Pen Displaced
Load kips
Unit Strain, micro-inches/inch
Assumed Start
Assumed Finish
E=3850
E=4360
E=4310
E=4280
E=4180
E=4155
E=4260
E=3920
E=4260
1000
2000
3000
10
20
30
40
Washington 2, D. C.
Chart No. 1012
O. S. PETERS CO.
Washington 2, D. C.

Fig. 15.

PROCEEDINGS PAPERS

The technical papers published in the past year are identified by number below. Technical-division sponsorship is indicated by an abbreviation at the end of each Paper Number, the symbols referring to: Air Transport (AT), City Planning (CP), Construction (CO), Engineering Mechanics (EM), Highway (HW), Hydraulics (HY), Irrigation and Drainage (IR), Pipeline (PL), Power (PO), Sanitary Engineering (SA), Soil Mechanics and Foundations (SM), Structural (ST), Surveying and Mapping (SU), and Waterways and Harbors (WW), Sedimen. Papers sponsored by the Board of Direction are identified by the symbols (BD). For titles and order coupons, refer to the appropriate issue of "Civil Engineering." Beginning with Volume 83 (January 1957) papers were published in Journals of the various Technical Divisions. To locate papers in the Journals, the symbols after the paper numbers are followed by a numeral designating the issue of a particular Journal in which the paper appeared. For example, Paper 1440 is identified as 1440 (HY 6) which indicates that the paper is contained in the sixth issue of the Journal of the Hydraulics Division during 1957.

VOLUME 83 (1957)

JULY: 1289(SM1), 1290(SM3), 1291(ES3), 1292(ES3), 1293(EM3), 1294(HW3), 1295(HW3), 1296(HW3), 1297(HW3), 1298(HW3), 1299(HW3), 1300(SM3), 1301(SM3), 1302(ST4), 1303(ST4), 1304(ST4), 1305(SU1), 1306(SU1), 1307(SU1), 1308(ST4), 1309(SM3), 1310(SU1)[c], 1311(SM3)[c], 1312(ST4), 1313(ST4), 1314(ST4), 1315(ST4), 1316(ST4), 1317(ST4), 1318(ST4), 1319(SM3)[c], 1320(ST4), 1321(ST4), 1322(SM3), 1323(AT1), 1324(AT1), 1325(AT1), 1326(AT1), 1327(AT1), 1328(AT1)[c], 1329(ST4)[c].

AUGUST: 1330(HY4), 1331(HY4), 1332(HY4), 1333(SA4), 1334(SA4), 1335(SA4), 1336(SA4), 1337(SA4), 1338(SA4), 1339(CO1), 1340(CO1), 1341(CO1), 1342(CO1), 1343(CO1), 1344(PO1), 1345(ST4), 1346(PO4)[c], 1347(IR6), 1348(HY4)[c], 1349(SA4)[c], 1350(PO4), 1351(PO4).

SEPTEMBER: 1352(IR2), 1353(ST5), 1354(ST5), 1355(ST5), 1356(ST5), 1357(ST5), 1358(ST5), 1359(IR3), 1360(IR2), 1361(ST5), 1362(IR2), 1363(IR3), 1364(IR3), 1365(WW3), 1366(WW3), 1367(WW3), 1368(WW3), 1369(WW3), 1370(WW3), 1371(HW4), 1372(HW4), 1373(HW4), 1374(HW4), 1375(PL3), 1376(PL3), 1377(IR3)[c], 1378(HW4)[c], 1379(IR2), 1380(HW4), 1381(WW4)[c], 1382(ST5)[c], 1383(PL3)[c], 1384(IR2), 1385(HW4), 1386(HW4).

OCTOBER: 1387(CP2), 1388(CP2), 1389(EM4), 1390(EM4), 1391(HY5), 1392(HY5), 1393(HY5), 1394(HY5), 1395(HY5), 1396(PO5), 1397(PO5), 1398(PO5), 1399(EM4), 1400(SA5), 1401(HY5), 1402(ST5), 1403(HY5), 1404(HY5), 1405(HY5), 1406(HY5), 1407(SA5), 1408(SA5), 1409(SA5), 1410(SA5), 1411(SA5), 1412(EM4), 1413(EM4), 1414(PO5), 1415(EM4)[c], 1416(PO5)[c], 1417(HY5)[c], 1418(EM4), 1419(PO5), 1420(PO5), 1421(PO5), 1422(SA5)[c], 1423(SA5), 1424(EM4), 1425(CP2).

NOVEMBER: 1426(EM4), 1427(EM4), 1428(EM4), 1429(EM4), 1430(EM4), 1430(EM4)[c], 1431(ST6), 1432(ST6), 1433(ST6), 1434(ST6), 1435(ST6), 1436(ST6), 1437(ST6), 1438(EM4), 1439(EM4), 1440(ST6), 1441(ST6), 1442(ST6)[c], 1443(SU2), 1444(SU2), 1445(SU2), 1446(SU2), 1447(SU2), 1448(SU2)[c].

DECEMBER: 1449(HY6), 1450(HY6), 1451(HY6), 1452(HY6), 1453(HY6), 1454(HY6), 1455(HY6), 1456(ST6)[c], 1457(PO6), 1458(PO6), 1459(PO6), 1460(PO6)[c], 1461(SA6), 1462(SA6), 1463(SA6), 1464(SA6), 1465(SA6), 1466(SA6)[c], 1467(AT2), 1468(AT2), 1469(AT2), 1470(AT2), 1471(AT2), 1472(AT2), 1473(AT2), 1474(AT2), 1475(AT2), 1476(AT2), 1477(AT2), 1478(AT2), 1479(AT2), 1480(AT2), 1481(AT2), 1482(AT2), 1483(AT2), 1484(AT2), 1485(AT2)[c], 1486(BD2), 1487(BD2), 1488(PO6), 1489(PO6), 1490(PO6), 1491(BD2), 1492(HY6), 1493(BD2).

VOLUME 84 (1958)

JANUARY: 1494(EM1), 1495(EM1), 1496(EM1), 1497(IR1), 1498(IR1), 1499(IR1), 1500(IR1), 1501(IR1), 1502(IR1), 1503(IR1), 1504(IR1)[c], 1505(IR2), 1506(IR1), 1507(IR1), 1508(ST1), 1509(ST1), 1510(ST1), 1511(ST1), 1512(ST1), 1513(WW1), 1514(WW1), 1515(WW1), 1516(WW1), 1517(WW1), 1518(WW1), 1519(ST1), 1520(EM1)[c], 1521(IR1)[c], 1522(ST1)[c], 1523(WW1)[c], 1524(EM1), 1525(HW1), 1526(HW1)[c], 1527(WW1).

FEBRUARY: 1528(HY1), 1529(PO1), 1530(HY1), 1531(HY1), 1532(HY1), 1533(SA1), 1534(SA1), 1535(SM1), 1536(SM1), 1537(SM1), 1538(PO1)[c], 1539(SA1)[c], 1540(SA1), 1541(SA1), 1542(SA1), 1543(SA1), 1544(SM1), 1545(SM1), 1546(SM1), 1547(SM1), 1548(SM1), 1549(SM1), 1550(SM1), 1551(SM1), 1552(SM1), 1553(PO1), 1554(PO1), 1555(PO1), 1556(PO1), 1557(SA1)[c], 1558(ST1)[c], 1559(SM1)[c].

MARCH: 1560(ST2), 1561(ST2), 1562(ST2), 1563(ST2), 1564(ST2), 1565(ST2), 1566(ST2), 1567(ST2), 1568(WW2), 1569(WW2), 1570(WW2), 1571(WW2), 1572(WW2), 1573(WW2), 1574(PL1), 1575(PL2), 1576(PL2)[c], 1577(PL1), 1578(PL1)[c], 1579(WW2)[c].

APRIL: 1580(EM2), 1581(EM2), 1582(HY2), 1583(HY2), 1584(HY2), 1585(HY2), 1586(HY2), 1587(HY2), 1588(PO2), 1589(IR2), 1590(IR1), 1591(IR2), 1592(SA2), 1593(SU2), 1594(SU2), 1595(SU2), 1596(SM2), 1597(PO2), 1598(PO2), 1599(PO2), 1600(PO2), 1601(PO2), 1602(PO2), 1603(HY2), 1604(SM2), 1605(SU2)[c], 1606(SA2), 1607(SA2), 1608(SA2), 1609(SA2), 1610(SA2), 1611(SA2), 1612(SA2), 1613(SA2), 1614(SA2)[c], 1615(IR2)[c], 1616(HY2)[c], 1617(SU2), 1618(PO2)[c], 2819(EM2)[c], 1620(CP1).

MAY: 1621(HW2), 1622(HW2), 1623(HW2), 1624(HW2), 1625(HW2), 1626(HW2), 1627(HW2), 1628(HW2), 1629(HW2), 1630(ST3), 1631(ST3), 1632(ST3), 1633(ST3), 1634(ST3), 1635(ST3), 1636(ST3), 1637(ST3), 1638(ST3), 1639(WW2), 1640(WW2), 1641(WW2), 1642(WW2), 1643(WW2), 1644(WW2), 1645(SM2), 1646(SM2), 1647(SM2), 1648(SM2), 1649(SM2), 1650(SM2), 1651(SM2), 1652(SM2)[c], 1653(WW2)[c], 1654(SM2), 1655(SA2), 1656(ST3)[c], 1657(SM2)[c].

JUNE: 1658(AT1), 1659(AT1), 1660(HY3), 1661(HY3), 1662(HY3), 1663(HY3), 1664(HY3), 1665(SA3), 1666(PL2), 1667(PL2), 1668(PL2), 1669(AT1), 1670(PO3), 1671(PO3), 1672(PO3), 1673(PL2), 1674(PL2), 1675(PO3), 1676(PO3), 1677(SA3), 1678(SA3), 1679(SA3), 1680(SA3), 1681(SA3), 1682(SA3), 1683(PO3), 1684(HY3), 1685(SA3), 1686(SA3), 1687(PO3), 1688(SA3)[c], 1689(PO3)[c], 1690(HY3)[c], 1691(PL2)[c].

JULY: 1692(WW3), 1693(EM3), 1694(ST4), 1695(ST4), 1696(ST4), 1697(ST4), 1698(SU2), 1699(SU2), 1700(SU2), 1701(SA4), 1702(SA4), 1703(SA4), 1704(SA4), 1705(HW3), 1706(HW3), 1707(HW3), 1708(ST4), 1709(ST4), 1710(HW3), 1711(ST4), 1712(PO4), 1713(PO4), 1714(SA4), 1715(SA4), 1716(SU2), 1717(SA4), 1718(EM3), 1719(EM3), 1720(SU2), 1721(ST4)[c], 1722(ST4), 1723(ST4), 1724(EM3)[c].

---

[c] Discussion of several papers, grouped by divisions.